Characterization of *Saccharomyces cerevisiae* kinesin Kip2

by total internal reflection fluorescence microscopy

Dissertation

zur Erlangung des akademischen Grades

Doctor rerum naturalium

(Dr. rer. nat.)

vorgelegt

der Fakultät Mathematik und Naturwissenschaften der

Technischen Universität Dresden

von

Anneke Hibbel

Geboren am 29. August 1981 in Baarn, Niederlande

Eingereicht am 30. März 2015

Die Dissertation wurde in der Zeit von Oktober 2011 bis März 2015

im Max-Planck-Institut für molekulare Zellbiologie und Genetik

angefertigt

Gutachter

1. Prof. Dr. Stefan Diez
2. Prof. Dr. Jonathon Howard

Table of contents   Page

Contributions

Abstract

Microtubule length control is indispensable for cytoskeletal functions such as mitotic spindle assembly and positioning. *In vivo* studies have shown that kinesin motor proteins can regulate microtubule length positively and negatively. The mechanisms by which kinesins act as depolymerases and catastrophe factors are well studied. By contrast, how kinesins promote microtubule growth is unknown. The aim of this work was to elucidate the mechanism by which budding yeast kinesin Kip2 regulates microtubule dynamics, using *in vitro* reconstitution assays combined with total internal reflection fluorescence (TIRF) and differential interference contrast (DIC) microscopy. Kip2 was shown to increase the mean length of microtubules through length-dependent polymerase and anti-catastrophe activities, both with porcine and yeast tubulin, in the absence of accessory proteins. Using single-molecule motility assays, Kip2 was shown to translocate in a highly processive, ATP-dependent manner and to processively target tubulin oligomers to microtubule plus-ends. Mutant studies to probe Kip2 structure-function relationships revealed that the N-terminus of Kip2 is dispensable for promotion of microtubule growth, while the C-terminus is not. An effort to functionally identify a tubulin/microtubule-binding domain in the C-terminus of Kip2 remained unfruitful. Finally, the combinatorial effect of Kip2 with interaction partners Bim1 and Bik1 on microtubule dynamics was reconstituted. This microtubule plus-end tracking complex promoted microtubule growth beyond the effect of Kip2 alone. Together, this work demonstrates that a kinesin motor can act directly as a length-dependent microtubule polymerase and anti-catastrophe factor in the absence of accessory proteins. Thereby, this work provides insight into how kinesins control microtubule length.

Abbreviations

ADP	Adenosine di-phosphate
AMP-PNP	Adenylyl-imidodi-phosphate
ATP	Adenosine triphosphate
BSA	Bovine serum albumin
CAP-gly	Cytoskeleton-associated protein, glycine-rich
Cin8	Chromosome instability 8
CLIP-170	Cytoplasmic linker protein 170
DIC	Differential interference contrast
eGFP	Enhanced green fluorescent protein
GDP	Guanosine di-phosphate
GMPCPP	Guanosine-5'-[(α,β)-methyleno]tri-phosphate
GTP	Guanosine tri-phosphate
Kar9	Karyogamy 9
KHC	Kinesin heavy chain
Kip2/3	Kinesin-like protein 2/3
KLC	Kinesin light chain
MAP	Microtubule-associated protein
MCAK	Mitotic centromere-associated kinesin
NCBI	National Center for Biotechnology Information
PBS	Phosphate-buffered saline
PCR	Polymerase chain reaction
SDS-PAGE	Sodium dodecyl sulfate polyacrylamide gel electrophoresis
Smy1	Suppressor of Myo2-66 1
SPB	Spindle pole body
TIRF	Total internal reflection fluorescence
XMAP215	*Xenopus* microtubule-associated protein 215
YFP	Yellow fluorescent protein
+TIP	Microtubule plus-end tracking proteins
6xHIS	Tag consisting of 6 histidine residues

List of Figures   Page

List of Tables   Page

1.   Introduction

1.1.   Microtubules in eukaryotic cells

The microtubule cytoskeleton is of vital importance for the shape and function of eukaryotic cells. Microtubules make up the mitotic spindle that segregates chromosomes during mitosis. In addition, microtubules provide mechanical support for cell shape and allow for cell motility as structural elements of cilia and flagella. Finally, microtubules function as tracks for motor proteins that transport cellular cargo (Hirokawa and Tanaka, 2015). The word cyto- (Greek for cell) skeleton suggests that microtubules are rigid structures, like the bones that make up our skeleton. By contrast, the microtubule cytoskeleton is highly dynamic: it assembles and disassembles on a time-scale of minutes.

        To exert cellular functions such as mitotic spindle assembly (Goshima et al., 2007; Reber et al., 2013) and positioning (Cottingham and Hoyt, 1997; Pecreaux et al., 2006), the lengths of individual microtubules need to be tightly controlled. Therefore, microtubule assembly dynamics are temporally and spatially regulated. To understand how this regulation occurs, it is important to dissect microtubule assembly dynamics on a molecular level.

1.2.   Microtubules are polymers of tubulin

In its unpolymerized form, tubulin is a α/β tubulin heterodimer, bound to two guanosine triphosphate (GTP) molecules (Amos, 2004). These α/β tubulin heterodimers assemble longitudinally in a non-covalent, head-to-tail manner to form protofilaments. Typically, ~13 protofilaments associate laterally to form a hollow microtubule with a diameter of 25 nm. The α-tubulin subunit is always exposed at the microtubule minus-end, whereas the β-tubulin subunit is exposed at the microtubule plus-end (Amos, 2004; Desai and Mitchison, 1997) (Figure 1.1). Thus, microtubules are inherently polar structures. In the cell, the minus-end is usually tethered to a microtubule-organizing center, such as the spindle pole body (SPB) in *Saccharomyces cerevisiae*. This tethering stabilizes the dynamics of this end of the

_____

polymer. By contrast, the plus-end is often free to explore the cellular space (Howard and Hyman, 2003).
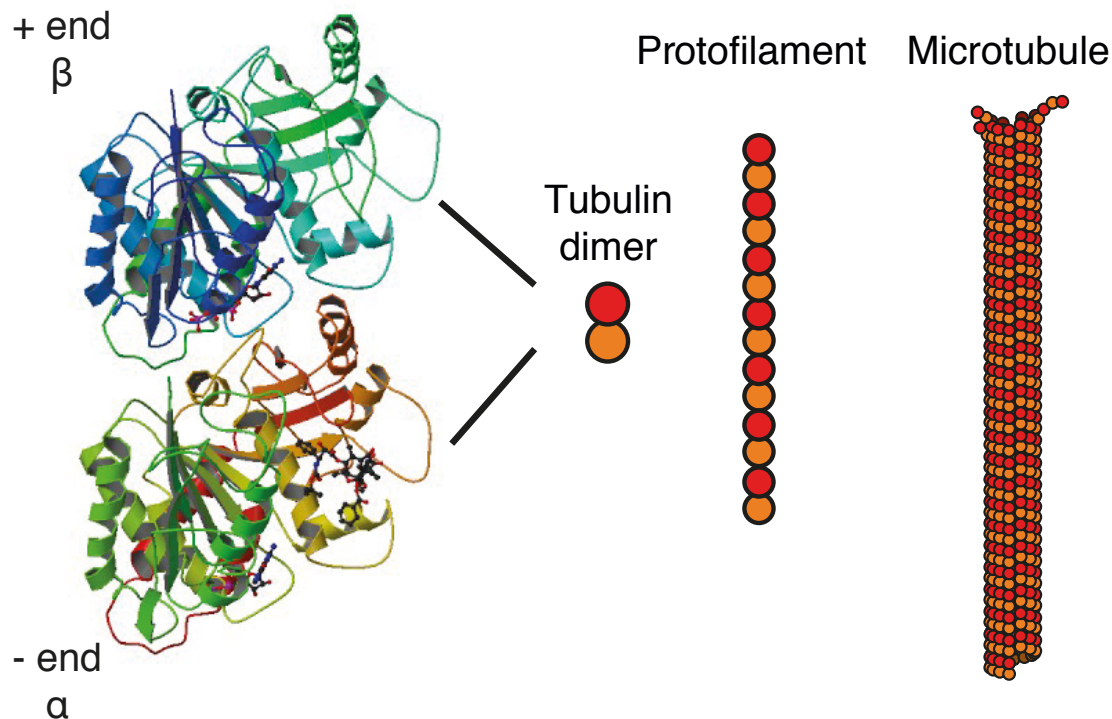
Figure 1.1. Schematic of a tubulin dimer, a protofilament and a microtubule. Modified from (Nogales et al., 1998).
Tubulin dimers associate in a head-to-tail manner to form protofilaments, which in turn form a hollow tube; the microtubule.

1.3.　　　Microtubules are inherently dynamic

Microtubules are inherently dynamic; they switch stochastically between phases of polymerization (growth) and depolymerization (shrinkage), a process termed dynamic instability that was discovered in 1984 (Mitchison and Kirschner, 1984a). The switching from slow growth to rapid shrinking is termed catastrophe, whereas the switching from shrinkage to growth is termed rescue (Walker et al., 1988) (Figure 1.2). The rate at which microtubules grow scales linearly with the concentration of free tubulin, while microtubule catastrophe is thought to only be loosely dependent on the microtubule growth rate (Walker et al., 1988).
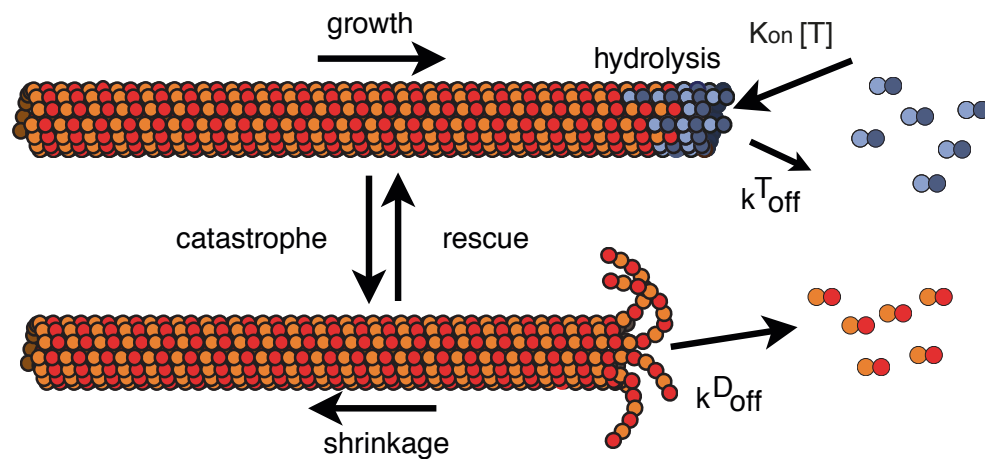
Figure 1.2. Microtubules switch between phases of slow growth and rapid shrinkage. Modified from (Bowne-Anderson et al., 2013).

Microtubule dynamics are determined by the on-rate of GTP-tubulin, the off-rate of GTP-tubulin, the off-rate of GDP-tubulin and the rate of hydrolysis of lattice-incorporated GTP-tubulin.

When a microtubule grows, GTP-tubulin, which has a straight conformation, associates with the microtubule plus-end. Upon incorporation in the lattice, the β-tubulin-associated GTP hydrolyzes, which causes a bent conformation of the tubulin dimer (Nogales et al., 1998). However, now that the tubulin is incorporated in the lattice, it is forced to remain a straight conformation. The release of this bending energy, which is stored in the microtubule lattice, drives depolymerization (Howard and Hyman, 2007; Nogales, 1999). Thus, microtubule catastrophe is fueled by GTP-hydrolysis, whereas microtubule growth is not (Hyman et al., 1992).

While the microtubule is growing, its plus-end is protected against disassembly by a stabilizing cap, which is thought to consist of GTP-tubulin (Caplow and Shanks, 1996; Drechsel and Kirschner, 1994; Maurer et al., 2014; Mickey and Howard, 1995). The switching from microtubule growth to shrinkage is believed to occur when the microtubule looses this stabilizing cap (Mitchison and Kirschner, 1984a; Tran et al., 1997; Walker et al., 1989). GTP-tubulin remnants embedded in the microtubule lattice are thought to contribute to rescue events, the switching from shrinkage to growth (Dimitrov et al., 2008; Tropini et al., 2012; Gardner et al., 2013).

The four parameters of dynamic instability define a threshold between unlimited microtubule growth and steady-state dynamics (Verde et al., 1992). These steady-state dynamics per se lead to a broad distribution of microtubule lengths (Howard and Hyman, 2007). In the cell, however, microtubule dynamics are

_____

regulated, which results in a more narrow distribution of microtubule lengths. This microtubule length control requires a precise balance between the phases of slow growth and rapid shrinkage at the microtubule plus-end (Figure 1.3). How this balance is achieved is still poorly understood.
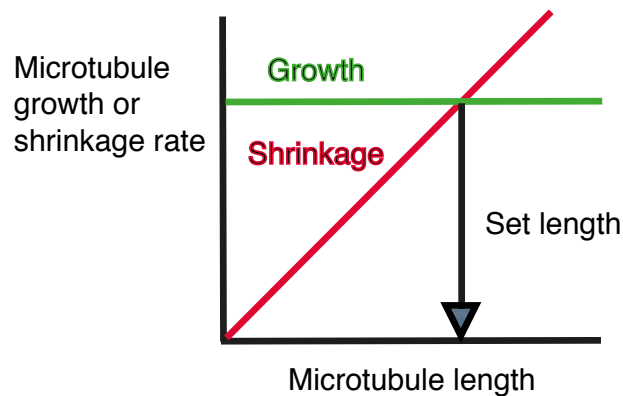
Figure 1.3. Microtubule length control. Modified from (Howard and Hyman, 2007).
The control of microtubule length requires a precise balance between phases of slow microtubule growth and rapid shrinkage at the microtubule plus-end.

1.4.1.   Microtubule-associated proteins regulate dynamics

In cells, microtubule dynamics are regulated by microtubule-associated proteins (MAPs) (Howard and Hyman, 2007; Vaart et al., 2009). Broadly speaking, these MAPs fall into three categories. The first class consists of proteins that increase microtubule growth rate, termed microtubule polymerases, such as XMAP215 (Gard and Kirschner, 1987). XMAP215 promotes fast microtubule elongation by catalytically adding multiple tubulin dimers to the growing plus-end, before it dissociates from the microtubule (Brouhard et al., 2008).

The second class of MAPs that regulate microtubule dynamics are proteins that track the growing microtubule plus-ends, termed +TIPs (reviewed in (Akhmanova and Steinmetz, 2010). The first identified +TIP was CLIP-170, that links endosomes to microtubules (Perez et al., 1999). In fission yeast, CLIP-170 functions as an anti-catastrophe factor (Brunner and Nurse, 2000), while *in vitro,* the N-terminal part of CLIP-170 promotes rescue (Arnal et al., 2004). CLIP-170 needs the famous +TIP End-Binding 1 (EB1, Mimori-Kiyosue et al., 2000) to track growing

microtubule plus-ends *in vitro* (Dixit et al., 2009). EB1 autonomously tracks growing microtubule plus-ends (Dixit et al., 2009) and functions as a hub for other MAPs (reviewed by Lansbergen and Akhmanova (2006). EB1 homologs regulate microtubule dynamics by increasing microtubule rescue frequency, as well as by decreasing the microtubule shrinkage rate (Morrison et al., 1998; Rogers et al., 2002; Tirnauer et al., 1999).

The third class of MAPs that regulate dynamics are proteins that disassemble microtubules, termed microtubule depolymerases. Microtubule depolymerases can remove the stabilizing GTP-cap (Kinoshita et al., 2006), which triggers microtubule catastrophe. In short, MAPs can influence microtubule growth positively and negatively. Among these MAPs that influence microtubule dynamics are molecular motors.

1.4.2.   Microtubule-based motor proteins

Before 1985, two cytoskeleton-based ATP-dependent force-generating molecular motors were known: actin-dependent myosin (Kühne, 1859; Pollard and Korn, 1973) and microtubule-dependent axonemal dynein (Gibbons and Rowe, 1965). In addition, cytoplasmic microtubules were identified to support organelle movement, which in turn was known to be ATP-dependent. Then, a novel molecular motor was identified as a protein capable of ATP-dependent microtubule plus-end directed movement of vesicles and organelles (Brady, 1985; Vale et al., 1985). This protein was named kinesin (Vale et al., 1985).

1.4.3.   The kinesin superfamily

Conventional kinesin, or kinesin-1, is the founding member of the kinesin superfamily. Conventional kinesin is a tetramer that consists of a homodimer of two kinesin-1 heavy chains (KHC) responsible for motor activity and two identical light chains (KLC) that connect the motor domain to the cargo (Marx et al., 2005). The structure of the enzymatically active domain was first determined by X-ray crystallography of truncated constructs derived from rat conventional kinesin (Kozielski et al., 1997) (Figure 1.4). By now, the motor domain structures of many kinesins from different

_____

organisms have been determined (reviewed in (Marx et al., 2005)). Kinesins are identified based on their sequence similarity to the highly conserved ATP-hydrolyzing motor head, a region of ~340 residues that consists of an ATP-binding site (Walker et al., 1982) and an adjacent microtubule-binding site (Yang et al., 1989).

Figure 1.4. The crystal structure of rat kinesin (Kozielski et al., 1997).
Ribbon structure showing the two heads of the kinesin dimer that are connected via a coiled–coil interaction of their necks.

Since the identification of conventional kinesin, more than 600 kinesin sequences have been found all throughout the eukaryotic lineage (Marx et al., 2005; Vicente and Wordeman, 2015). To classify these kinesins, a superfamily was proposed that is divided into 14 subfamilies (Dagenbach and Endow, 2004; Lawrence et al., 2004). Kinesins within the same subfamily are thought to perform more or less similar functions in the cell (Dagenbach and Endow, 2004). Kinesins exist in monomeric, dimeric and oligomeric functional units. The motor domain can be located on the N-terminus, centrally in the sequence or on the C-terminus (Vale and Fletterick, 1997). The directionality of the motor correlates with the location of the motor domain within the protein sequence.

In general, kinesins use the chemical energy of ATP to drive a conformational change; the power stroke that generates force and the production of mechanical work (Howard, 2001; Svoboda and Block, 1994; Vale and Milligan, 2000). In solution, both kinesin-1 motor heads contain tightly bound ADP. Binding of one kinesin head to the microtubule results in rapid release of ADP from this head, followed by binding of ATP and the power stroke. This power stroke brings the second motor head in close

_____

proximity to the microtubule. The now trailing head hydrolyzes ATP and releases Pi. The leading head binds to the microtubule, exchange ADP for ATP, undergoes the power stroke etcetera. In the ADP state, kinesin-1 is loosely bound to the microtubule, whereas in the apo-state or with the non-hydrolyzable ATP analog AMP-PNP, kinesin-1 is tightly bound to the microtubule (Hackney, 1994; Hancock and Howard, 1999; Friel and Howard, 2012).

Kinesin-1 walks hand-over-hand (Yildiz et al., 2004) and hydrolyzes one ATP molecule per 8 nm step (Coy et al., 1999; Schnitzer and Block, 1997). Many kinesins are processive; they take multiple steps before dissociating from the microtubule (Svoboda et al., 1993). Alternatively, some kinesins are non-processive, such as *Drosophila* kinesin-10 Nod (Cui et al., 2005), or have an unconventional ATP-hydrolysis cycle, such as *Xenopus* kinesin-13 MCAK (Friel and Howard, 2011) that targets the microtubule end by diffusion and uses ATP-hydrolysis to remove tubulin dimers (Hunter et al., 2003).

In contrast to the highly conserved kinesin motor domain, the kinesin N-termini and/or C-termini have diverged extensively during evolutionary diversification of lineages (Wickstead et al., 2010). This structural diversification reflects the wide variety of functions that kinesins have in eukaryotic cells. These functions can be broadly classified into three categories: directional cargo transport along microtubules (reviewed in (Hirokawa et al., 2009), microtubule sliding relative to each other (Fink et al., 2009; Jolly and Gelfand, 2014; Su et al., 2013), and regulation of microtubule dynamics (Drummond, 2011; Howard and Hyman, 2007; Su et al., 2012).

1.4.4.   Kinesins as regulators of microtubule dynamics

Motors of the kinesin superfamily (Dagenbach and Endow, 2004; Lawrence et al., 2004; Wickstead et al., 2010) employ diverse strategies to regulate the microtubule cytoskeleton. Kinesin-8 and kinesin-13 family members promote microtubule depolymerization through direct activity at the plus-end (kinesin-8) or at both ends (kinesin-13) (Gupta et al., 2006; Kline-Smith and Walczak, 2002; Varga et al., 2006; Walczak et al., 1996). Kinesin-8 family members can also slide microtubules relative to each other in the mitotic spindle. *In vivo* studies have shown that this microtubule sliding opposes kinesin-8's disassembly activity and leads to increased spindle length (Su et al., 2013). Other kinesins have been reported to promote microtubule

_____

growth. For example, the non-processive kinesin-10 Nod increases microtubule mass *in vitro* in an ATP-independent manner, as assayed by sedimentation (Cui et al., 2005). In addition, the processive kinesin-1, kinesin-5 and kinesin-7 were found to increase the percentage of microtubules that elongated *in vitro* assays (Sardar et al., 2010). However, the mechanisms by which these kinesins promote growth are poorly understood. Moreover, it is not known whether any of them act directly as microtubule polymerases.

1.5.1.   Kinesins in *Saccharomyces cerevisiae*

The *Saccharomyces cerevisiae* (budding yeast) genome contains 6 kinesin motor proteins: Cin8, Kip1, Kip2 and Kip3, Kar3 and Smy1. In addition to these 6 kinesins, budding yeast has one cytoplasmic dynein heavy chain: Dyn1 (Hildebrandt and Hoyt, 2000) (Figure 1.5).
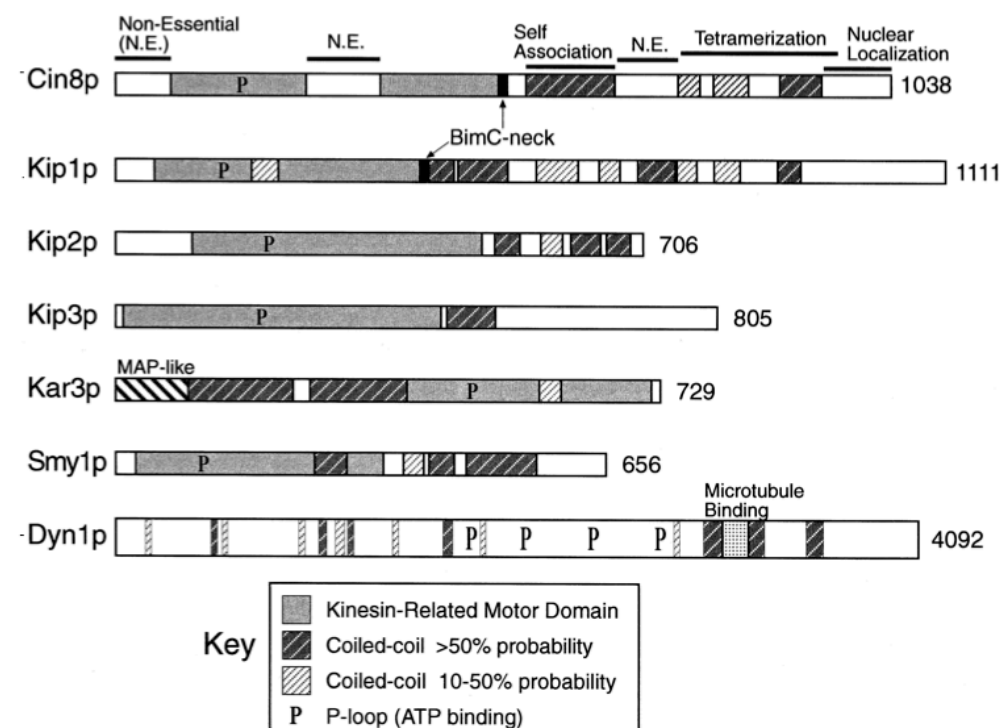
Figure 1.5. Microtubule-based molecular motors in budding yeast (Hildebrandt and Hoyt, 2000).

Primary sequences of the 7 microtubule-based molecular motors with annotated domains, drawn to scale except for dynein. The lengths in amino acids is indicated at the right of each protein.

These budding yeast motor proteins serve three cellular functions: cargo transport, attachment of microtubules to the cortex and the regulation of microtubule dynamics. Due to functional overlap, none of the 6 kinesins or dynein is uniquely required for cell viability (Hildebrandt and Hoyt, 2000). Kinesin-1 Smy1 has a motor domain sequence that is highly divergent compared to other kinesin proteins (Dagenbach and Endow, 2004) and is involved in polarized cell growth (Lillie and Brown, 1994). The other budding yeast kinesins, as well as dynein, are involved in mitotic spindle function and positioning, most of them by regulating microtubule dynamics throughout the cell cycle.

1.5.2.   Microtubules throughout the budding yeast cell cycle

Budding yeast has a closed mitosis, which means that the nuclear envelope does not break down during the cell cycle. As a result, cytoplasmic microtubules and spindle microtubules, which grow out of opposite sides of the SPB, form two different populations that are functionally separated from each other. In a summary of events, spindle microtubules assemble in the center of the mother cell body during G1 of the cell cycle. A small spindle forms with an anti-parallel microtubule mid-zone. In this mid-zone, the forces are created that push the two duplicated SPBs apart. Each of the 16 budding yeast chromosomes associates with a single microtubule from each spindle pole body. Thus, the whole spindle is comprised of only 32 kinetochore microtubules, in addition to approximately 8 interpolar microtubules. During anaphase A, these kinetochore microtubules separate the chromosomes and move them towards the poles. Next, the spindle rapidly elongates in anaphase B, followed by spindle disassembly and cytokinesis in telophase (Hildebrandt and Hoyt, 2000).

In addition to spindle microtubules, cytoplasmic microtubules also play an important role during the budding yeast cell cycle (Carminati and Stearns, 1997; Palmer et al., 1992; Sullivan and Huffaker, 1992). To ensure the proper segregation of the genomic material during the asymmetric cell division, these cytoplasmic microtubules position the nucleus in the neck between the mother cell and the bud. This process, termed nuclear migration, involves both translocation and reorientation of the spindle and starts during G1. From the SPB, dynamic microtubules grow out towards the emerging bud cortex (Byers and Goetsch, 1975), where they associate with cortical dynein (Yeh et al., 1995). This association is important for directing

_____

nuclear migration into the mother-bud neck (Eshel et al., 1993; Li et al., 1993). The nucleus then rotates to orient the SPB towards the bud (Snyder et al., 1991). At anaphase, the spindle is positioned parallel to the mother-bud axis and as the spindle elongates, one spindle pole is pulled through the neck and into the bud, while the other pole stays in the mother cell (Kahana et al., 1995; Yeh et al., 1995).

Proper regulation of cytoplasmic microtubule length is crucial for nuclear migration: when microtubule dynamics are misregulated, the spindle is mispositioned. Failure to correct nuclear migration results in anaphase nuclear division taking place in the mother cell, which in turn leads to a binucleate mother and an anucleate bud (Cottingham and Hoyt, 1997).

1.5.3.   Kinesins throughout the budding yeast cell cycle

Kinesins (and dynein) play vital roles in budding yeast mitotic spindle positioning. Cytoplasmic dynein, while anchored at the cell cortex, positions the mitotic spindle during mitosis by pulling the cytoplasmic networks towards itself (reviewed in (Moore et al., 2009)). *DYN1* deletion mutants display spindle-positioning defects (Eshel et al., 1993; Li et al., 1993).

The kinesin-5 motors Cin8 and Kip1 localize to the mitotic spindle and have redundant functions in mitotic spindle assembly (Hoyt et al., 1992); double mutants arrest in mitosis, whereas one of these proteins suffices for cell viability (Roof et al., 1992). Kip1 is a bi-directional motor that tracks and stabilizes spindle microtubule plus-ends (Fridman et al., 2013). Cin8 is also bi-directional (Roostaalhu et al., 2011) and promotes bipolar spindle assembly in cooperation with Kip3 (Su et al., 2013).

The kinesin-14 Kar3 is important for nuclear fusion during mating (Meluh and Rose, 1990). Kar3 translocates as a heterodimer with the non-motor proteins Cik1 or Vik1 to microtubule minus-ends (Mieck et al., 2015). Kar3 in combination with Vik1 cross-links parallel microtubules during mitosis (Gardner et al., 2008; Manning et al., 1999), whereas Kar3 in combination with Cik1 slides anti-parallel microtubules in mitosis (Hepperla et al., 2014).

The Kinesin-8 Kip3 is probably the best-studied budding yeast motor. It localizes to both spindle and cytoplasmic microtubules (Gupta et al., 2006) and has multiple functions: it slides anti-parallel microtubules apart in the spindle, in conjunction with Cin-8 (Su et al., 2013). In addition, Kip3 scales spindle length with

cell size in anaphase, by suppressing the polymerization of microtubules in the spindle mid-zone (Rizk et al., 2014). Kip3 is also involved in nuclear migration: Kip3 deletion strains have cytoplasmic microtubules that are longer than in wild-type, which leads to a higher percentage of binucleate cells (Cottingham and Hoyt, 1997). Finally, Kip3 is involved in the regulation of microtubule dynamics to maintain mitotic arrest in cells with mispositioned spindles (Fukuda et al., 2014).

On a molecular level, Kip3 was identified as a plus-end directed motor (Gupta et al., 2006; Varga et al., 2006) with a long run-length that disassembles microtubules in a length-dependent manner (Varga et al., 2006). Kip3 binds randomly to the microtubule lattice and walks processively to the microtubule plus-end, where it dwells until the next Kip3 molecule arrives to bump it off. Kip3 depolymerizes the microtubule plus-end by removing on average one or two tubulin dimers when it gets bumped from the microtubule. As microtubules elongate, the number of Kip3 molecules on the lattice grows proportionally: longer microtubules have a higher flux of Kip3 to their plus-end. The rate at which tubulin dimers are removed, therefore, increases proportionally to the length of the microtubule. In other words, Kip3 is a length-dependent microtubule depolymerase (Varga et al., 2009). During mitosis, the microtubule depolymerizing activity of Kip3 is antagonized by another budding yeast kinesin: Kip2 (Cottingham and Hoyt, 1997).

1.5.4.   Identification of budding yeast kinesin Kip2

The budding yeast kinesin Kip2 was identified in 1992 (Roof et al., 1992) in a PCR screen on yeast genomic DNA using degenerate primers for regions of the highly conserved kinesin motor domain. In this screen, two kinesins were found; Kip1 and Kip2 (KIP stands for kinesin related protein). Kip2 has an open reading frame of 706 amino acids on the left arm of chromosome 16. Kip2 has 38% identity to Drosophila melanogaster KHC and its conserved regions include the ATP-binding pocket consensus sequence GX4GKT (Roof et al., 1992).

Initially, Kip2 was thought to be a member of the Kinesin-7 family, based on its conserved motor domain that is closest in homology to kinesin-7 Cenp-E. However, the N-terminus and C-terminus of Kip2 have diverged significantly from all other kinesins. The 90 amino acid long N-terminus is serine rich (Roof et al., 1992) and shows no homology to other proteins. Therefore, its phylogenetic origin of Kip2 is

now considered to be untraceable: Kip2 is thought of as an 'orphan' kinesin motor (B. Wickstead, personal communication). The N-terminus is 137 amino acids long and has three heptad repeat regions, which are predicted to form an alpha-helical coiled-coil, consistent with the formation of a dimer (Roof et al., 1992).

Both Kip2 mRNA levels (Spellman et al., 1998) and Kip2 protein levels (Carvalho et al., 2004) are cell-cycle regulated and peak during mitosis, when cytoplasmic microtubules are most stable. In addition to this regulation during the budding yeast cell-cycle, Kip2 is post-translationally modified: purified Kip2 transports as a doublet by SDS-PAGE, two bands correspond to different phosphorylated forms (Roberts et al., 2014).

1.5.5.   Kip2 is involved in mitotic spindle positioning

Kip2 is expressed in vegetative yeast cells. To test the viability of these cells in the absence of Kip2, a deletion mutation was made removing residues 94 to 667. This null mutant strain did not portray phenotypes in mitosis, meiosis or karyogamy (Roof et al., 1992). Kip2 was first shown to be involved in mitotic spindle positioning by (Cottingham and Hoyt, 1997). These authors showed that *KIP2* deletion strains had elevated levels of binucleate cells, as a result of nuclear migration defects. Interestingly, deletion of *KIP2* could suppress the nuclear migration defects seen in *dyn1Δ kip3Δ* double mutants and *dyn1Δ kar3Δ* double mutants. From these results, it was hypothesized that the spindle positioning functions of Kar3 and Kip3 are antagonized by the function of Kip2 and that without Dyn1, both Kar3 and Kip3 are necessary for proper mitotic spindle positioning. Investigation of microtubule phenotypes with anti-tubulin immuno-staining revealed that *kip2Δ* cells had shorter and lower numbers of cytoplasmic microtubules than wild-type. In addition, *kip2Δ* cells had a decreased resistance to the microtubule depolymerizing drug benomyl (Cottingham and Hoyt, 1997). This loss of cytoplasmic microtubule length and numbers in kip2Δ was partially rescued in a *kip2Δ kar3Δ* double mutant (Huyett et al., 1998). These studies concluded that Kip2 is required to stabilize microtubules against depolymerization (Cottingham and Hoyt, 1997; Huyett et al., 1998). The phenotype of low cytoplasmic microtubule numbers was especially striking during telophase, suggesting that stabilization of microtubules by Kip2 occurs during this cell stage (Miller et al., 1998). In addition, (Miller et al., 1998) found that kip2Δ *kar9Δ*

double mutants were unviable, which provided evidence for two distinct pathways in yeast nuclear positioning: one pathway that requires Dyn1 and another pathway that requires Kar9. The mutant studies described above implicate that Kip2 is involved in both pathways.

1.5.6.   Kip2 transports MAPs to microtubule plus-ends

Using both fluorescence microscopy and immunofluorescence microscopy, Kip2 was shown to localize exclusively to cytoplasmic microtubules throughout the cell cycle, both in the mother cell and in the bud (Miller et al., 1998). On these cytoplasmic microtubules, Kip2 was implicated to transport cortical adaptor protein Kar9 (Kurihara et al., 1994) from the SPB to the microtubule plus-ends that contact the bud neck in G1/S phase (Maekawa et al., 2003).

More evidence for a cellular function as translocase came from a study on the Kip2 fission yeast homolog, called Tea2, which was discovered by (Verde et al., 1995). Similar to *kip2Δ, TEA2* mutants have short microtubule phenotypes (Verde et al., 1995). Tea2 co-localized with cytoplasmic microtubules in interphase and at cell tips at the end of cytoplasmic microtubules. In the absence of Tea2, the fission yeast CLIP-170 homolog Tip1 was mislocalized. Therefore, it was suggested that Tip1 travels to microtubule plus-ends as a cargo of Tea2 (Browning et al., 2000). Bieling and colleagues (2007) showed *in vitro* that Tea2 indeed transports Tip1 along microtubules and that the fission yeast EB1 homolog Mal3 is required to load the Tea2-Tip1 complex onto the microtubule lattice.

This motor-based transport of CLIP-170 seems to be conserved in fungi: in budding yeast, Kip2 was shown to processively target the budding yeast CLIP-170 homolog Bik1 to microtubule plus-ends (Figure 1.5). Bik1-3YFP was shown by live-cell imaging to localize primarily to microtubule plus-ends. In addition, Bik1-3YFP moved as speckles along cytoplasmic microtubules towards the plus-end (Figure 1.6). Co-localization studies showed that Kip2 and Bik1 co-migrate along these microtubules and that the budding yeast EB1 homolog Bim1 is not required for this transport (Carvalho et al., 2004). Once Bik1 is at the microtubule plus-end, it tracks this plus-ends autonomously through its CAP-Gly domain (Caudron et al., 2008).
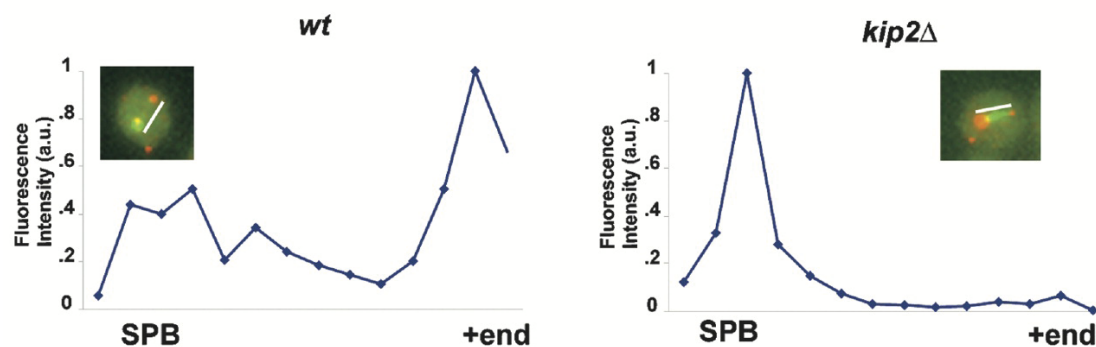
Figure 1.6. Kip2 transports Bik1 along cytoplasmic microtubules (Carvalho et al., 2004). Fluorescence intensity showing the relative distribution of Bik1-3YFP between the microtubule plus-end and the minus-end (at the SPB) in wild-type (left) and *Kip2Δ* cells (right).

In addition to Kar9 and Bik1, Kip2 transports the minus-end directed microtubule-based motor Dyn1 (Carvalho et al., 2004; Caudron et al., 2008; Roberts et al., 2014). Using an *in vitro* reconstitution approach, (Roberts et al., 2014) showed that Kip2 forms a complex with Bik1 and Bim1. This complex binds to a second complex composed of Dyn1 and Lis1. When either Bik1 or Lis1 is missing, Kip2 does not associate with Dyn1. In order to processively transport Dyn1 to the microtubule plus-end, while resisting it's minus-end directed motility, Kip2 requires both Bik1 and Bim1. This suggests that Bik1 and Bim1 function as processivity factors for Kip2 to overcome the minus-end directed forces exerted by Dyn1 (Roberts et al., 2014).

1.5.7.   Kip2 as an indirect regulator of microtubule dynamics

Kip2 affects the length of cytoplasmic microtubules. To study whether Kip2 affects microtubule dynamics, *KIP2* was over-expressed under control of the inducible GAL1 promoter. Kip2 over-expression in wild-type cells resulted in very long, stable cytoplasmic microtubules (Figure 1.7). This hyper-elongation coincided with Bik1-3YFP localizing exclusively to microtubule plus-ends. Strikingly, *KIP2* over-

_____

expression in *bik1Δ* cells did not result in the hyper-elongated microtubule phenotype. As a control, *KIP2* was over-expressed in *bim1Δ* cells. In these cells, elevated *KIP2* levels resulted in microtubule hyper-elongation (Carvalho et al., 2004). Therefore, it was suggested that Kip2 controls microtubule dynamics by targeting the +TIP Bik1 to cytoplasmic microtubule plus-ends (Carvalho et al., 2004; Caudron et al., 2008).
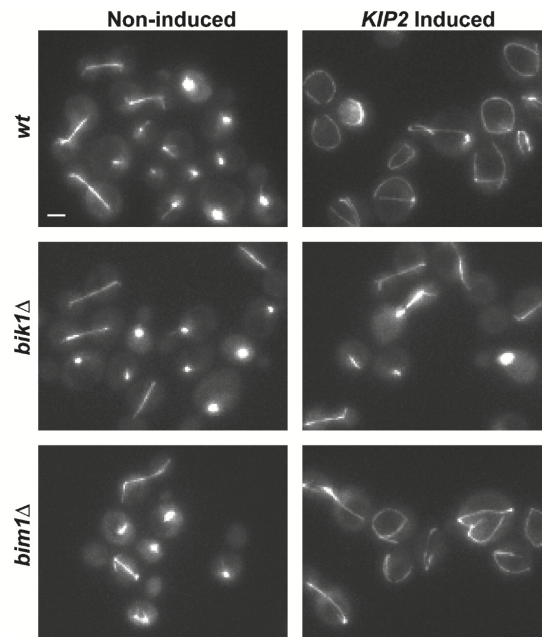
Figure 1.7 Kip2 stabilizes microtubules in the presence of Bik1 (Carvalho et al., 2004). Over-expression of Kip2 results in hyper-elongated, stable cytoplasmic microtubules in wild-type and *bim1Δ* cells but not in *bik1Δ* cells.

In summary, Kip2 has been suggested to promote microtubule growth, but only indirectly. Deletion of this kinesin results in shorter, less abundant cytoplasmic microtubules, whereas Kip2 over-expression results in hyper-elongated cytoplasmic microtubules (Carvalho et al., 2004; Caudron et al., 2008; Cottingham and Hoyt, 1997; Huyett et al., 1998; Miller et al., 1998). Kip2 translocates processively to the plus-end of these cytoplasmic microtubules, transporting a protein complex that includes the CLIP-170 homolog Bik1 and dyn1 (Carvalho et al., 2004; Caudron et al., 2008; Roberts et al., 2014). Based on these genetic studies showing that Kip2-dependent growth promotion is dependent of Bik1, it has been proposed that Kip2 indirectly promotes microtubule growth by bringing Bik1 to the microtubule plus end. However, whether Kip2 can directly promote microtubule growth is unknown.

_____

1.6.   *In vitro* reconstitution of microtubule dynamics

Genetic studies have revealed a plethora of MAPs that are involved in the regulation of microtubule length. However, these genetic 'top-down' studies often fail to elucidate underlying molecular mechanisms. An alternative approach to probing protein function is *in vitro* reconstitution (Liu and Fletcher, 2009). In this 'bottom-up' approach, purified proteins are used to reconstitute a minimal model of the process of interest. The purification of tubulin from calf and pig brain (Weisenberg et al., 1968; Weisenberg and Timasheff, 1970) started a new field of *in vitro* reconstitution of microtubules. Since the pioneering experiments by Mitchison and Kirchner that reconstituted microtubule dynamics (Mitchison and Kirschner, 1984a; 1984b), a large body of work has been performed to improve purification protocols (Gell et al., 2011; Lee and Timasheff, 1977; Widlund et al., 2012), to develop novel microscopy based assays to probe microtubule dynamics (Gell et al., 2010), and to reconstitute microtubule dynamics under physiological conditions (Kinoshita et al., 2001; Zanic et al., 2013). In addition, *in vitro* assays have been used to reconstitute microtubule plus-end tracking (Bieling et al., 2007; Braun et al., 2013; Dixit et al., 2009), to mechanistically probe microtubule dynamics (Gardner et al., 2011) and to characterize multiple MAPs that are capable of tuning microtubule dynamics (Brouhard et al., 2008b; Hunter et al., 2003; Podolski et al., 2014; Varga et al., 2006). Thus, the bottom-up approach of *in vitro* reconstitution, combined with advanced imaging techniques, allows for the elucidation of molecular mechanisms of protein interactions.

_____

2.   Aim of this study

The aim of this project was to decipher the mechanism by which budding yeast kinesin Kip2 regulates microtubule dynamics, in order to provide insight into how kinesins control microtubule length. The approach was to dissect protein-protein interactions using *in vitro* reconstitution assays, combined with Total Internal Reflection Fluorescence (TIRF) microscopy.

The key objectives of this project were:

1. **To characterize the effect of Kip2 on microtubule dynamics *in vitro.***
   This objective was addressed by reconstituting the interaction of purified Kip2 with dynamic microtubules grown with purified tubulin in TIRF and Differential Interference Contrast (DIC) microscopy experiments.

2. **To identify biophysical properties of Kip2 on microtubules *in vitro.***
   This objective was addressed by reconstituting the interaction of Kip2 single-molecules on stabilized and dynamic microtubules in single-molecule motility TIRF microscopy experiments.

3. **To reconstitute the Kip2-based microtubule plus-end tracking protein complex.**
   This objective was addressed by reconstituting the combinatorial interactions of purified Kip2, Bik1 and Bim1 with dynamic microtubules in TIRF microscopy experiments.

3.   Results

3.1.   Characterization of dynamic microtubules *in vitro*

3.1.1.   Purification of Kip2 and Kip2-eGFP

Kip2 affects the stability of cytoplasmic microtubules *in vivo* (Carvalho et al., 2004; Caudron et al., 2008; Cottingham and Hoyt, 1997; Huyett et al., 1998; Miller et al., 1998), but whether Kip2 alone affects microtubule dynamics is unknown. To test this, full-length 6xHis-Kip2 and 6xHis-Kip2-eGFP (Figure 3.1A,B) were expressed in SF+ cells using baculovirus expression and purified using affinity chromatography over His-affinity columns.
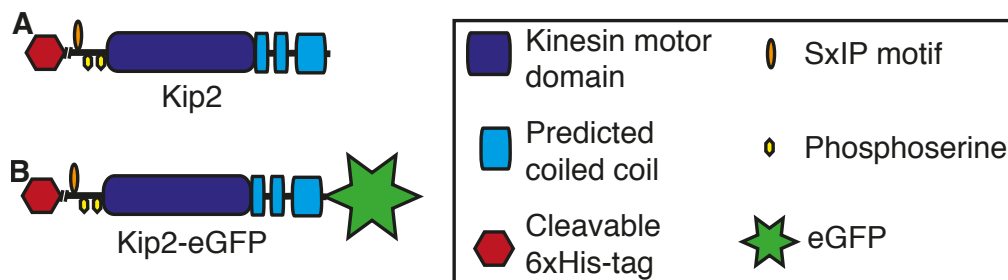
Figure 3.1. Kip2 constructs.

A). Schematic of full-length Kip2 with cleavable 6xHis-tag on the N-terminus.

B). Schematic of full-length Kip2 with cleavable 6xHis-tag on the N-terminus and eGFP on the C-terminus.

Affinity column purification success was checked by SDS-PAGE and Western blot using anti-6xHis antibody. Next, 6xHis-tags were enzymatically cleaved from the protein using PreScission protease. Finally, Kip2 and Kip2-eGFP were purified to homogeneity by gel filtration over a Sephadex 200 column, which was pre-washed with protein storage buffer (Figure 3.2, Figure 3.3). Protein stability was confirmed by SDS-PAGE and enzymatic cleavage of the 6xHis-tag from the protein of interest was confirmed by Western blot using anti-6xHis-antibody (Appendix 1). Final protein purity was checked by mass spectroscopy at the MPI-CBG in house Mass Spec facility.
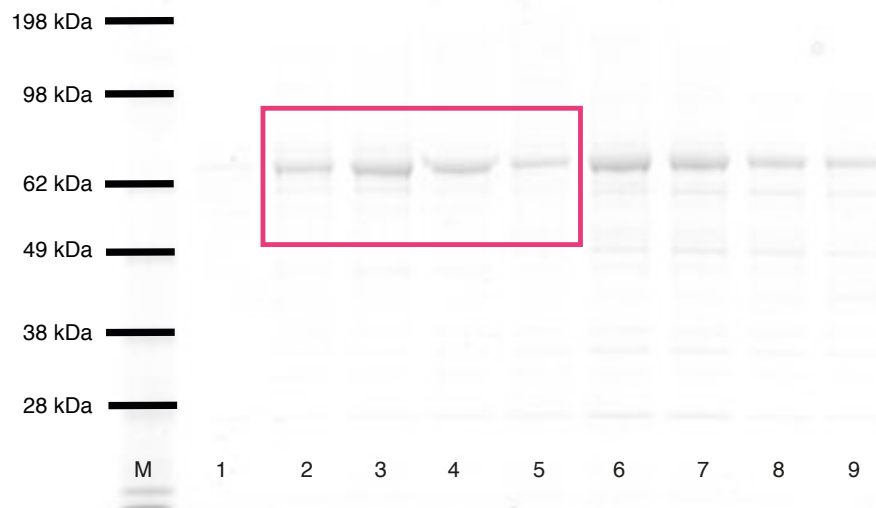
Figure 3.2. SDS-PAGE gel of gel-filtrated Kip2 fractions.

Per lane, 7 µl purified Kip2 (78 kDa) was loaded. Lane M: Seeblue Plus2 prestained protein marker, Lane 1-9: elution fractions of gel filtration. The fractions within the red box were pooled and used for *in vitro* reconstitution assay experiments. The final concentration of the pooled fractions was 4.6 µM (see Methods, Appendix 2).

Figure 3.3. SDS-PAGE gel of gel filtrated Kip2-eGFP fractions.

Per lane, 10 µl purified Kip2-eGFP (105 kDa) was loaded. Lane M: Seeblue Plus2 prestained protein marker, Lane 1-9: elution fractions of gel filtration. The fractions within the red box were pooled and used for *in vitro* reconstitution assay experiments. The final concentration of pooled fractions was 1.7 µM (see Methods, Appendix 3).

3.1.2.   *In vitro* reconstitution of microtubule dynamics

In vivo studies in yeast deletion strains suggest that Kip2 increases the length of cytoplasmic microtubules by transporting the +TIP protein Bik1 to the microtubule plus-end (Carvalho et al., 2004; Caudron et al., 2008). To determine whether Kip2 alone promotes microtubule growth *in vitro*, dynamic microtubules were grown at 12 µM free Alexa-488-labeled porcine tubulin from the ends of GMPCPP-stabilized microtubule seeds made from rhodamine-labeled porcine tubulin (Gell et al., 2010; 2011) (dynamic microtubule assay, Figure 3.4). Stabilized microtubule seeds were imaged using EPI-fluorescence, whereas dynamic microtubule extensions were imaged using TIRF microscopy at a frame rate of 0.33 Hz. The mean length of the freshly polymerized (green) microtubules was measured ten minutes after addition of Kip2 and tubulin to the surface-bound microtubule seeds.
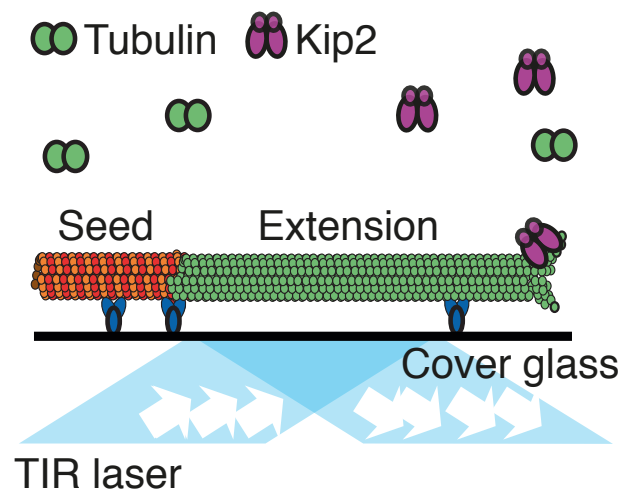
Figure 3.4. Dynamic microtubule assay.
Schematic of the experimental design. Alexa-488-labeled porcine tubulin (green) in solution polymerizes onto the ends of GMPCPP-stabilized, rhodamine-labeled microtubules (red) bound to the coverslip with anti-rhodamine antibodies (blue). The surface of the flow chamber is imaged using TIRF microscopy, which minimizes background from the fluorescent tubulin in solution.

3.1.3. Kip2 increases the length of dynamic microtubules *in vitro*

In the presence of 1 mM ATP in solution, unlabeled Kip2 induced a dramatic increase in average microtubule length (Figure 3.5A, Table 1). Average microtubule length increased from 0.99 ± 0.12 μm without Kip2 to 8.9 ± 0.64 μm at 40 nM Kip2 (Figure 3.5B, n = 56 and 26 microtubules respectively, $p < .0001$ (Welch's unpaired t-test)). All errors are standard errors of the mean unless otherwise stated. The half-maximal stimulation of growth occurred at about 5 nM Kip2. At later time-points, it became increasingly difficult to measure microtubule length at high Kip2 concentrations, as microtubules extensions frequently bent out of the TIRF field.
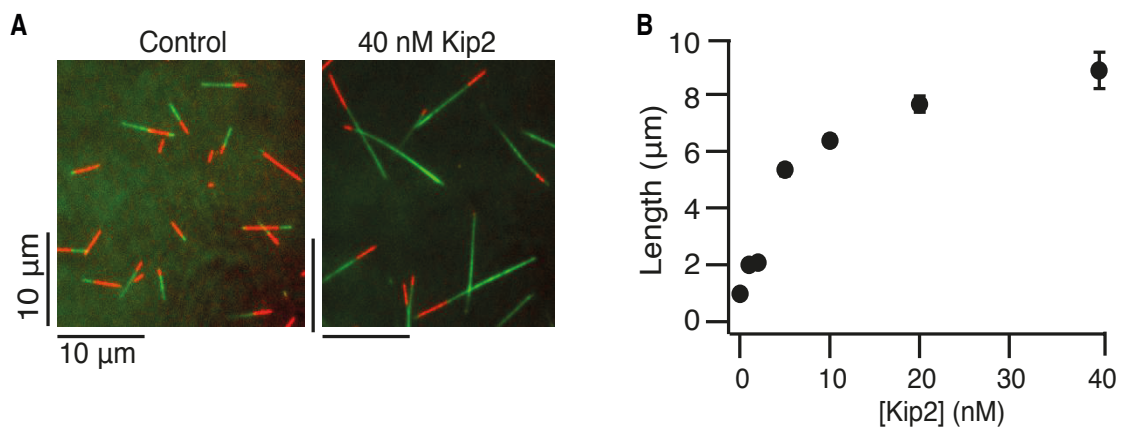
Figure 3.5. Kip2 increases the length of dynamic microtubules.

A). Microscopy images of green dynamic microtubules grown with 12 μM porcine tubulin from red stabilized seeds without (left) and with (right) of 40 nM Kip2, ten minutes after flushing tubulin and Kip2 into the flow chamber.

B). Microtubule length as a function of Kip2 concentration (mean ± SE) in 1 mM ATP, measured ten minutes after flushing 12 μM porcine tubulin and Kip2 into the flow chamber.

To validate the effect of Kip2 on microtubule length, the experiment was repeated with and without 40 nM Kip2-eGFP (Figure 3.6). Kip2-eGFP also increased the length of dynamic microtubules, from 1.6 ± 0.15 μm without Kip2-eGFP to 9.4 ± 0.40 μm at 40 nM Kip2-eGFP (n = 40 and 33 respectively, $p < .0001$ (Welch's unpaired t-test)). In summary, Kip2 increases average microtubule length *in vitro*, in the absence of accessory proteins. Both purified Kip2 and Kip2-eGFP show this microtubule length-enhancing effect. Thus, the C-terminal -eGFP tag does not impair Kip2's microtubule-length promoting function.
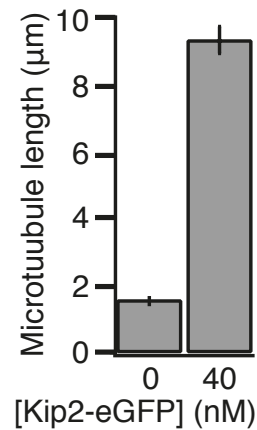
Figure 3.6. Kip2-eGFP increases the length of dynamic microtubules *in vitro*.
Microtubule length (mean ± SE) in the absence and presence of 40 nM Kip2-eGFP in 1 mM ATP, measured ten minutes after flushing 12 µM porcine tubulin and Kip2 into the flow chamber.

3.1.4. Kip2 is a microtubule polymerase with porcine tubulin

The increase in average microtubule length as a function of Kip2 concentration strongly suggests that Kip2 alters the dynamic properties of microtubules. To quantify how Kip2 influences microtubule dynamics, kymographs were created from the time-lapse images of the dynamic microtubule assay described above (Figure 3.7A). These kymographs revealed that microtubules undergo catastrophe, the switching from slow growth to rapid shrinkage, both with and without Kip2 present in the assay. Thus, dynamic instability of microtubules was successfully reconstituted *in vitro*.

Next, to characterize the effect of Kip2 on microtubule dynamics, the four parameters of dynamic instability were analyzed (see Table 2). From the kymographs of the dynamic microtubule assay, the slope of all growing microtubules was measured to calculate the average microtubule growth rate per condition (Table 3). In the presence of ATP, the microtubule growth rate increased up to 3-fold from 0.32 ± 0.02 µm/min without Kip2 to 0.94 ± 0.05 µm/min at 40 nM Kip2 (Figure 3.7B, *n* = 172 and 18 growth events respectively, *p* < .0001 (Welch's unpaired t-test)). The half-maximal stimulation in growth rate occurred at about 6 nM Kip2.

To validate that Kip2 is a microtubule polymerase, the experiment was repeated with and without 40 nM Kip2-eGFP (Figure 3.7C). In the presence of 1 mM ATP, Kip2-eGFP increased the microtubule growth rate 2.8 fold, from 0.37 ± 0.01 µm/min without Kip2-eGFP to 1.0 ± 0.06 µm/min at 40 nM Kip2-eGFP (*n* = 121 and 22

respectively, p < .0001 (Welch's unpaired t-test)). In summary, Kip2 increases the growth rate of microtubules grown with 12 µM porcine tubulin up to threefold.
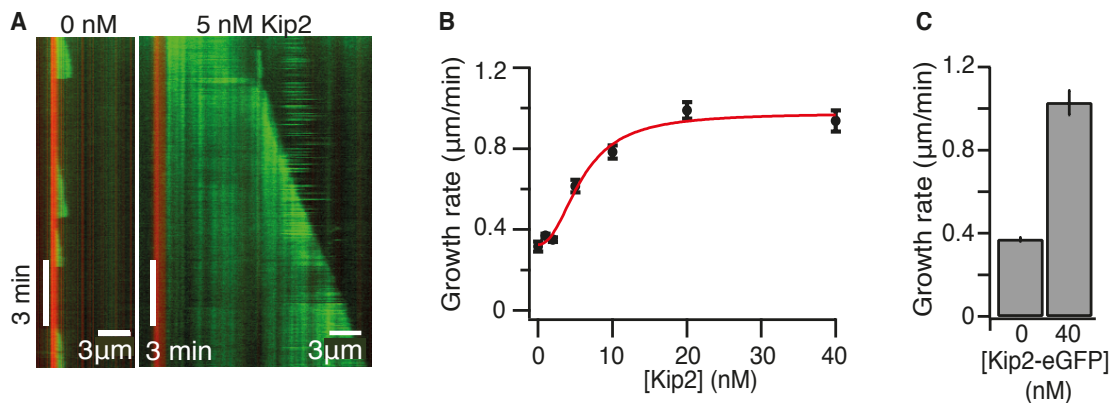
Figure 3.7. Kip2 is a microtubule polymerase of microtubules grown with porcine tubulin.

A). Kymographs showing typical microtubule growth with 12 µM porcine tubulin without (left) and with 5 nM Kip2 (right) in 1 mM ATP. Kip2 increases microtubule growth rate.

B). Microtubule growth rate as a function of Kip2 concentration at 12 µM porcine tubulin in 1 mM ATP (mean ± SE). The data was fitted (red line) using equation $f(x) = v_0 + (v_{max} - v_0) \, x^n / (x^n + x_0^n)$, where n is the Hill coefficient and x_0 is the Kip2 concentration for half-maximal stimulation. The parameter values are: $V_0 = 0.33 \pm 0.04$ µm/min, $V_{max} = 0.98 \pm 0.05$ µm/min, $n = 2.2 \pm 0.77$ and k_m is 5.9 ± 0.95 nM.

C). Bar chart of microtubule growth rate (mean ± SE) with and without 40 nM Kip2-eGFP at 12 µM porcine tubulin in 1 mM ATP.

3.1.5.   Kip2 is an anti-catastrophe factor with porcine tubulin

Figure 3.7A suggests that in the presence of Kip2, microtubules undergo catastrophe less frequently than in the absence of Kip2. To quantify the effect of Kip2 on catastrophe frequency, the total number of catastrophes observed per experimental condition was divided by the total duration of microtubule growth of all microtubules in that experimental condition (Table 4). This microtubule catastrophe frequency (K_{cat}, see Table 2) strongly decreased from 0.17 ± 0.02 per minute without Kip2 to <0.005 per minute at 40 nM Kip2 (Figure 3.8A, $n = 126$ and 1 catastrophe events respectively, p < .0001 (Welch's unpaired t-test)). The half-maximal inhibition in catastrophe occurred at about 7 nM Kip2.

To validate that Kip2 is an anti-catastrophe factor, the experiment was repeated with and without 40 nM Kip2-eGFP (Figure 3.8B). In the presence of 1 mM ATP, Kip2-eGFP also strongly decreased K_{cat} from 0.16 ± 0.02 per minute without Kip2-eGFP to <0.005 per minute at 40 nM Kip2-eGFP (n = 88 and 0 catastrophe events respectively, $p <$ .0001 (Welch's unpaired t-test)). In summary, Kip2 reduces the catastrophe frequency of microtubules grown with 12 µM porcine tubulin.
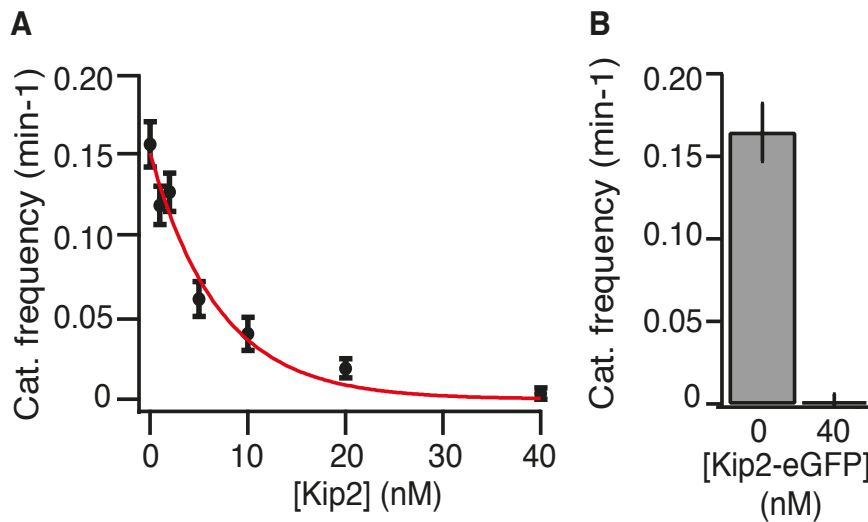
Figure 3.8. Kip2 is an anti-catastrophe factor of microtubules grown with porcine tubulin.

A). Catastrophe frequency as a function of Kip2p concentration at 12 µM porcine tubulin in 1 mM ATP (mean ± SE). The data was fitted (red line) using the equation: $f(x) = A \exp(-x / x_0)$, where the catastrophe rate is one half maximal when the Kip2 concentration is $1/x_0$. The parameter values are: A = 0.0027 ± 0.0002 and x_0 = 0.14 ± 0.02 nM.

B). Bar chart of catastrophe frequency with and without 40 nM Kip2-eGFP at 12 µM porcine tubulin in 1 mM ATP (mean ± SE).

_____

3.1.6.   Kip2 increases the rescue frequency of porcine microtubules

Next, microtubule rescue frequency (per unit distance) was calculated per Kip2 concentration as the total number of rescues observed, divided by the total distance that microtubules shrank upon catastrophe (K_{res}, see Table 2). Kip2 increased K_{res} from 0.03 ± 0.01 per µm without Kip2 to 0.19 ± 0.08 per µm at 20 nM Kip2 (Figure 3.9, Table 5, n = 7 and 6 respectively, p < .05 (Student's t-test)). At 40 nM Kip2, catastrophe events were too rare to quantify K_{res}. Thus, Kip2 increases the rescue frequency of porcine microtubules. However, at higher Kip2 concentrations, microtubule catastrophe is so rare that the effect of rescue on microtubule length is expected to become negligible.
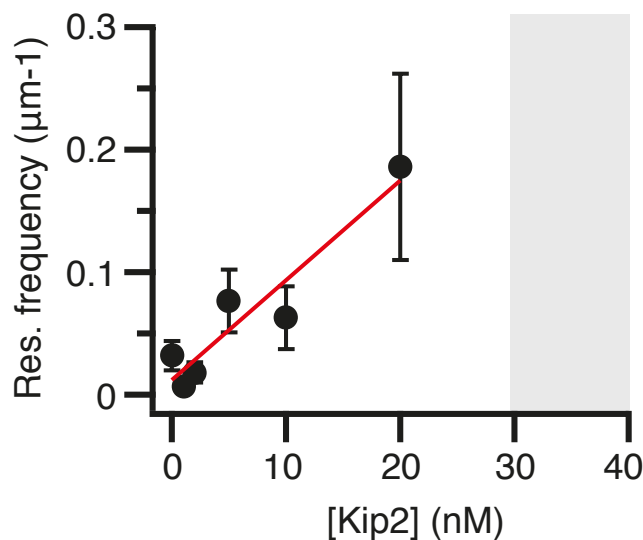
Figure 3.9. Kip2 increases the rescue frequency of microtubules grown with porcine tubulin.

Rescue frequency as a function of Kip2 concentration (mean ± SE, see Table 2) of microtubules grown with 12 µM porcine tubulin and 1 mM ATP. The slope of the linear regression through the data is significantly different from zero (Y = 0.008*X + 0.012, p < .05 (Student's t-test)).The grey box indicates the Kip2 concentration regime in which microtubule catastrophe is very rare and rescue frequency was not quantified.

3.1.7.   Kip2 does not affect porcine microtubule shrinkage rate

Finally, microtubule shrinkage rate was quantified from the slope of microtubules that experienced catastrophe, for all microtubules per experimental condition. Kip2 did not affect microtubule shrinkage rate between 0 - 10 nM Kip2 (Figure 3.10, Table 6). Above 10 nM Kip2, catastrophe events were too rare to reliably quantify microtubule shrinkage velocity. In summary, microtubule shrink at a rate of ~30 µm/min, regardless of whether Kip2 is present in the assay.
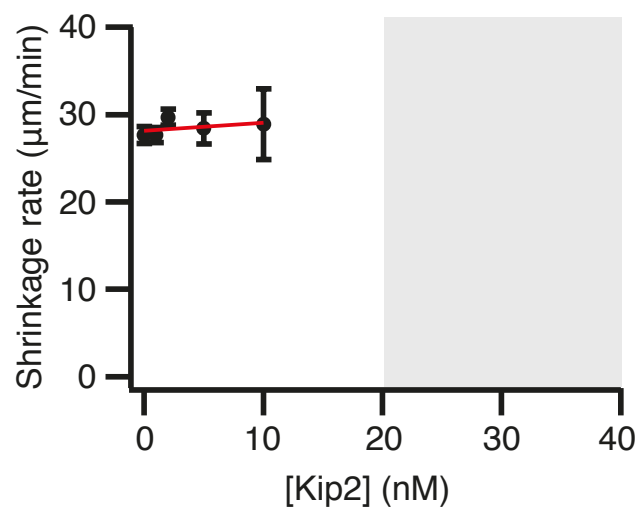
Figure 3.10. Kip2 does not affect the shrinkage rate of microtubules grown with porcine tubulin.

Average microtubule shrinkage rate as a function of Kip2 concentration (mean ± SE, see Table 2) of microtubules grown with 12 µM porcine tubulin and 1 mM ATP. The slope of the linear regression through the data does not differ from zero (Y = 0.09*X + 28.1, *p* = .48 (Student's t-test)). The grey box indicates the Kip2 concentration regime in which microtubule catastrophe is very rare and microtubule shrinkage rate was not quantified.

3.1.8.   Measured growth rates and catastrophe frequencies account for the measured increase in length

Quantifications of the four parameters of microtubule dynamics as a function of Kip2 concentration revealed that Kip2 increases microtubule growth rate and decreases catastrophe frequency. To validate that these effects on microtubule dynamics account for the measured increase in microtubule length, the theoretical microtubule length at t = 10 minutes after flushing in 12 µM free tubulin and Kip2 was calculated for every Kip2 concentration (see Table 7) as :

Theoretical length = (10 minutes - microtubule lifetime) * growth rate.

The measured rescue frequencies were not used in the calculations, because due to their low frequency, rescues should only have a minor effect on average microtubule length. Figure 3.11 shows both the theoretical and the measured average microtubule lengths at t = 10 minutes per Kip2 concentration.
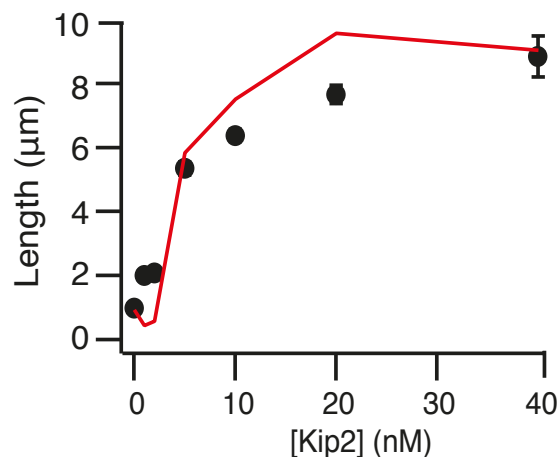
Figure 3.11. Theoretical versus measured microtubule length.
Microtubule length as a function of Kip2 concentration in 1 mM ATP. The black markers depict the measured microtubule lengths (mean ± SE). The red line through the data depicts the theoretical microtubule lengths based on the measured growth rates and catastrophe frequencies per Kip2 concentration (Table 1, 7).

The theoretical curve (red) approximates the measured average microtubule lengths. In conclusions, Kip2 increases the average microtubule length of microtubules grown with porcine tubulin by increasing microtubule growth rate while reducing the catastrophe frequency.

3.1.9.   Kip2 is a microtubule polymerase with yeast tubulin

The effects of Kip2 on microtubules discussed so far were obtained with tubulin purified from pig brains (Gell et al., 2011). However, tubulins from different sources differ with respect to sequence and post-translational modifications (Janke and Chloë Bulinski, 2011; Schatz et al., 1986). This raises the possibility that the measured effects of Kip2 on porcine microtubule dynamics may be specific to brain tubulin and not to budding yeast tubulin, which is the relevant substrate for Kip2. In addition, tubulin labeling could affect the properties of the tubulin dimers and/or affect the interaction of Kip2 with microtubules. To exclude these possible confounding effects, the dynamic microtubule assay experiments and analyses were repeated using 4 µM conspecific, unlabeled budding yeast tubulin (Podolski et al., 2014; Widlund et al., 2012) and DIC microscopy (Figure 3.12, Table 8).
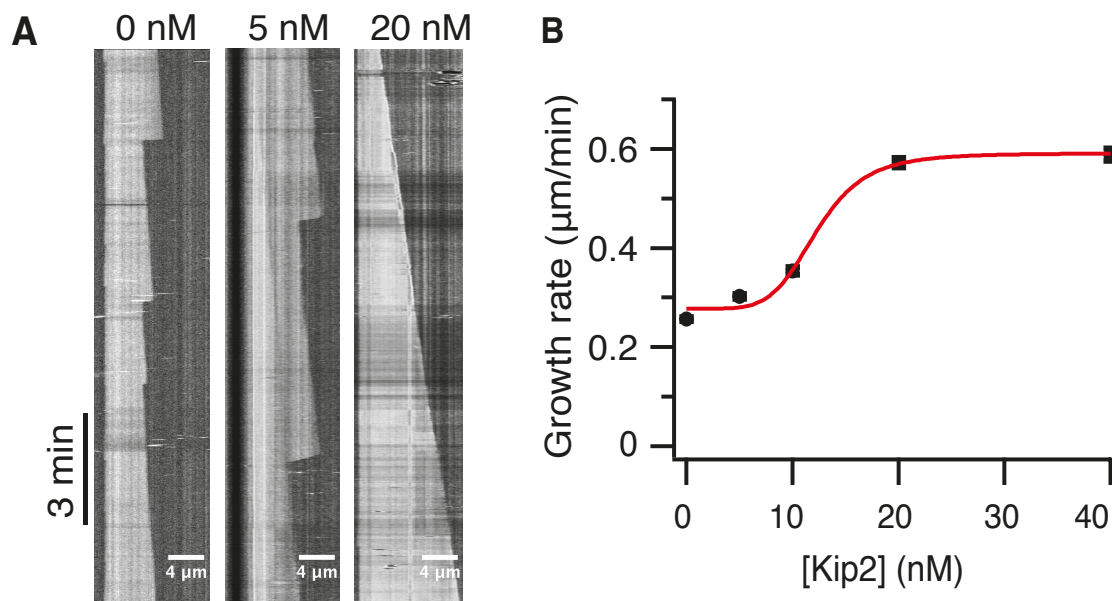
Figure 3.12. Kip2 is a microtubule polymerase with yeast tubulin.

A). Kymographs from DIC microscopy showing typical microtubule growth with 4 µM unlabeled yeast tubulin in the absence (left) and presence of Kip2 (5 nM, center, 20 nM, right) in 1 mM ATP.

B). Microtubule growth rate (mean ± SE) as a function of Kip2 concentration of microtubules grown with 4 µM yeast tubulin in 1 mM ATP. The data was fitted (red line) as in Figure 3.7B. The parameter values are: $V_0 = 0.28 \pm 0.02$ µm/min, $V_{max} = 0.59 \pm 0.03$ µm/min, $n = 5.4 \pm 3.2$ and k_m is 12.3 ± 1.9 nM.

28

In accordance with the results obtained with porcine tubulin, Kip2 increased the growth rate of yeast microtubules 2.3-fold, from 0.26 ± 0.004 µm/min without Kip2 to 0.59 ± 0.01 µm/min at 40 nM Kip2 (Figure 3.12B, n = 300 and 48 growth events respectively, $p < .0001$ (Welch's unpaired t-test)). The half-maximal effects were seen at about 12 nM Kip2 (Figure 3.12B). The measured increase in microtubule growth rate was slightly less for yeast (2.3-fold) than for porcine tubulin (2.8-fold for Kip2 and 2.9-fold for Kip2-eGFP). Nonetheless, the results on yeast microtubule growth rates show that Kip2 is a microtubule polymerase of both porcine and yeast tubulin.

3.1.10.   Kip2 is an anti-catastrophe factor with yeast tubulin

Analysis of K_{cat} of yeast microtubules as a function of Kip2 concentration revealed that Kip2 is also an anti-catastrophe factor of yeast microtubules (Figure 3.13, Table 9). K_{cat} decreased very strongly from 0.23 ± 0.02 per minute without Kip2 to 0.009 ± 0.004 per minute at 40 nM Kip2 (n = 192 and 5 catastrophe events respectively, $p < .0001$ (Welch's unpaired t-test)). The half-maximal effects were seen at about 10 nM Kip2. In summary, Kip2 has similar effects on yeast as on porcine tubulin, confirming that Kip2 is a microtubule polymerase and an anti-catastrophe factor. The effects of Kip2 on yeast microtubule rescue frequencies and shrinkage rates were not quantified.
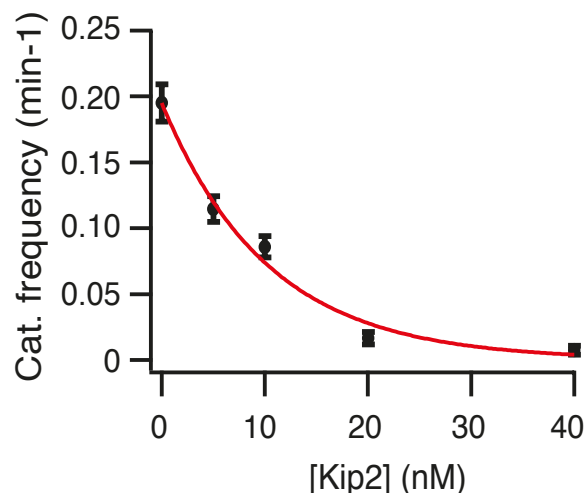
Figure 3.13. Kip2 is an anti-catastrophe factor of yeast microtubules.
Catastrophe frequency (mean ± SE) as a function of Kip2 concentration of microtubules grown with 4 µM yeast tubulin in 1 mM ATP (see Table 2). The data was fitted (red line) as in Figure 3.8A. The parameter values are: A = 0.0039 ± 0.0002 and x_0 = 0.10 ± 0.01 nM.

3.1.11.   Kip2 increases the tubulin association rate constant

Kip2 alters microtubule dynamics, which strongly suggests that Kip2 affects microtubule assembly kinetics. To investigate whether Kip2 affects the tubulin on-rate and/or off-rate, the average porcine microtubule growth rate was measured as a function of tubulin concentration. As expected from experimental (Walker et al., 1988) and theoretical (Bowne-Anderson et al., 2013) studies, the rate of microtubule elongation increased linearly with the tubulin concentration, both in the presence and absence of Kip2 (Figure 3.14).

   Without Kip2 in solution, no microtubule growth was observed below 8 µM at 28°C and only 2 growth events were observed at 8 µM. Therefore, the red 8 µM data point is omitted from the graph. By contrast, with Kip2 in solution, microtubules grew at tubulin concentrations as low as 4 µM, indicating that Kip2 facilitates microtubule nucleation off GMPCPP-stabilized seeds.
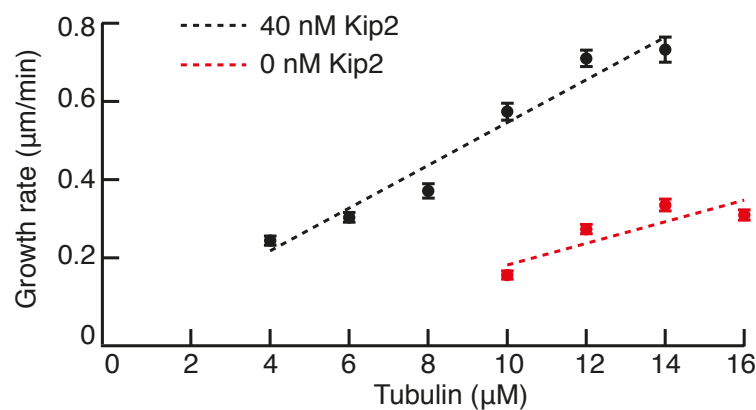
Figure 3.14. Kip2 increases the tubulin on-rate constant
Microtubule growth rate as a function of tubulin concentration (mean ± SE). The red data depict microtubule growth rates in the absence of Kip2. The black data depict microtubule growth rates with 40 nM Kip2 in solution. The dotted lines are the linear fits through the data sets, weighted by the SE. The tubulin association rate constants are given by the slopes of the fit lines. The dissociation rate constants are given by the y-intercepts of the fit lines.

Microtubule growth rate is given by the equation:

$$\text{Growth rate} = k_{on}\,[T] - k_{off} \qquad\qquad (1)$$

The tubulin association rate constant (k_{on}) was calculated from the slope of the linear regression lines through the data sets. Kip2 increased the on-rate from 0.70 ± 0.30 $\mu M^{-1} \cdot s^{-1}$ to 1.47 ± 0.16 $\mu M^{-1} \cdot s^{-1}$ (assuming 1604 tubulin dimers per μm, $p < .005$ (Student's t-test)). Thus, Kip2 increases microtubule growth rate by increasing the on-rate of tubulin. The *y*-intercept of the linear regression lines through the data sets did not differ significantly from zero, both with and without Kip2. Therefore, this experiment did not allow to resolve any putative effect of Kip2 on the GTP-tubulin off-rate constant.

3.1.12.   Kip2 lowers the GTP-tubulin off-rate constant

To test whether Kip2 influences the GTP-tubulin dissociation rate, the microtubule shrinkage rate was measured of GMPCPP-stabilized or taxol-stabilized microtubules, incubated with or without 40 nM Kip2 (in the absence of free tubulin). The rationale behind this experiment was that the spontaneous depolymerization of GMPCPP-stabilized microtubules mimics the GTP-tubulin off-rate of growing microtubules. In the presence of ATP, Kip2 decreased the shrinkage rate of GMPCPP-stabilized microtubules 3-fold, from 0.015 ± 0.002 $\mu m/min$ without Kip2 to 0.005 ± 0.001 $\mu m/min$ at 40 nM Kip2 (Figure 3.15, $n = 29$ and 31 microtubules respectively, $p < .0005$ (Welch's unpaired t-test)).
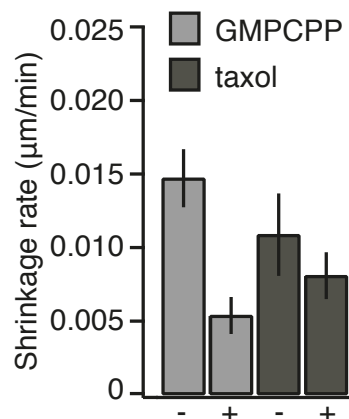
Figure 3.15. Kip2 lowers the tubulin off-rate constant for GMPCPP-stabilized microtubules.
Microtubule shrinkage rates of GMPCPP-stabilized (light grey) or taxol-stabilized (dark grey) microtubules in the absence of free tubulin (mean $\pm$ SE) in 1 mM ATP. Shrinkage rates were measured in the absence (-) and in the presence (+) of 40 nM Kip2. Kip2 lowers the shrinkage rate of GMPCPP-stabilized microtubules in ATP.

Thus, assuming that GMPCPP-tubulin is a good analog for GTP-tubulin, this result suggests that Kip2 decreases the GTP-tubulin dissociation rate up to 3-fold in the absence of free tubulin. Kip2 did not decrease the GDP-tubulin dissociation rate of taxol-stabilized microtubules in ATP (0.011 ± 0.003 µm/min without Kip2 (n = 19) compared to 0.008 ± 0.002 µm/min at 40 nM Kip2 (n = 28, p = .39 (Welch's unpaired t-test)).

3.1.13.   Kip2 requires ATP-hydrolysis to increase the tubulin association rate

Kip2 increases the tubulin association rate and decreases the tubulin dissociation rate in the presence of ATP. To test whether these effects on tubulin association and dissociation require ATP-hydrolysis, dynamic microtubules were grown with or without 40 nM unlabeled Kip2 in the presence of the slowly hydrolyzable ATP analog AMP-PNP. In AMP-PNP, Kip2 had only a minimal positive effect on average microtubule length (Figure 3.16, red circles). In the presence of Kip2, microtubule growth rate remained low (0.41 ± 0.01 µm/min in AMP-PNP compared to 0.94 ± 0.05 µm/min in ATP) and catastrophe frequency remained high (0.11 ± 0.01 per minute in AMP-PNP compared to <0.005 per minute in ATP). Thus, Kip2 did not increase the tubulin association rate in AMP-PNP (unlike in the presence of ATP).
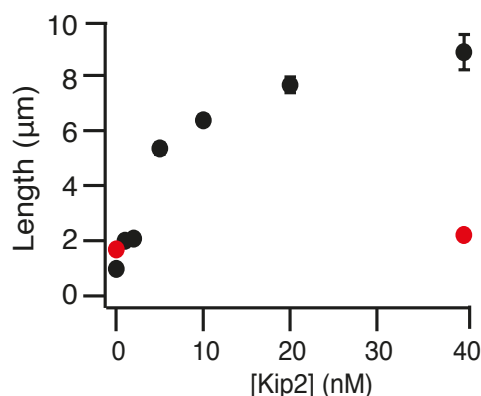
Figure 3.16. Kip2 increases the tubulin association rate in an ATP-dependent manner. Microtubule length as a function of Kip2 concentration (mean ± SE, error bars fall within the symbols) in 1 mM ATP (black markers) or 1 mM AMP-PNP (red markers), measured ten minutes after flushing 12 µM porcine tubulin and Kip2 into the flow chamber. In the presence of the non-hydrolyzable ATP analog AMP-PNP, microtubule length does not increase as a function of Kip2 concentration.

3.1.14.   Kip2 does not require ATP-hydrolysis to lower the GTP-tubulin dissociation rate

To test whether Kip2 requires ATP-hydrolysis to lower the tubulin dissociation rate, the microtubule shrinkage experiments were repeated with 1 mM AMP-PNP, as well as 1 mM ADP, instead of ATP (Figure 3.17). In AMP-PNP, Kip2 did not decrease the GTP-tubulin dissociation rate of GMPCPP-stabilized microtubules (0.015 ± 0.004 µm/min without Kip2 ($n = 56$) compared to 0.008 ± 0.002 µm/min at 40 nM Kip2 ($n = 39$), $p = 0.08$ (Welch's unpaired t-test)). However, Kip2 did reduce the shrinkage rate of taxol-stabilized microtubules from 0.020 ± 0.003 µm/min to 0.006 ± 0.001 µm/min ($n = 31$ and 24 respectively, $p < .0001$ (Welch's unpaired t-test)). In ADP, Kip2 decreased the GTP-tubulin dissociation rate of GMPCPP-stabilized microtubules (0.025 ± 0.002 µm/min without Kip2 ($n = 58$) compared to 0.009 ± 0.001 µm/min at 40 nM Kip2 ($n = 47$), $p < .0001$ (Welch's unpaired t-test)). Kip2 also reduced the shrinkage rate of taxol-stabilized microtubules from 0.008 ± 0.001 µm/min to 0.0026 ± 0.0005 µm/min ($n = 57$ and 66 respectively, $p < .0001$ (Welch's unpaired t-test)). Thus, Kip2 does not require ATP-hydrolysis to decrease the GTP-tubulin dissociation rate.
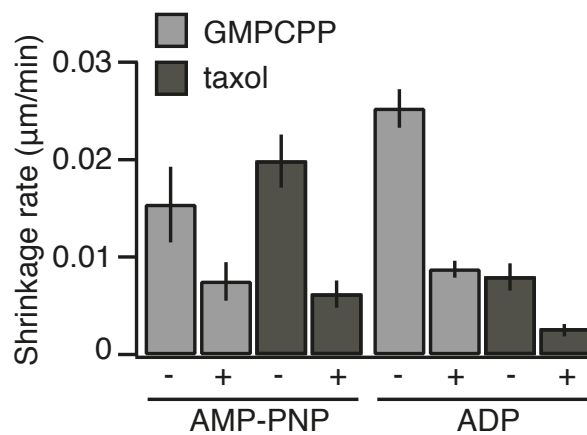
Figure 3.17. Kip2 does not strictly require at ATP-hydrolysis to lower the tubulin dissociation rate.

Microtubule shrinkage rates of GMPCPP-stabilized (light grey) or taxol-stabilized (dark grey) microtubules in the absence of free tubulin (mean ± SE) in 1 mM AMP-PNP or 1 mM ADP. Shrinkage rates were measured in the absence (-) and in the presence (+) of 40 nM Kip2. Kip2 lowers the shrinkage rate of taxol-stabilized microtubules in AMP-PNP, as well as of GMPCPP-stabilized and taxol-stabilized microtubules in ADP.

3.15.   Kip2 increases microtubule growth rate in a length-dependent manner

Kip2 regulates microtubule dynamics, reminiscent of microtubule depolymerizing kinesin-8 Kip3 that disassembles microtubules in a length-dependent manner (Varga et al., 2006). Therefore, it was hypothesized that microtubule growth promotion by Kip2 may also be length-dependent. To test this, microtubule growth rate was analyzed as a function of total microtubule length (the seed plus the dynamic extension). In the absence of Kip2, microtubules grown with 12 µM porcine tubulin grew at a constant rate independent of their length (Figure 3.18, black triangles, $n = 165$, $p = .06$ (Student's t-test)). By contrast, at low (1-2 nM, purple circles) and intermediate (5-10 nM, blue squares) Kip2 concentrations, long microtubules grew faster than short microtubules ($n = 325$ and 103 respectively, $p < .0001$ (Student's t-test)). At 1-2 nM Kip2, the slope of the curve was less steep than at 5-10 nM Kip2 ($n = 325$ and 103, $p < .05$ (Welch's unpaired t-test)). Finally, at high Kip2 concentrations (20-40 nM), the measured microtubules grew at a constant rate independent of their length (green diamonds, $n = 62$, $p = .36$ (Student's t-test)). Analysis of yeast microtubule growth rates as a function of microtubule length yielded similar results (Figure 18B). Thus, Kip2 is a length-dependent microtubule polymerase: at low and intermediate Kip2 concentrations, microtubules grow increasingly faster as the microtubule becomes longer. At high Kip2 concentrations, microtubule growth rate saturates almost immediately upon the start of microtubule growth, presumably because the microtubule plus-end is saturated with Kip2. At these high Kip2 concentrations, microtubules rarely experience catastrophe. Therefore, it was impossible to resolve the length-dependent acceleration of microtubule growth rates at high Kip2 concentrations in this experiment.
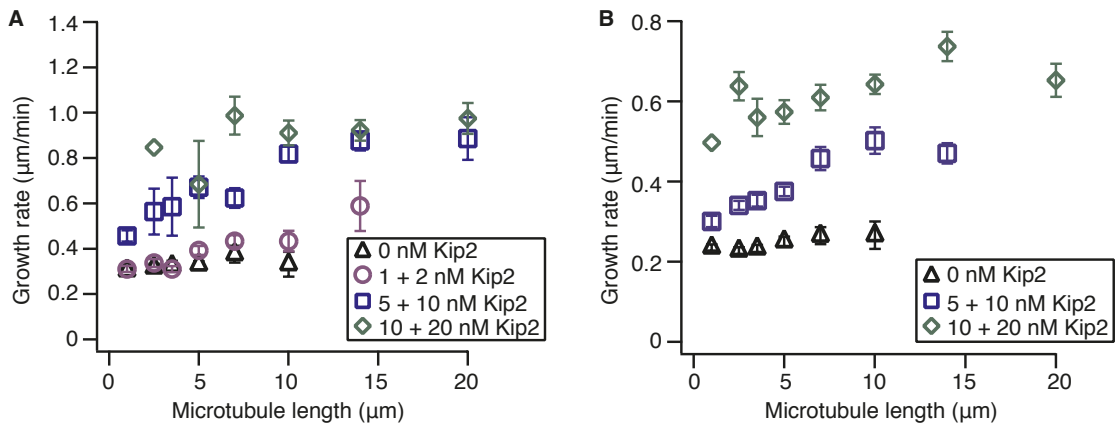
Figure 3.18. Kip2 increases microtubule growth rate in a length-dependent manner.

A). Microtubule growth rates (mean ± SE) as a function of length of microtubules grown with 12 µM porcine tubulin. The data in the plot was binned for 1-2 nM Kip2 (purple circles), 5-10 nM Kip2 (blue squares) and 20-40 nM Kip2 (green diamonds). The measured microtubule lengths were binned for 0-2 µm, 2-3 µm, 3-4 µm, 4-6 µm, 6-8 µm, 8-12 µm, 12-16 µm and 16-24 µm.

B). Microtubule growth rates (mean ± SE) as a function of length of microtubules grown with 4 µM yeast tubulin. The data in the plot was binned for 5-10 nM Kip2 (blue squares) and 20-40 nM Kip2 (green diamonds). The measured microtubule lengths were binned for 0-2 µm, 2-3 µm, 3-4 µm, 4-6 µm, 6-8 µm, 8-12 µm, 12-16 µm and 16-24 µm.

3.1.16.   Kip2 prevents catastrophe in a length-dependent manner

To test whether Kip2 also prevents catastrophe in a length-dependent manner, the average microtubule length was measured at the moment of catastrophe for microtubules grown with 12 µM porcine tubulin. Next, these microtubules were binned in two categories: short (< 4 µm) or long (> 4 µm). The total distance that microtubules grew in each bin (4 µm minus seed length, and/or final length minus 4 µm) was divided by the number of catastrophes that occurred in that bin (Figure 3.19A). In the absence of Kip2, the likelihood of catastrophe increased with microtubule length, which resulted in a reduced average length at catastrophe for long ('old') microtubules compared to short ('young') microtubules ($n = 34$ and 86

catastrophes respectively, *p* < .05 (Welch's unpaired t-test)). This length-dependent increase in catastrophe in the absence of MAPs is expected as a result of microtubule ageing (Gardner et al., 2011).
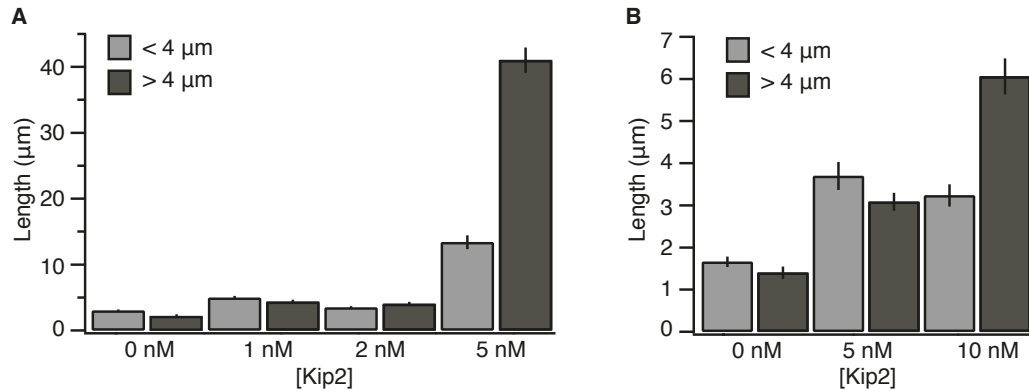
Figure 3.19. Kip2 prevents catastrophe in a length-dependent manner.

A). Bar graph showing microtubule length (mean ± SE) at the moment of catastrophe for microtubules grown at 12 µM porcine tubulin in the presence of 0, 1, 2 and 5 nM Kip2. Bars depict microtubules that reached a total length of less than 4 µm (light grey) or more than 4 µm (dark grey).

B). Bar graph showing microtubule length (mean ± SE) at the moment of catastrophe for microtubules grown at 4 µM yeast tubulin in the presence of 0, 5 and 10 nM Kip2.

By contrast, at 5 nM Kip2, long microtubules showed an increased average length at catastrophe compared to short microtubules (*n* = 11 and 12 respectively, *p* < .0001 (Welch's unpaired t-test)). Thus, in the presence of 5 nM Kip2, long microtubules are less likely to undergo catastrophe than short microtubules. These measurements were repeated on microtubules grown from 4 µM yeast tubulin. Yeast microtubules experienced a length-dependent prevention of catastrophe at 10 nM Kip2 (Figure 3.19B, *n* = 33 and 47 respectively, *p* < .0001 (Welch's unpaired t-test)).

Thus, whereas catastrophe frequency increases as a function of microtubule length in the absence of MAPs, Kip2 decreases the catastrophe frequency as a function of microtubule length. In summary, both the increase in microtubule growth rate and the prevention of catastrophe by Kip2 are length-dependent processes.

3.2.   Biophysical properties of Kip2 *in vitro*

3.2.1.   A single-molecule motility assay to study biophysical properties of Kip2-eGFP

Kip2 has a highly conserved kinesin motor domain (Dagenbach and Endow, 2004; Roof et al., 1992; Wickstead et al., 2010) and was shown *in vivo* to processively translocate along microtubules and to localize at the microtubule plus-end (Carvalho et al., 2004). In addition, Kip2 affects microtubule plus-end dynamics *in vitro* (Chapter 3.1). Together, these data predict that Kip2 localizes to microtubule plus-ends in the dynamic microtubule assay. To investigate how Kip2 could affect microtubule plus-end dynamics, its biophysical properties were measured in single-molecule motility assays (Figure 3.20). To ensure single-molecule Kip2 concentrations, typically less than 1nM Kip2-eGFP was added to red surface-bound GMPCPP-stabilized or taxol-stabilized microtubules, without free tubulin in solution. Stabilized microtubules were imaged using EPI-fluorescence, whereas single Kip2-eGFP molecules were imaged using TIRF microscopy at a frame rate of 0.5 Hz, or by continuous streaming at ~10 Hz.
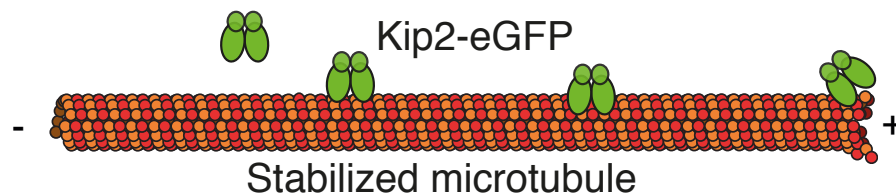
Figure 3.20. Single-molecule motility assay.
Schematic of the experimental design.

3.2.2.   Kip2-eGFP is a slow, processive motor in ATP

To study the behavior of Kip2 on stabilized microtubules, kymographs were created from the single-molecule motility assays. Individual Kip2-eGFP traces revealed that in 1 mM ATP, single Kip2-eGFP molecules associated with GMPCPP-stabilized microtubule lattices and walked processively (Figure 3.21A) towards the microtubule plus-end (see Figure 3.29C for proof of plus-end directionality) at a velocity of 5.0 ± 0.9 µm/min at 28° C (mean ± SD, *n* = 674). Kip2-eGFP walked at the same velocity

_____

on taxol-stabilized microtubules (4.9 ± 1.1 μm/min, *n* = 525,   *p* = .25 (Welch's unpaired t-test)). Thus, Kip2 processively translocates at 5 μm/min irrespective of the nucleotide state of the microtubule lattice (assuming that taxol-stabilized microtubules are in a GDP-state). By contrast, in the non-hydrolyzable ATP analog AMP-PNP, Kip2 tightly bound to the microtubule lattice and did not translocate (Figure 3.21B).
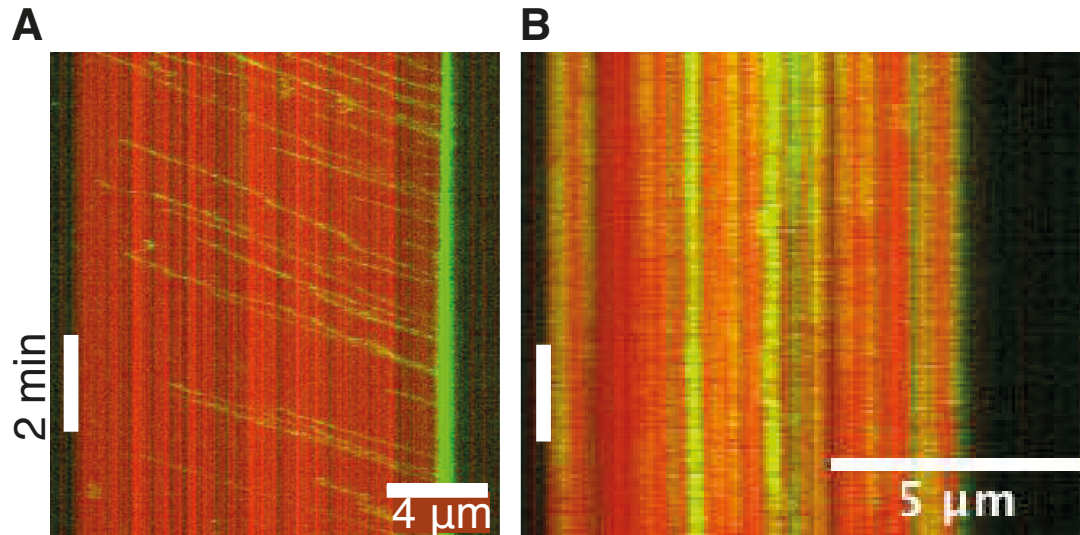
Figure 3.21. Kip2-eGFP processively translocates along GMPCPP-stabilized microtubules in ATP but not in AMP-PNP.

A). Kymograph of 0.1 nM Kip2-eGFP in 1mM ATP, showing processive motility of single-molecules towards and accumulation at the GMPCPP-stabilized microtubule plus-end.

B). Kymograph of 0.1 nM single Kip2-eGFP molecules tightly bound to the GMPCPP-stabilized microtubule lattice in 1 mM AMP-PNP.

The Kip2-eGFP velocities in ATP on both GMPCPP- and taxol-stabilized microtubules were not normally distributed (statistical value = 0.99 and 0.98 respectively, cut-off value = 0.05 and 0.06 respectively, *p* < .05 (One-sample Kolmogorov-Smirnov test)).

In summary, Kip2 is a processive kinesin that uses its ATP-hydrolyzing motor domain to translocate at a velocity of 5 μm/min, which is one order of magnitude slower than the canonical vesicle transporting kinesin-1 (Svoboda and Block, 1994).

_____
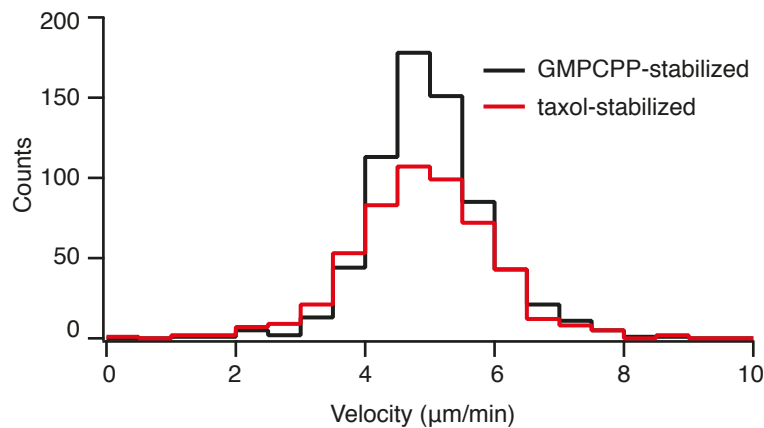
Figure 3.22. Distribution of Kip2-eGFP velocities

Histogram showing velocities of single Kip2-eGFP molecules along GMPCPP-stabilized (black) or taxol-stabilized (red) microtubules in 1 mM ATP.

3.2.3.   Kip2-eGFP is a highly processive motor

In addition to the velocity of Kip2-eGFP, the run-length of single Kip2-eGFP molecules was assessed from the single-molecule motility assay experiments described in §3.2.1. To measure run-length, Kip2-eGFP traces along stabilized microtubules were imaged using TIRF microscopy by continuous streaming at ~10 Hz (Figure 3.23). Run-length was quantified as the sum of all distances translocated by Kip2-eGFP molecules, divided by the total number of dissociations from the lattice (before reaching the microtubule plus-end). The Kip2-eGFP traces revealed that on GMPCPP-stabilized microtubules, Kip2-eGFP had a run-length of 4.1 ± 0.2 µm (Figure 3.24, mean ± SE, n = 117). The run-length of Kip2-eGFP on taxol-stabilized microtubules was 7.0 ± 0.5 µm/min (n = 91, $p <$ .0001 (Welch's unpaired t-test)). Others have also observed shorter run-lengths of kinesin on GMPCPP-stabilized microtubules compared to taxol-stabilized microtubules that are presumably composed of GDP-tubulin (McVicker et al., 2011). For the remainder of this thesis, only the measured Kip2-eGFP run-length of 4.1 ± 0.2 µm on GMPCPP-stabilized microtubules will be considered, because the dynamic microtubule assays in Chapter 3.1 were performed with GMPCPP-stabilized microtubules.

Of note, it is unclear whether the Kip2-eGFP traces in the kymographs terminated due to dissociation of Kip2-eGFP from the microtubule, or due to bleaching of the eGFP fluorophore. Therefore, the measured average length of 4.1 µm on GMPCPP-stabilized microtubules potentially underestimates the true run-length.

_____
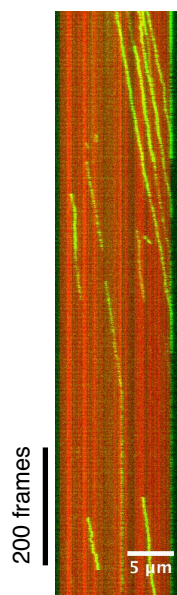
Figure 3.23. Kip2-eGFP is a highly processive motor.

Kymograph showing traces of single Kip2-eGFP molecules on a GMPCPP-stabilized microtubule.
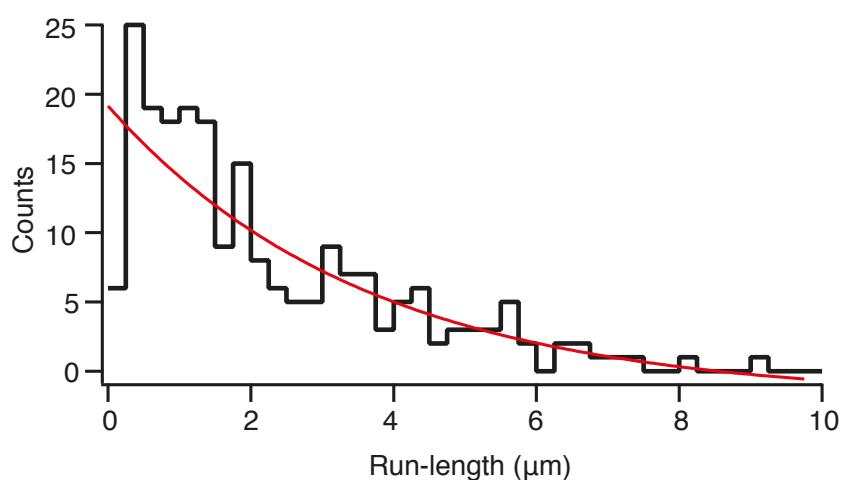
Figure 3.24. Distribution of run-lengths on GMPCPP-stabilized microtubules.

Histogram composed of 40 bins with a bin width of 0.25 µm, showing the distribution of Kip2-eGFP run-lengths on GMPCPP-stabilized microtubules. The run-length of Kip2 is predicted to be exponentially distributed, as dissociation from the microtubule lattice is expected to be a random process. The distribution does not follow a simple exponential (red line, $f(x) = A \exp(-x/x_0)$), where A = 21.1 and x_0 = 0.28); run-lengths between 0 and 0.5 µm are under-represented. This is likely due to the short duration of these run-lengths. A run-length of 0.5 µm would take 6 s (Kip2-eGFP translocates at a velocity of 5 µm/min), which is 60 pixels at a frame-rate of ~10 Hz.

_____

3.2.4.   Kip2-eGFP dwells at microtubule plus-ends

Both Figure 3.21A and Figure 2.23 show that Kip2-eGFP dwells at the microtubule plus-end upon arrival. The end-residence times of single Kip2-eGFP molecules at the microtubule plus-end were measured from the kymographs of the single-molecule motility assay experiments imaged at a frame rate of 0.5 Hz (Figure 3.25). Once Kip2-eGFP reached the microtubule plus-end, it resided there for 30 ± 26 s before dissociating from GMPCPP-stabilized microtubules or 29 ± 28 s before dissociating from taxol-stabilized microtubules (mean ± SD, n = 40 and 12 respectively, p = .88 (Welch's unpaired t-test)). Thus, when Kip2 reaches the stabilized microtubule plus-end, it resides there without dissociating for up to a minute. This long end-residence results in an accumulation of Kip2-eGFP at the stabilized microtubule plus-end over time (Figure 3.21A).
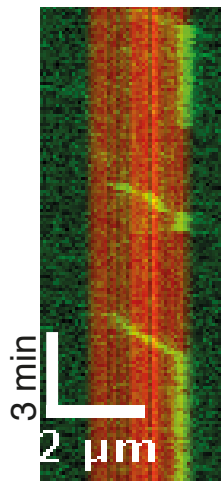
Figure 3.25. Kip2-eGFP dwells at microtubule plus-ends.

Kymograph showing end-residence of single Kip2-eGFP molecules on a GMPCPP-stabilized microtubule in 1 mM ATP. Upon arrival at the plus-end, Kip2-eGFP does not immediately dissociate from the microtubule.

3.2.5   Kip2-eGFP requires ATP-hydrolysis for directed motility

The highly processive motility of Kip2-eGFP in ATP strongly suggests that translocation of Kip2 is fueled by ATP-hydrolysis. However, alternative mechanisms of translocation are also possible: kinesin-13 MCAK has an unconventional ATPase cycle and reaches both the microtubule plus-end and the minus-end by diffusion (Friel and Howard, 2011; Helenius et al., 2006). To test whether Kip2-eGFP requires ATP-hydrolysis to target the microtubule plus-end, the single-molecule motility assay experiment was repeated in 1 mM ADP. In ADP, Kip2-eGFP diffused along the lattice of surface-bound GMPCPP-stabilized microtubules and did not reach the microtubule plus-end over time (Figure 3.26). To quantify whether Kip2-eGFP is in a truly diffusive state in ADP, the mean squared displacement over time should be calculated. However, that analysis is beyond the scope of this work. The non-processivity of Kip2-eGFP in the ADP nucleotide state, as well as in AMP-PNP (§3.2.2), shows that Kip2 requires ATP-hydrolysis for directed motility.
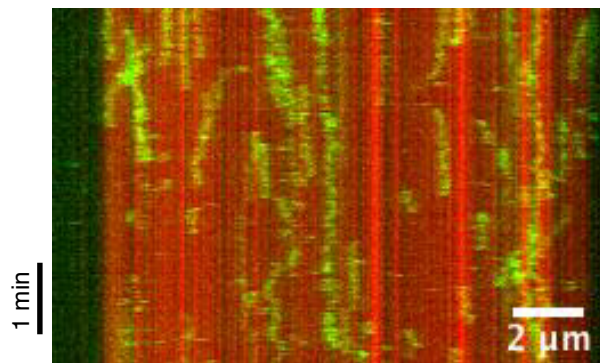
Figure 3.26. Kip2-eGFP diffuses along the microtubule lattice in ADP.
Kymograph showing diffusive movements of single Kip2-eGFP molecules on a GMPCPP-stabilized microtubule in 1 mM ADP.

_____

3.2.6. Kip2 targets tubulin to microtubule plus-ends by processive motility

Kip2 promotes microtubule growth (Chapter 3.1) and the processive nature of this kinesin, together with its prolonged end-residence time at the microtubule plus-end (Figure 3.25), suggests that Kip2 might promote growth as a processive microtubule polymerase that accelerates tubulin subunit addition to the microtubule polymer, like the non-motor XMAP215 (Brouhard et al., 2008). Alternatively, Kip2 could promote microtubule growth as a tubulin shuttle, targeting tubulin to the microtubule plus-end to increase the local tubulin concentration at the microtubule plus-end.

To test whether Kip2 binds tubulin from solution, the single-molecule motility assay was modified. Red surface-immobilized GMPCPP-stabilized microtubules were pre-loaded with unlabeled Kip2 in the presence of 1 mM AMP-PNP. Next, 1 µM 60% Alexa-488-labeled porcine tubulin was flushed into the channel in the presence of 1 mM AMP-PNP. Finally, soluble tubulin was washed out using 1 mM AMP-PNP buffer (Figure 3.27A). Control channels without Kip2 did not show tubulin decoration along stabilized microtubules (Figure 3.27B). In channels with Kip2 pre-loaded on the microtubules, these microtubules were decorated with green tubulin (Figure 3.27C), indicating that Kip2 binds tubulin from solution along the microtubule lattice. To test whether Kip2 can also transport this tubulin to the microtubule plus-end, unlabeled Kip2 and green tubulin was added to channels with stabilized red microtubules in the presence of 1 mM ATP. Kymographs along microtubules revealed that Kip2 indeed transports tubulin to microtubule plus-ends, leading to a local accumulation of tubulin at these plus-ends (Figure 3.27D,E). Thus, Kip2 targets tubulin to the microtubule plus-end by processive motility.
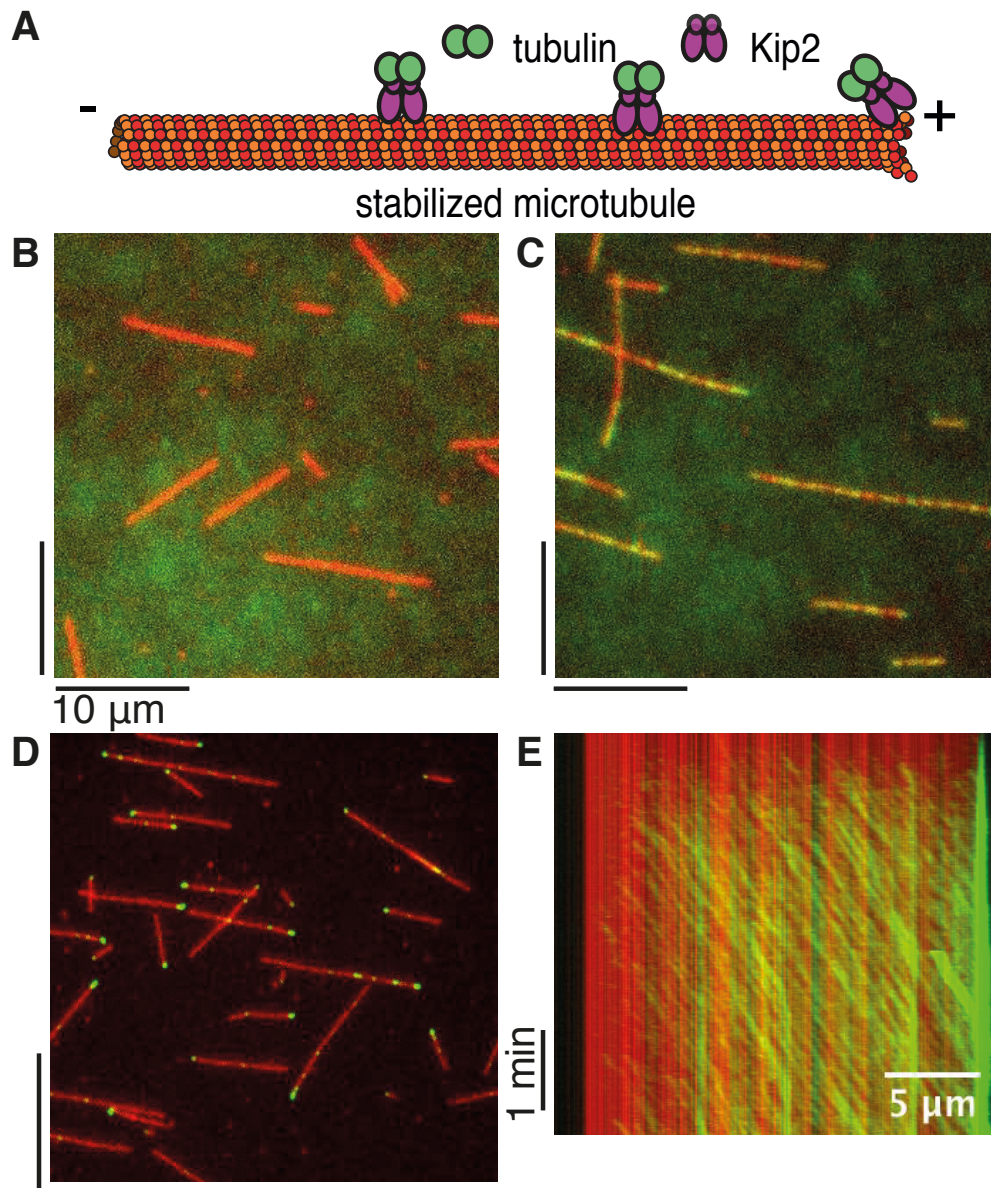
Figure 3.27. Kip2 processively targets tubulin to microtubule plus-ends.

A). Schematic of the experimental design.

B). Without Kip2 in solution, 1 µM green tubulin in solution does not associate with the microtubule lattice.

C). In 1 mM AMP-PNP, 40 nM Kip2 binds 1 µM green tubulin to the microtubule lattice.

D). In 1 mM ATP, 40 nM Kip2 transports 1 µM green tubulin to the microtubule plus-end.

E). Kymograph showing transport of 1 µM green tubulin by 40 nM unlabeled Kip2 towards the microtubule plus-end. Over time, green tubulin accumulates at the microtubule plus-end.

3.2.7.   Kip2 transports tubulin oligomers

To estimate the number of tubulin dimers carried by Kip2 per transported particle, the integral fluorescence intensity of transported particles was measured using Motiontracking software. This integral fluorescence intensity was compared to the intensity of tubulin dimers on the cover slip, as in (Brouhard et al., 2008) (Figure 3.28).
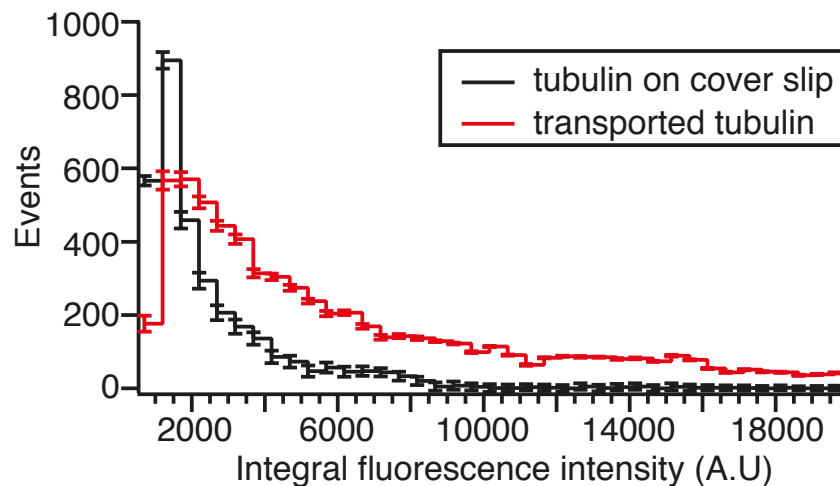
Figure 3.28. Kip2 transports tubulin oligomers.

Histogram of integral fluorescence intensities of Kip2:tubulin complexes on microtubules (red) and surface-bound tubulin dimers (black, summed integral intensities ± SD of 3 experiments). Integral fluorescence intensities below 700 were discarded as background noise. Assuming transported particles are spherical (as would approximately be the case for single-molecules), the mode of the background fluorescence intensity (A.U.) is 1288, which is interpreted to represent individual tubulin dimers (see Brouhard et al., 2008). The mode of the fluorescence intensity of transported particles is 2739. The Alexa-488 labeling ratio of the transported tubulin was 60%. Thus, most Kip2 molecules carry oligomers 3 tubulin dimers ((2739/1288)*~1.6). The mean fluorescence intensity of transported particles was 7138 ± 833 (SE). Thus, assuming transported particles are spherical, these particles contain on average 8-9 tubulin dimers. The number of Kip2 molecules per transported particle is unknown.

The transported particles contained on average 9 ± 0.5 tubulin dimers (mean ± SE, *n* > 1000), assuming the transported particles were approximately spherical (as would be the case for single-molecules). When the single-molecule assumption of spherical shape was dropped, the average per transported particles increased up to ~12

tubulin dimers. Thus, every Kip2 molecule carries multiple tubulin dimers in the tubulin transport assay.

Interestingly, tubulin transport was observed over distances several times longer than the average Kip2 run-length of 4.1 µm (Figure 3.27E). In addition, inspection of kymographs revealed the fusing of smaller transport particles into larger ones. Therefore, it is possible that each of the transported tubulin particles is associated with more than 1 Kip2 molecule. In summary, the average number of tubulin dimers transported per particle in the tubulin transport assay is on the order of 10, whereas the number of Kip2 molecules per transported particle is unknown.

3.2.8 The Kip2 flux on the dynamic microtubule extension is lower than on the stabilized microtubule seed

Kip2 carries tubulin to the microtubule plus-end and this shuttling of tubulin may, or may not, account for the measured increase in microtubule growth rate. To test this, a spiking experiment was performed on stabilized microtubules to measure the flux of Kip2 to the microtubule plus-end. Surface-bound GMPCPP-stabilized microtubules were incubated with a mixture of 20 nM or 40 nM unlabeled Kip2 plus 0.09 nM Kip2-eGFP in the presence of 1 mM ATP (Figure 3.29A,B). In addition, to compare the flux of Kip2-eGFP on stabilized microtubules with the flux on dynamic extensions, this spiking assay was repeated on dynamic microtubules. In the dynamic spiking assay, 20 nM or 40 nM unlabeled Kip2 and 1 nM Kip2-eGFP, as well as 8 µM unlabeled tubulin, was added to stabilized microtubule seeds in the presence of 1 mM ATP. This allowed the visualization the growing plus-end while still allowing for resolution of single molecules (Figure 3.29C).

From the kymographs of these spiking assays, the flux of Kip2-eGFP molecules to either the stabilized or the growing microtubule plus-end was measured, from which the number of molecules that arrived at the plus-end per second could be back calculated (Figure 3.30). To quantify the flux on stabilized microtubules (J_s, see Table 2), the total number of Kip2-eGFP molecules that arrived at the stabilized microtubule plus-end was divided by the total duration of the experiment. To quantify the flux of Kip2 on dynamic microtubules (J_d, see Table 2), the total number of Kip2-eGFP molecules that arrived at the growing microtubule plus-end was divided by the total time of observed microtubule growth.
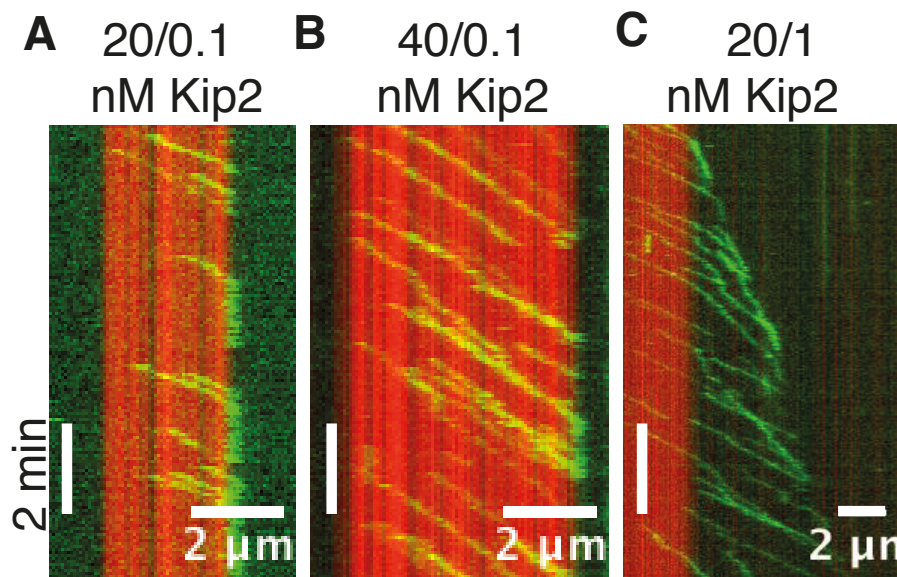
Figure 3.29. Kip2 flux on stabilized and dynamic microtubules.

A). Kymograph showing the flux of 20 nM Kip2 spiked with 0.1 nM Kip2-eGFP on a GMPCPP-stabilized microtubule in 1 mM ATP.

B). Kymograph showing the flux of 40 nM Kip2 spiked with 0.1 nM Kip2-eGFP on a GMPCPP-stabilized microtubule in 1 mM ATP.

C). Kymograph showing the flux of 20 nM Kip2 spiked with 1 nM Kip2-eGFP on a dynamic microtubule grown with 8 μM unlabeled tubulin in 1 mM ATP.

In this way, it was extrapolated that the Kip2 flux to the stabilized microtubule plus-end was 4.2 ± 0.01 molecules/s at 20 nM Kip2 compared to 11.3 ± 0.02 molecules/s at 40 nM Kip2 (Figure 3.30, mean ± SE, n = 654 and 547 respectively, $p < .0001$ (Welch's unpaired t-test)). The flux to the growing microtubule plus-end was 0.5 ± 0.01 molecules/s at 21 nM Kip2 and 1.5 ± 0.01 molecules/s at 41 nM Kip2 (Figure 3.30, n = 220 and 296 Kip2-eGFP molecules respectively, $p < .0001$ (Welch's unpaired t-test)). Thus, the flux of Kip2 is higher on stabilized microtubules than on dynamic extensions, both at 20 nM and 40 nM Kip2 ($p < .0001$ (Welch's unpaired t-test)). As expected, increasing the Kip2 concentration led to an increase in the flux of Kip2 to the microtubule plus-end, both on stabilized and dynamic extensions. The more than 2-fold increase in flux resulting from a doubling of the Kip2 concentration suggests cooperativity in the binding of Kip2 to microtubules.
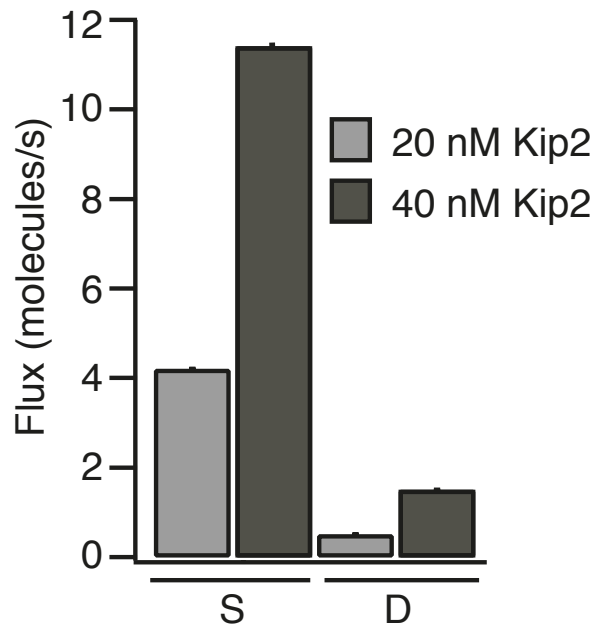
Figure 3.30. Quantification of the Kip2 flux on stabilized and dynamic microtubules.
Bar chart of Kip2 flux on GMPCPP-stabilized microtubules (S) and on dynamic extensions (D) grown with 8 µM unlabeled tubulin for varying Kip2-concentrations (mean ± SE, see Table 2) in 1 mM ATP.

3.2.9.   Kip2 decreases its own end-residence time

The highly processive kinesin-8 Kip3 decreases its own end-residence time (Varga et al., 2009), by bumping off the Kip3 molecules that dwell at the microtubule plus-end. To test whether Kip2 can also bump itself from the microtubule, its end-residence time at 20 and 40 nM Kip2 was quantified from the spiking assays described in §3.2.8, and compared to the end-residence time at 1 nM Kip2 (§3.2.4). On stabilized microtubules, an increase in the Kip2 concentration from 1 nM to 40 nM led to a decrease in end-residence time from 30 ± 26 s at 1 nM Kip2 to 5.5 ± 1.2 s at 40 nM Kip2 (Figure 3.31, mean ± SD, n = 40 and 81 respectively, $p <$ .0001 (Welch's unpaired t-test)). In the spiking assays on dynamic microtubules, the end-residence time of Kip2 was 5.9 ± 1.6 s at 21 nM Kip2 and 5.5 ± 1.2 s at 41 nM Kip2 (Figure 3.31, n = 31 and 57 events respectively, p = .83 (Welch's unpaired t-test)). Thus, the end-residence time of Kip2 decreases as the concentration of Kip2 increases. This indicates that incoming Kip2 motors bump off the motors in front of them, as was observed for Kip3 (Varga et al., 2009).
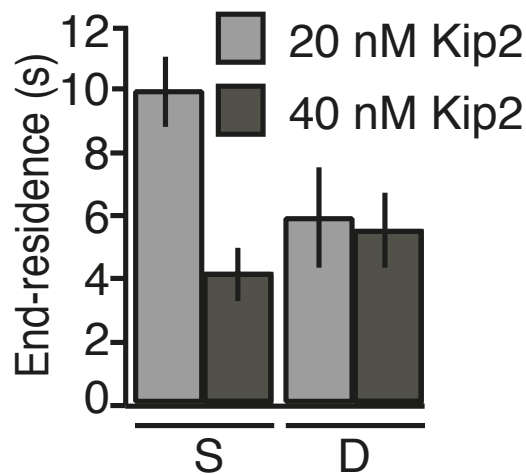
Figure 3.31. Kip2 decreases its own end-residence time.
Bar chart of Kip2 end-residence time on GMPCPP-stabilized microtubules (S) and dynamic extensions (D) grown with 8 µM unlabeled tubulin with 20 nM and 40 nM Kip2-concentrations in 1 mM ATP (mean ± SE).

3.2.10.   Kip2 senses the dynamic microtubule extension

The kymographs of the spiking assay on dynamic microtubules revealed a lower velocity of Kip2-eGFP on dynamic microtubule extensions than on stabilized microtubule seeds. In this assay, Kip2-eGFP walked along the GMPCPP-tubulin seeds at a velocity of 4.2 ± 1.1 µm/min, which is slower than the Kip2-eGFP velocity of 5.0 ± 0.9 µm/min measured in the nondynamic assays with GMPCPP-stabilized microtubules (mean ± SD, $n = 100$ and 675 Kip2-eGFP traces respectively, $p < .0001$ (Welch's unpaired t-test)). On dynamic microtubules, Kip2-eGFP moved along the extensions at a velocity of 2.8 ± 1.0 µm/min, both at 21 nM and 41 nM Kip2 (mean ± SD, $n = 185$ and 81 respectively). At 1 nM Kip2-eGFP (with no added unlabeled Kip2) Kip2-eGFP walked at a pace of 2.1 ± 0.9 µm/min (mean ± SD, $n = 28$), excluding the possibility that the reduced speed on dynamic microtubules is due to crowding on the lattice. Thus, Kip2-eGFP moves at approximately one half the speed on dynamic microtubule extensions compared to stabilized microtubules. However, Kip2 is still faster than the polymerization rates of dynamic microtubules; Kip2 remains fast enough to catch up with the growing microtubule plus-end.

3.2.11. Kip2 binds to the stabilized microtubule seed at the same rate as to the dynamic extension

Kip2 senses the dynamic microtubule extension, which raises the question whether the binding rate of Kip2 to the microtubule extension differs from the binding rate to the microtubule seed. From the kymographs of the spiking experiments described in § 3.2.6, the binding rate of Kip2 to stabilized microtubules (k_s) was calculated as:

$$k_s = \frac{N}{L \cdot T} \qquad (2)$$

where N is the number of binding events, L is the length of the microtubule seed (in µm) and T is the total duration of the experiment (in seconds). For dynamic microtubule extensions, the Kip2 binding rate (k_d) was calculated as:

$$k_d = \frac{2N}{v_+ \cdot T^2} \qquad (3)$$

where N is the number of binding events and v_+ is the microtubule growth rate (in µm/s). At 21 nM Kip2, k_s was 0.09 ± 0.05 µm$^{-1} \cdot$s^{-1} and k_d was 0.07 ± 0.04 µm$^{-1} \cdot$s^{-1} (mean ± SD, $n = 7$ microtubules, $p = .30$ (Welch's unpaired t-test)). At 41 nM Kip2, K_s was 0.30 ± 0.19 µm$^{-1} \cdot$s^{-1} and K_d was 0.19 ± 0.11 µm$^{-1} \cdot$s^{-1} (Figure 3.32, mean ± SD, $n = 8$ microtubules, $p = .18$ (Welch's unpaired t-test)). Thus, Kip2 binds to stabilized seeds and dynamic microtubule extensions at the same rate.
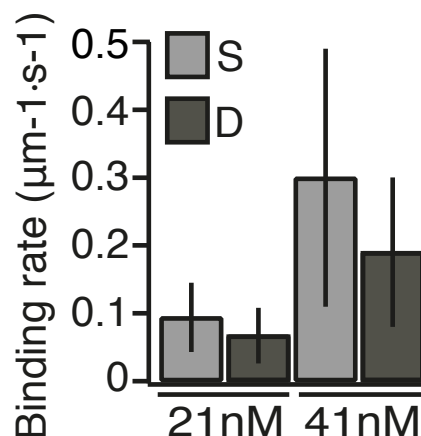
Figure 3.32. Binding rates of Kip2.
Bar chart of Kip2 binding rate on GMPCPP-stabilized microtubules (S) and dynamic extensions (D) grown with 8 µM unlabeled tubulin with varying Kip2-concentrations in 1 mM ATP (mean ± SD).

3.3.   Kip2 mutant studies to probe structure-function relationships

3.3.1.   Purification of Kip2 truncation mutants

In the previous chapters, it was shown that purified Kip2 is a highly processive motor that promotes microtubule growth *in vitro.* In this chapter, a mutant approach was taken to gain understanding of how the structure of Kip2 is related to its function. As a first step, the N-terminus or C-terminus of Kip2 were truncated (Figure 3.33).
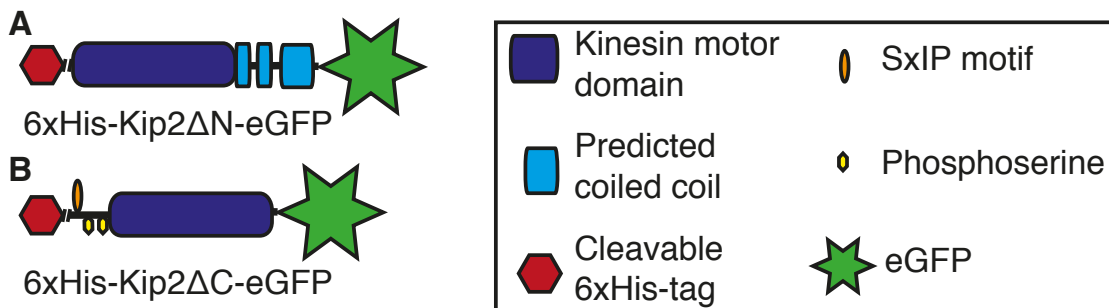
Figure 3.33. Kip2 truncation constructs

A). Schematic of 6xHis-Kip2ΔN-eGFP

B). Schematic of 6xHis-Kip2ΔC-eGFP

These truncation mutant proteins were expressed in SF+ cells using baculovirus expression and purified using affinity chromatography over His-affinity columns. Affinity column purification success was checked by SDS-PAGE (Figure 3.34, 3.35) and Western blot using anti-6xHis antibody. High protein purity was not a priority for the crude, preliminary experiments to probe structure-function relationships described below. Therefore, the eluted proteins were not further purified, nor were the 6xHis-tag removed. The elution fractions were exchanged into storage buffer over a buffer exchange column (Amicon) and snap-frozen at 80 °C.

Figure 3.34. SDS-PAGE gel of purified 6xHis-Kip2ΔN-eGFP fractions.

Per lane, 7 µl 6xHis-Kip2ΔN-eGFP (96 kDa) was loaded. Lane M: Seeblue Plus2 pre-stained protein marker, Lane 1: Crude lysate. Lane 2: Supernatant after centrifuge spin, Lane 3: Flow-through, Lane 4: Flow-though after 10 mM imidazole wash, Lane 5: Flow-though after 50 mM imidazole wash. Lane 6: Flow-though after 100 mM imidazole wash. Lane 7: Elution fraction (300 mM imidazole). The elution fraction was used for *in vitro* reconstitution assay experiments. Protein concentration was estimated using Bradford.

Figure 3.35. SDS-PAGE gel of purified 6xHis-Kip2ΔC-eGFP fractions.

Per lane, 7 µl 6xHis-Kip2ΔC-eGFP (82 kDa) was loaded. Lane M: Seeblue Plus2 pre-stained protein marker, Lane 1: Supernatant after centrifuge spin, Lane 2: Flow-through, Lane 3: Flow-though after 10 mM imidazole wash, Lane 4: Flow-though after 50 mM imidazole wash. Lane 5: Flow-though after 100 mM imidazole wash. Lane 6: Elution fraction (300 mM imidazole). The elution fraction was used for *in vitro* reconstitution assay experiments. Protein concentration was estimated using Bradford.

_____

3.3.2.   The N-terminus of Kip2 is dispensable for promotion of microtubule growth

As a first test of Kip2 structure-function relationships, a dynamic microtubule assay (§ 3.1.2) was performed in the presence of either ~100 nM 6xHis-Kip2ΔN-eGFP or ~100 nM 6xHis-Kip2ΔC-eGFP (hereafter called Kip2ΔN and Kip2ΔC), to test whether these truncation mutants were still able to promote microtubule growth. The mean length of the freshly polymerized microtubules was measured ten minutes after addition of Kip2Δ and 12 µM free porcine tubulin to the surface-bound microtubule seeds.
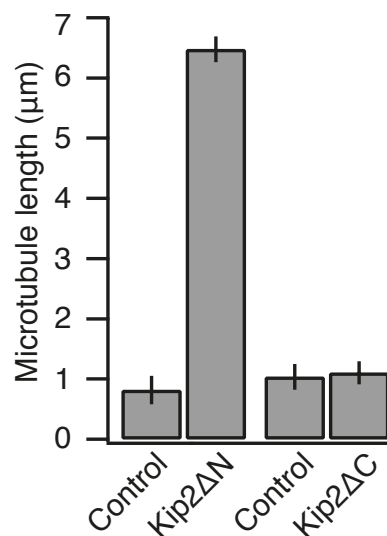
Figure 3.36. Microtubule growth is promoted by Kip2ΔN but not by Kip2ΔC.
Microtubule length (mean ± SE) with and without ~100 nM Kip2ΔN or Kip2ΔC in 1 mM ATP, measured ten minutes after flushing 12 µM porcine tubulin and Kip2Δ into the flow chamber.

This experiment revealed that Kip2ΔN increased the average microtubule length from 0.81 ± 0.24 µm/min without Kip2Δ (control), to 6.5 ± 0.22 µm/min at ~100 nM Kip2ΔN (Figure 3.36, $n = 7$ and 24 respectively, $p < .0001$ (Welch's unpaired t-test)). By contrast, Kip2ΔC did not affect microtubule length (1.0 ± 0.21 µm/min without Kip2Δ (control), compared to 1.1 ± 0.19 µm/min at ~100 nM Kip2ΔC, $n = 20$ and 24 respectively, $p = .82$ (Welch's unpaired t-test)). Thus, the N-terminal tail appears to be dispensable for the microtubule growth promoting function of Kip2 *in vitro*. By contrast, the C-terminal tail is indispensable, possibly because this region harbors coiled-coil domains essential for dimerization of the protein.

3.3.3.   The N-terminus of Kip2 is dispensable for processive motility

To test whether the N-terminal and C-terminal truncation mutants are still able to processively translocate along stabilized microtubules, a single-molecule motility assay was performed as in § 3.2.1. Kymographs revealed that in 1 mM ATP, Kip2ΔN maintained the ability to walk processively towards the microtubule plus-end. By contrast, Kip2ΔC did not show directed motility, but instead only briefly interacted with the GMPCPP-stabilized microtubule lattice in a diffusive manner (Figure 3.37).
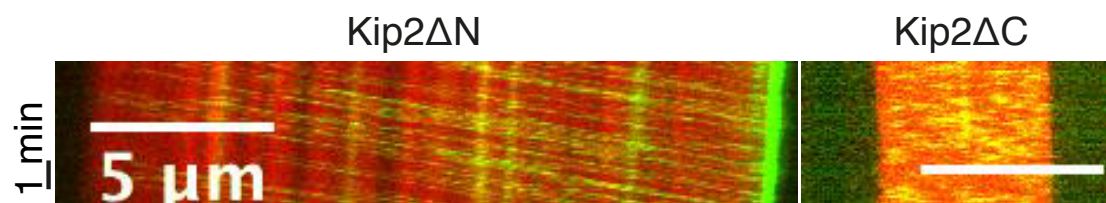
Figure 3.37. The N-terminus of Kip2 is dispensable for processive motility.
Kymographs of single Kip2Δ molecules on GMPCPP-stabilized microtubules in 1 mM ATP. Kip2ΔN translocates processively, whereas Kip2ΔC diffuses along the microtubule lattice.

This experiment shows that the N-terminus of Kip2 is dispensable for processive motility, whereas the C-terminus is indispensable. The most plausible explanation for the loss of processivity in Kip2ΔC is that this protein is a monomer, as the coiled-coil regions for dimerization are located in the C-terminus of the protein. However, the possibility that Kip2ΔC-eGFP dimerizes via the -eGFP tail (A. Hyman, personal communication; Norris et al., 2015) was not ruled out by this experiment. Nonetheless, as is clear from the kymograph, this putative artificial dimerization does not allow for processive motility of the C-terminally truncated protein.

3.3.4.   Both Kip2ΔN and Kip2ΔC bind tubulin from solution

To test whether Kip2ΔN and Kip2ΔC are able to bind tubulin from solution, surface-bound, biotinylated GMPCPP-stabilized microtubules were incubated with either ~100 nM Kip2ΔN or Kip2ΔC in 1 mM AMP-PNP. Both proteins labeled the microtubules (Figure 3.38, left panels). Next, rhodamine labeled tubulin was added in the presence of 1 mM AMP-PNP, incubated for 1 minute and subsequently flushed

_____

out using imaging buffer supplemented with 1 mM AMP-PNP. Snap shots were taken using a 488 nm laser to visualize the -eGFP labeled Kip2Δ decorating the unlabeled microtubules and EPI-fluorescence to visualize tubulin bound to microtubules. Both Kip2ΔN and Kip2ΔC decorated the stabilized microtubules in AMP-PNP (Figure 3.38, left panels) and were able to bind tubulin from solution (Figure 3.38, right panels). This suggests that tubulin from solution either binds to the centrally located kinesin motor domain that is unaltered in both protein constructs, or that there is more than 1 tubulin binding domain in the Kip2 sequence; 1 on each terminus. Of note, potentially the 6xHis-tag on both proteins is responsible for the binding of tubulin from solution in this experiment. The rhodamine signal on microtubules incubated with Kip2ΔN compared to Kip2ΔC was not quantified. Therefore, no conclusions should be drawn from the apparent stronger signal of the Kip2ΔC-decorated microtubules.

_____

Kip2ΔN   rhodamine-tubulin

Kip2ΔC   rhodamine-tubulin
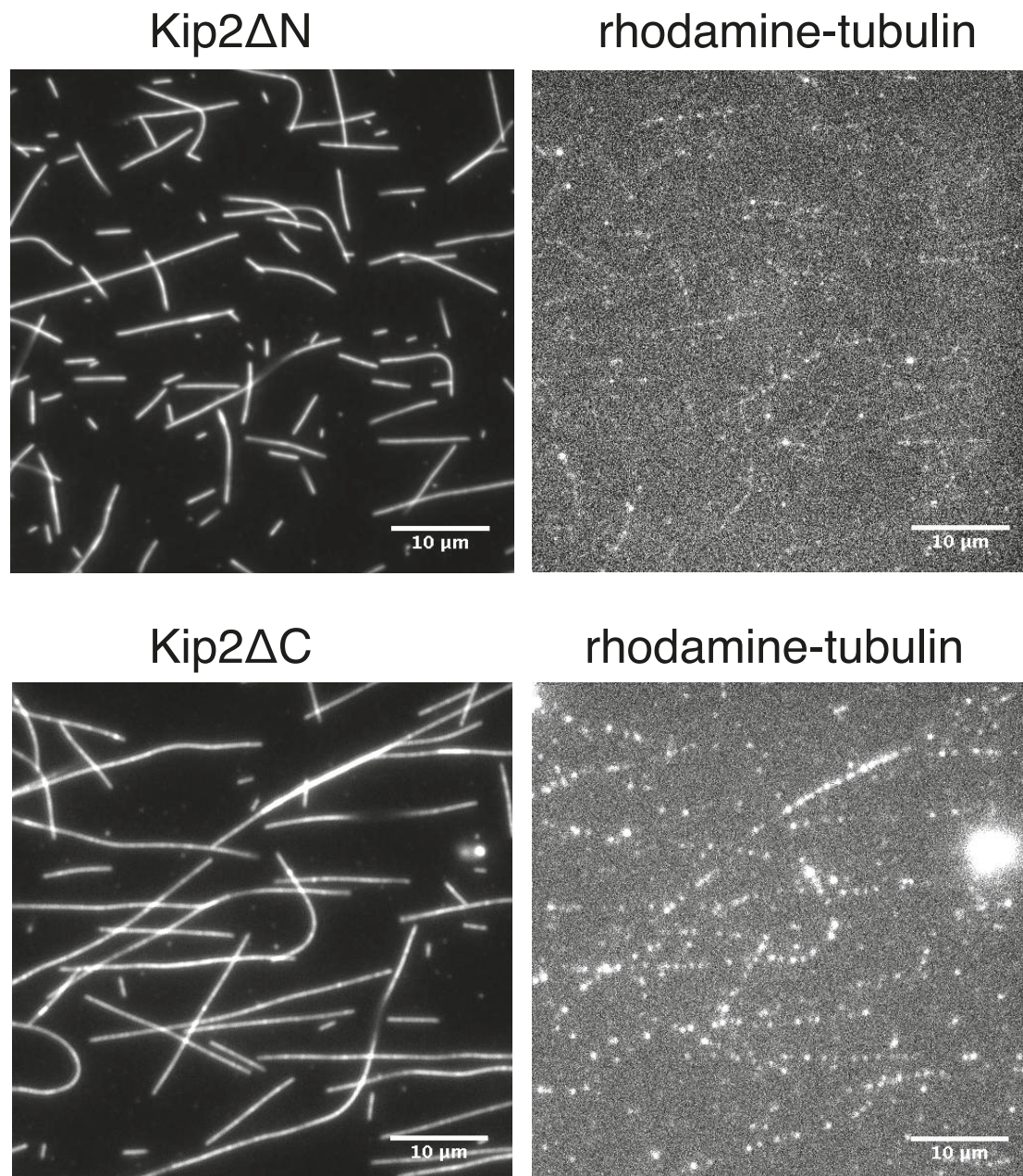
Figure 3.38. Both Kip2ΔN and Kip2ΔC bind tubulin from solution.

Microscopy images of unlabeled GMPCPP-stabilized microtubules incubated with ~100 nM eGFP labeled Kip2ΔN (upper left panel) or Kip2ΔC (bottom left panel). Rhodamine-labeled tubulin covers microtubules incubated either with Kip2ΔN (top right panel) or with Kip2ΔC (bottom right panel).

3.3.5.   Identification of a putative microtubule- or tubulin-binding domain in the Kip2 sequence

The polymerase activity of Kip2 suggests that this protein may have a binding domain for either tubulin dimers (§ 3.2.6) or microtubules (§ 3.2.3). The identification of such a putative tubulin/microtubule-binding domain in the Kip2 sequence was performed in collaboration with Dr. Ian Henry. *In silico* comparisons of multiple known tubulin/microtubule-binding domains from other proteins such as XMAP215 revealed no obvious conserved sequence motives. However, what these identified tubulin/ microtubule-binding domains have in common, is a region of positively charged residues at the end of helices, on the surface of the protein. The known Kip2 microtubule binding domain (Yang et al., 1989) also consists of a short run of positively charged arginine, lysine and histidine residues.

If Kip2 would have a tubulin/microtubule-binding domain that is important for microtubule growth promotion, then one would expect this domain to be conserved through evolution. The truncation studies described in § 3.3.2 - 3.3.4 suggest that such a domain would be located in the C-terminus of Kip2 (as the N-terminus is dispensable for growth promotion, processive motility and tubulin binding). Thus, to identify a putative tubulin/microtubule-binding domain, the Kip2 homologs in the NCBI homologene database were aligned using ClustalW. This alignment revealed a conserved stretch of positively charged residues in the C-terminus of Kip2 (Figure 3.39).
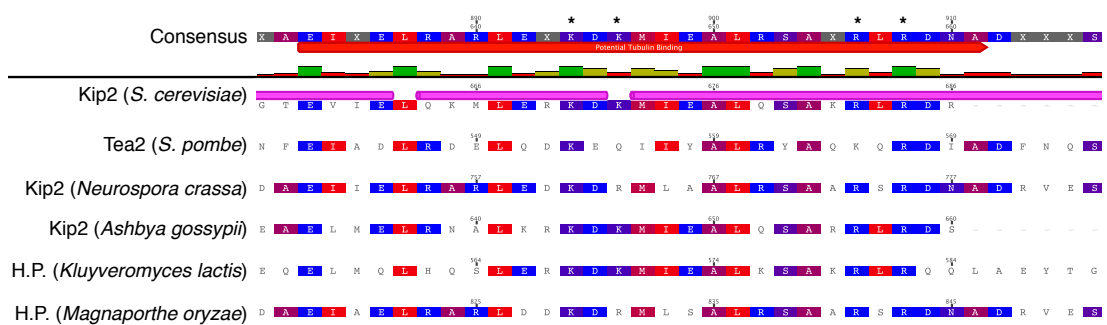
Figure 3.39. The C-terminus of Kip2 harbors a conserved stretch of positively charged residues.

Alignment of Kip2 and five homologs from fungi, courtesy of Dr. Ian Henry. Residue charges are color-coded according to hydrophobicity. Stars above the consensus sequence indicate the amino acids that were mutated to alanine.

_____

A structural model of this C-terminal region, created using I-Tasser and Chimera software packages, revealed that these conserved residues potentially form a positively charged domain on the surface of Kip2, as would be predicted for a tubulin/ microtubule-binding domain (Figure 3.40).
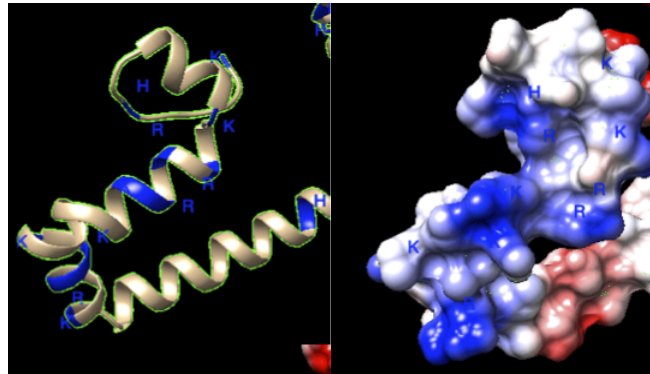
Figure 3.40. A putative tubulin/microtubule-binding site in the C-terminus of Kip2.
Left panel: Ribbon diagram of a region in the C-terminus that is predicted to form a domain with basic residues (blue) on the surface of Kip2. Right panel: Space filling model of the same basic region in the Kip2 C-terminus. Images are courtesy of Dr. Ian Henry.

To test whether this conserved, positively charged domain in the C-terminus of Kip2 is important for the microtubule growth promoting function of this protein, two lysine residues and two arginine residues (indicated in Figure 3.39) were mutated to alanine by means of alanine substitution mutagenesis (see methods). The resulting protein sequence with these four point mutations, expressed in insect cells with a C-terminal -eGFP, was named Kip2_ala-eGFP.

3.3.6.   Purification of Kip2_ala-eGFP

6xHis-Kip2_ala-eGFP was expressed in SF+ cells using baculovirus expression and purified using Ni-NTA superflow resin. For this purification, a resin was chosen instead of a His-affinity column, because the protein repeatedly precipitated on the column. Affinity purification success was checked by SDS-PAGE (Figure 3.41) and Western blot using anti-6xHis antibody. Next, 6xHis-tags were enzymatically cleaved from the protein using PreScission protease. Enzymatic cleavage of the 6xHis-tag was checked by Western blot using anti-6xHis-antibody (Appendix 4). Kip2_ala-eGFP was not further purified by gel filtration, because the protein also repeatedly

_____

precipitated on the Sephadex 200 column. The pooled elution fractions were supplemented with 10% glycerol and snap-frozen at 80 °C.
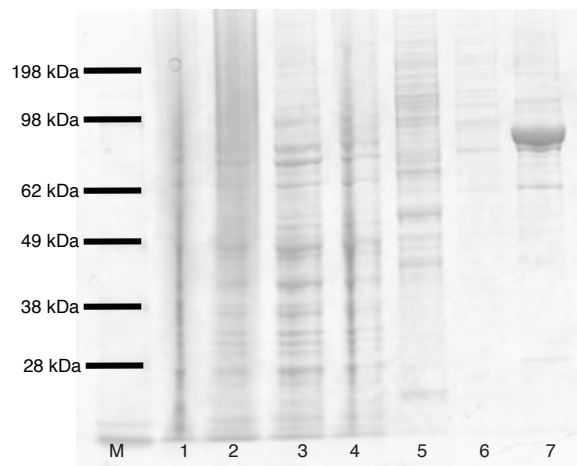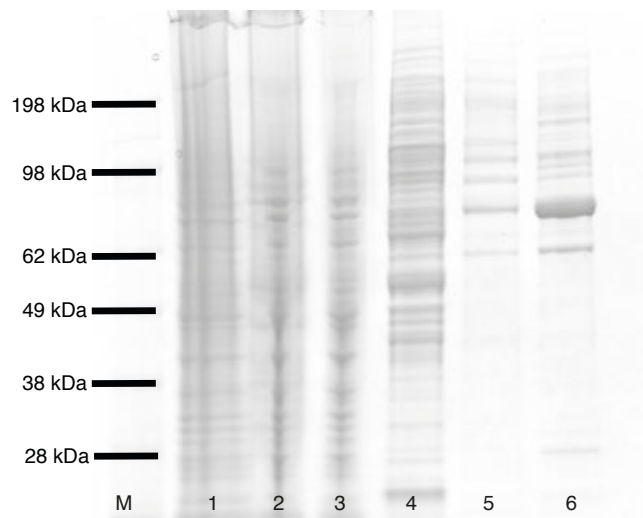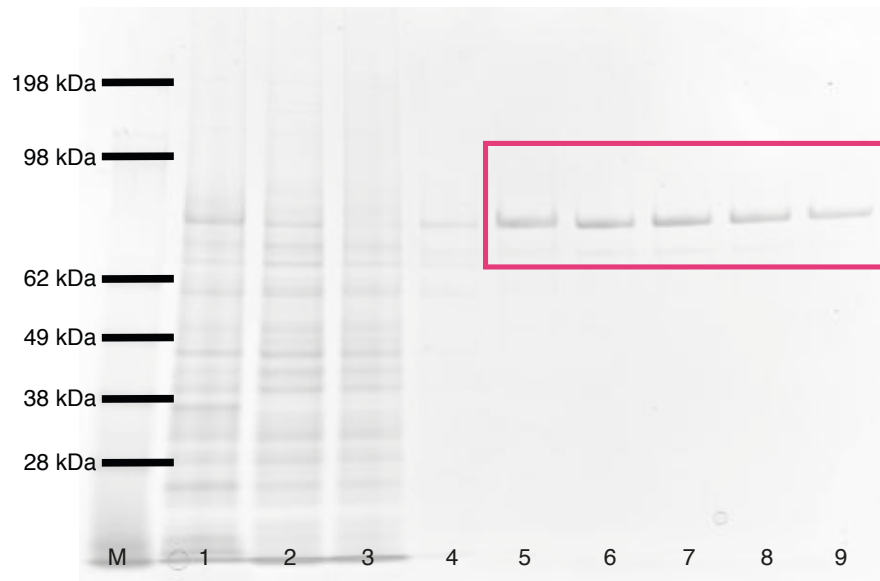

Figure 3.41. SDS-PAGE gel of purified 6xHis-Kip2_ala-eGFP fractions.
Per lane, 7 µl Kip2_ala-eGFP (105 kDa) was loaded. Lane M: Seeblue Plus2 pre-stained protein marker, Lane 1: Crude lysate, Lane 2: Supernatant after centrifuge spin, Lane 3: Flow-through, Lane 4: Flow-though after wash, Lane 5-9: Elution fractions. The fractions 5-9 (within the red box) were pooled and used for *in vitro* reconstitution assay experiments. The final concentration of the pooled fractions was 1.9 µM.

3.3.7.   Kip2_ala-eGFP increases microtubule growth rate to the same extent as wild-type Kip2-eGFP

To test whether Kip2_ala-eGFP promotes microtubule growth, the growth rate of microtubules grown with 12 µM porcine tubulin was quantified with and without 40 nM Kip2_ala-eGFP and compared to the microtubule growth rate with 40 nM Kip2-eGFP as a positive control. To match experimental conditions, the reaction buffer for the Kip2-eGFP experiments was supplemented with elution buffer and 1:50x diluted PreScission protease. Kip2_ala-eGFP increased microtubule growth rate 2.5-fold from 0.39 ± 0.02 µm/min ($n = 59$) to 1.0 ± 0.03 µm/min ($n = 35$) (Figure 3.42, $p < .0001$ (Welch's unpaired t-test)). This increase in growth rate did not differ from that by Kip2-eGFP (1.0 ± 0.04 µm/min, $n = 41$, $p = .99$ (Welch's unpaired t-test)). Thus, mutation of the C-terminal basic region to an uncharged region did not affect the ability of Kip2 to increase microtubule growth rate.
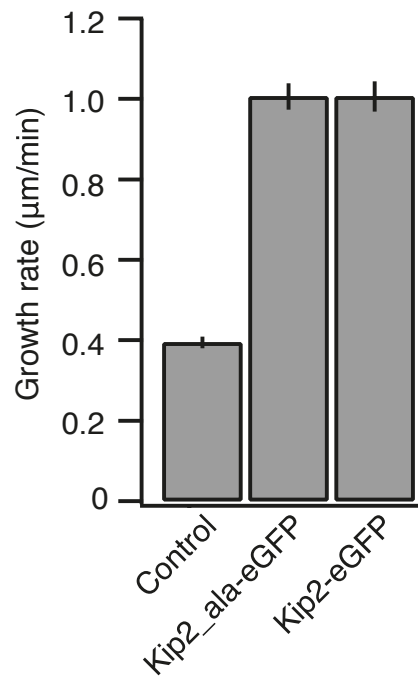
Figure 3.42. Kip2_ala-eGFP increases microtubule growth rate.

Bar chart showing microtubule growth rates (mean ± SE) of microtubules grown with 12 µM porcine tubulin without or with 40 nM Kip2_ala-eGFP or 40 nM Kip2-eGFP.

3.3.8.   Kip2_ala-eGFP has unaltered biophysical properties

To test whether biophysical properties of Kip2 were altered by the mutations in the basic region in the C-terminus, single-molecule motility assays were performed with Kip2_ala-eGFP as described in Chapter 3.2, with Kip2-eGFP as a positive control. To match experimental conditions, the reaction buffer for the Kip2-eGFP experiments was supplemented with elution buffer and 1:50x diluted PreScission protease.

To measure velocities, single Kip2_ala-eGFP and Kip2-eGFP molecules were imaged using TIRF microscopy at a frame rate of 0.5 Hz. The individual Kip2-eGFP traces in kymographs revealed that in 1 mM ATP, single Kip2_ala-eGFP molecules associated with the GMPCPP-stabilized microtubule lattice and walked processively towards the microtubule plus-end at the same velocity as Kip2-eGFP (Figure 3.43, 4.1 ± 0.7 µm/min ($n = 260$) compared to 4.2 ± 1.0 µm/min, mean ± SD, $n = 235$, $p = .31$ (Welch's unpaired t-test)).
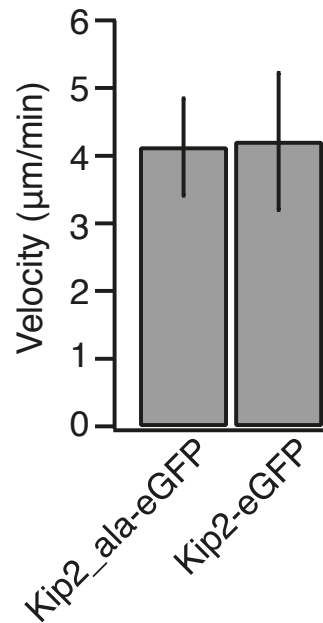
Figure 3.43. Kip2_ala-eGFP walks along microtubules at the same velocity as Kip2-eGFP.

Bar chart showing velocities (mean ± SD) of single Kip2_ala-eGFP and Kip2-eGFP molecules along GMPCPP-stabilized microtubules in 1 mM ATP.

Thus, the mutation of the basic region in the Kip2 C-terminus to an uncharged region did not affect the velocity of Kip2 on stabilized microtubules.

Next, the run-length of Kip2_ala-eGFP on GMPCPP-stabilized microtubules was quantified and compared to that of Kip2-eGFP. To measure run-length, Kip2_ala-eGFP and Kip2-eGFP molecules were imaged using TIRF microscopy by constant streaming at a frame rate of ~10 Hz. Single-molecule traces of Kip2_ala-eGFP walked for 4.3 ± 0.3 μm ($n = 35$) before dissociation (or bleaching) compared to 4.6 ± 0.4 μm for Kip2-eGFP (Figure 3.44, $n = 30$, $p = .56$ (Welch unpaired t-test)). Thus, mutation of the basic region in C-terminus of Kip2 to a uncharged region did not affect the run-length of Kip2 on stabilized microtubules.
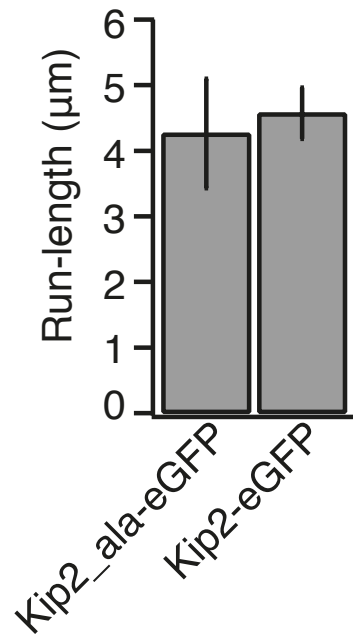
Figure 3.44. Kip2_ala-eGFP translocates the same distance along microtubules as Kip2-eGFP.
Bar chart showing run-lengths (mean ± SE) of single Kip2_ala-eGFP and Kip2-eGFP molecules along GMPCPP-stabilized microtubules in 1 mM ATP.

Finally, the end-residence times of single Kip2_ala-eGFP molecules at the microtubule plus-end were measured from the kymographs of the single-molecule motility assay experiments imaged at a frame rate of 0.5 Hz and compared to the dwell-time of Kip2-eGFP. The end-residence time of Kip2_ala-eGFP was the same as that of Kip2-eGFP (Figure 3.45, 21 ± 29 s compared to 24 ± 26 s, n = 8 and 12 respectively, p = .83 (Welch's unpaired t-test)).

In summary, the mutation in the C-terminus of Kip2 did not result in any change in velocity, run-length or end-residence time of the motor. Together with the unimpaired polymerase function of Kip2_ala-eGFP (§ 3.3.7), it is concluded that the positively charged C-terminal domain in the Kip2 sequence is unimportant for the growth promoting function of Kip2.
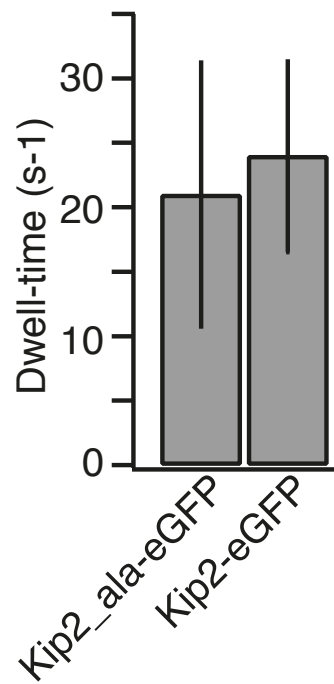
Figure 3.45. Kip2_ala-eGFP resides at the microtubule plus-end for the same amount of time as Kip2-eGFP.

Bar chart showing end-residence time (mean ± SE) of single Kip2_ala-eGFP and Kip2-eGFP molecules along GMPCPP-stabilized microtubules in 1 mM ATP.

3.3.9   Over-expression of Kip2_ala in budding yeast results in cytoplasmic microtubules of intermediate length.

To test whether the *in vivo* microtubule growth promoting function of Kip2 is preserved in the Kip2_ala mutant, the Kip2_ala-HA3 was over-expressed under control of an inducible GAL1-promoter in wild-type budding yeast cells expressing fluorescent α-tubulin. As a positive control, full-length Kip2-HA3 was over-expressed. Protein expression was checked by Western blot using anti-HA-antibody. Cell-lines with similar levels of Kip2-HA3 and Kip2_ala-HA3 protein expression were chosen for imaging (Appendix 5).

The rationale of this experiment was that wild-type Kip2 present in budding yeast will exert its normal cellular function, such as transport of Bik1 and dynein to the microtubule plus-ends (see § 1.6.5). In case the microtubule growth-promoting function would be maintained in the over-expressed mutant Kip2, one would expect hyper-elongated cytoplasmic microtubules, as is the case with over-expression of wild-type Kip2 (Figure 1.6). By contrast, if the over-expressed mutant Kip2 had lost its microtubule growth-promoting function, one would expect cytoplasmic microtubules of wild-type length.

Following the imaging protocol of (Carvalho et al., 2004), budding yeast cells were imaged by confocal microscopy using a 488 nm laser line at t = 45 minutes after induction of either full-length Kip2-HA3 or Kip2_ala-Ha3 by addition of galactose to the growth medium. As a negative control, uninduced cells from the same cell lines were imaged (Figure 3.46). Average microtubule length was measured from maximum intensity projections of the obtained Z-stacks. Microtubule length was measured by hand in Fiji using the Freehand Line tool. Of note, the 2-D representation of 3-D data could potentially cause aberrations in the measurements. In addition, this experiment was performed twice, instead of in biological triplicate as good research practice dictates. Finally, as protein expression levels were judged by eye, small differences in protein levels between the Kip2 and Kip2_ala cell lines are probable. Therefore, the following data should be considered to be preliminary.

Over-expression of full-length Kip2-HA3 increased the average microtubule length   from 1.0 ± 0.07 μm ($n = 71$) to 3.4 ± 0.35 μm ($n = 90$, $p < .0001$ (Welch's unpaired t-test) Figure 3.47). The Kip2-ala-Ha3 mutant also increased the average length of cytoplasmic microtubules from 0.99 ± 0.06 μm ($n = 86$) to 2.3 ± 0.15 μm ($n = 60$, $p < .0001$ (Welch's unpaired t-test)), but to a lesser extent than full-length

_____

Kip2 (*p* < .01 (Welch's unpaired t-test)). Uninduced Kip2-HA3 and Kip2_ala-Ha3 cell lines had microtubules of equal length (*p* = .66 (Welch's unpaired t-test)). In summary, although the Kip2_ala mutant increases cytoplasmic microtubule length *in vivo*, it may have partly lost its microtubule growth promoting effect.
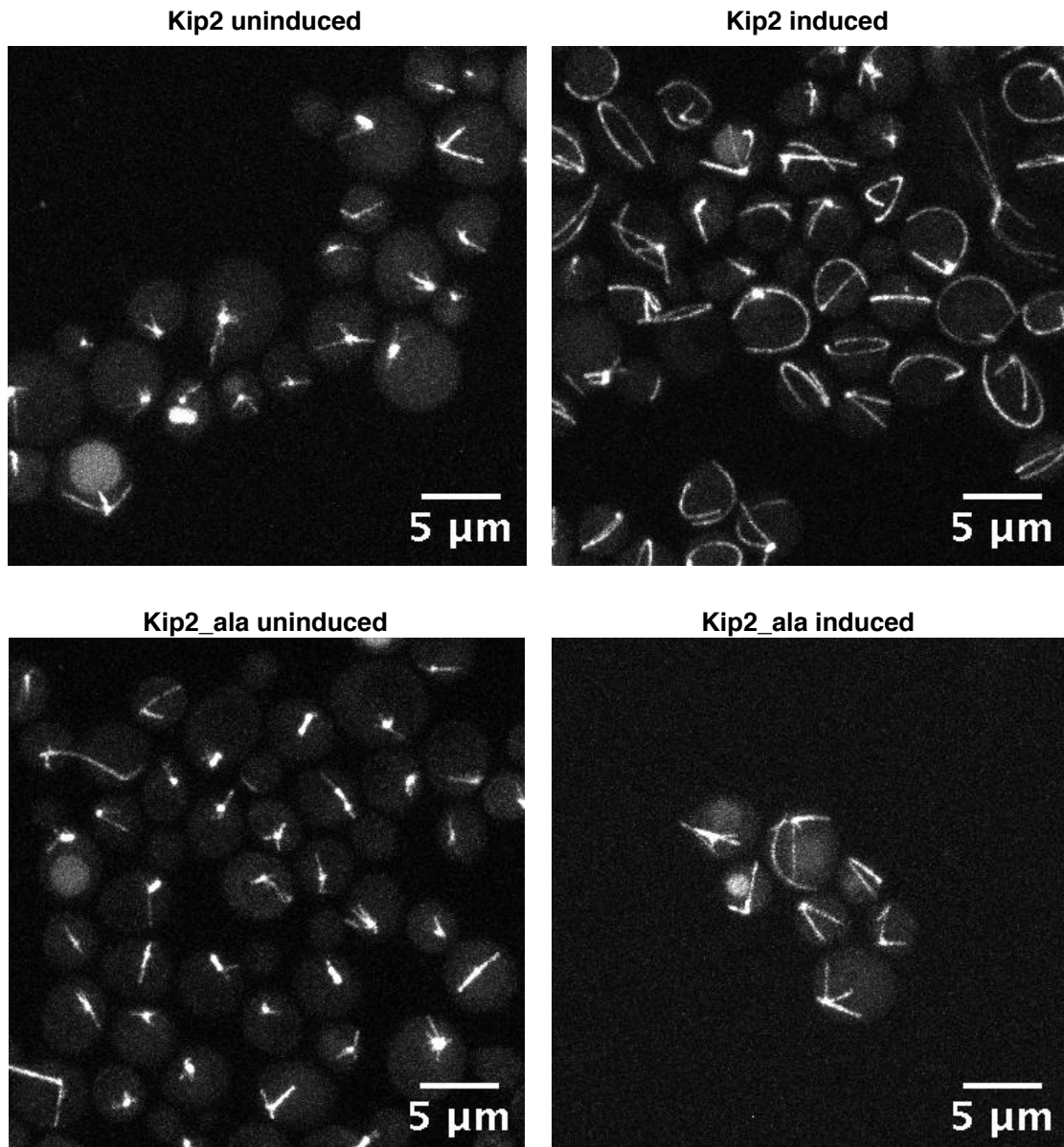
Figure 3.46. Over-expression of Kip2 and Kip2_ala results in hyper-elongated cytoplasmic microtubules *in vivo*.

Maximum intensity projections of budding yeast cells expressing fluorescent α-tubulin and either Kip2 (upper panels) or Kip2_ala (lower panels), 45 minutes after induction of protein expression by addition of galactose (right panels) or without induction (left panels).
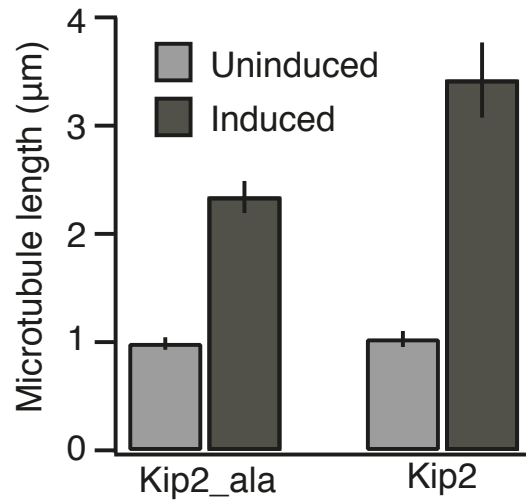
Figure 3.47. Kip2 and Kip2_ala increase cytoplasmic microtubule length *in vivo*.
Bar chart showing microtubule length (mean ± SE) at t = 45 minutes after mock treatment or induction of either Kip2_ala or Kip2 by addition of galactose to the medium.

3.4.   Combinatorial regulation of microtubule dynamics by Kip2-Bim1-Bik1.

3.4.1.   Reconstitution of the microtubule plus-end tracking protein complex Kip2-Bim1-Bik1

In Chapter 3.1, purified Kip2 on its own was shown to promote microtubule growth. In the cell, however, Kip2 transports the +TIP Bik1 to the microtubule plus-end (Carvalho et al., 2004; Caudron et al., 2008). In addition, Kip2 forms a complex *in vitro* with both Bik1 and Bim1 (Roberts et al., 2014). In the absence of Kip2, Bik1 and Bim1 form a heterotetramer that affects microtubule dynamics in the same way as Bim1 alone does (Blake-Hodek et al., 2010). Therefore, to fully understand how Kip2 regulates microtubule dynamics, it is important to probe these dynamics in the presence of all three microtubule plus-end tracking proteins. In this Chapter, the protein complex Kip2-Bim1-Bik1 was reconstituted on dynamic microtubules. To test the binding properties of Bik1 and Bim1 to microtubules, these proteins were tagged with eGFP.

3.4.2.   Purification of Bik1-eGFP from SF+ cells

Full-length 6xHis-Bik1-eGFP was expressed in SF+ cells using baculovirus expression and purified using affinity chromatography over His-affinity columns, as described in (Blake-Hodek et al., 2010). Affinity column purification success was checked by SDS-PAGE and Western blot using anti-6xHis as a primary antibody. Next, 6xHis-tags were enzymatically cleaved from the protein using PreScission protease. Finally, Bik1-eGFP was purified to homogeneity by gel filtration over a Sephadex 200 column, which was pre-washed with protein storage buffer (Figure 3.48). Protein stability was confirmed by SDS-PAGE and enzymatic cleavage of the 6xHis-tag from the protein of interest by Western blot using anti-6xHis-antibody.

Figure 3.48. SDS-PAGE gel of gel filtrated Bik1-eGFP fractions.

Per lane, 10 µl Bik1-eGFP (78 kDa) was loaded. Lane M: Seeblue Plus2 prestained protein marker, Lane 1-7: elution fractions of gel filtration. Fractions indicated by the red box were pooled and used for *in vitro* reconstitution assay experiments. The final concentration of the pooled fractions was 1.6 µM (see Methods).

3.4.3.   Purification of Bim1-eGFP from *E. coli*

Purification of Bim1-eGFP was kindly performed by Dr. Aliona Bogdanova. Full-length 6xHis-Bim1-eGFP was expressed in *E.coli* and purified using affinity chromatography over His-affinity columns, as described in (Blake-Hodek et al., 2010). Affinity column purification success was checked by SDS-PAGE and Western blot using anti-6xHis as a primary antibody. Next, 6xHis-tags were enzymatically cleaved from the protein using PreScission protease. Finally, Bim1-eGFP was purified to homogeneity by gel filtration over a Sephadex 200 column, which was pre-washed with protein storage buffer (Figure 3.49). Protein stability was confirmed by SDS-PAGE and enzymatic cleavage of the 6xHis-tag from the protein of interest by Western blot using anti-6xHis-antibody.

_____
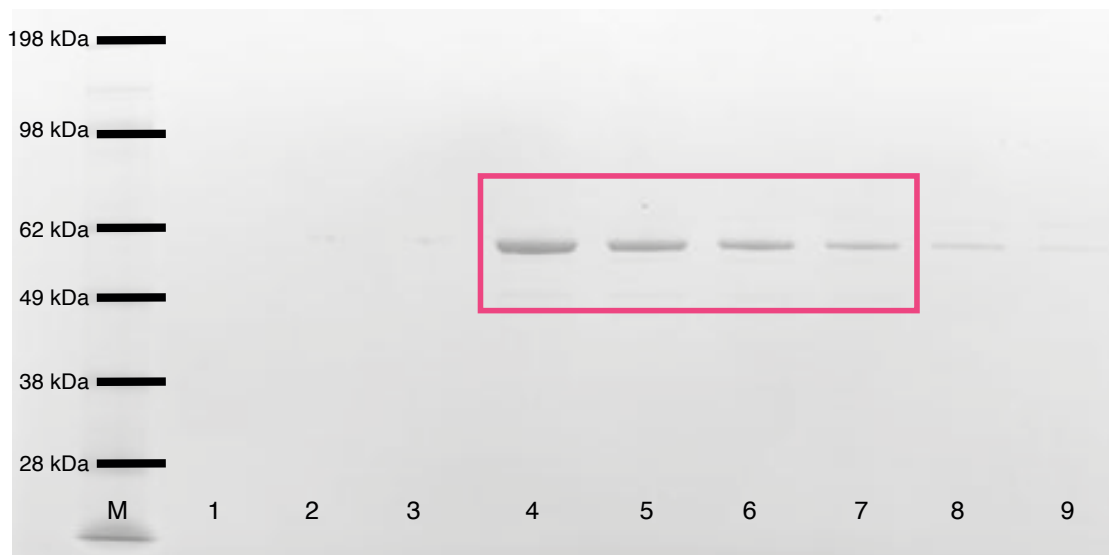
Figure 3.49. SDS-PAGE gel of gel filtrated Bim1-eGFP fractions.

Per lane, 15 µl protein (65 kDa) was loaded. Lane M: Seeblue Plus2 prestained protein marker, Lane 1-9: elution fractions of gel filtration. Fractions indicated by the red box were pooled and used for *in vitro* reconstitution assay experiments. The final concentration of the pooled fractions was 1.8 µM (see Methods).

3.4.4.   Combinatorial regulation of microtubule length by the complex Kip2-Bim1-Bik1

Genetic studies in budding yeast suggest that Kip2 increases cytoplasmic microtubule length by transporting Bik1 to the microtubule plus-end (Carvalho et al., 2004; Caudron et al., 2008). By contrast, this work shows that Kip2 alone is sufficient to promote microtubule growth (Chapter 3.1). To quantify how Bik1 and Bim1 influence microtubule length *in vitro*, the dynamic microtubule assay described in Chapter 3.1 was repeated with 12 µM porcine tubulin and (combinations of) 40 nM Kip2, 22 nM Bik1-eGFP and 200 nM Bim1-eGFP, in the presence of 1 mM ATP. The Kip2 concentration of 40 nM was chosen, because the effect on growth rate and catastrophe frequency was saturated at this concentration (Figure 3.7 and Figure 3.8). The concentrations of Bik1-eGFP and Bim1-eGFP were chosen subsequently to reflect the relative physiological concentrations of the proteins in the cell with respect to Kip2, based on (Ghaemmaghami et al., 2003). Microtubule lengths of freshly polymerized (green) microtubules were measured ten minutes after addition of 200 nM Bim1-eGFP and/or 22 nM Bik1-eGFP and 12 µM free tubulin to the surface-

_____

bound microtubule seeds (Figure 3.50). As a positive control, the effect of 40 nM Kip2 on microtubule length was quantified.
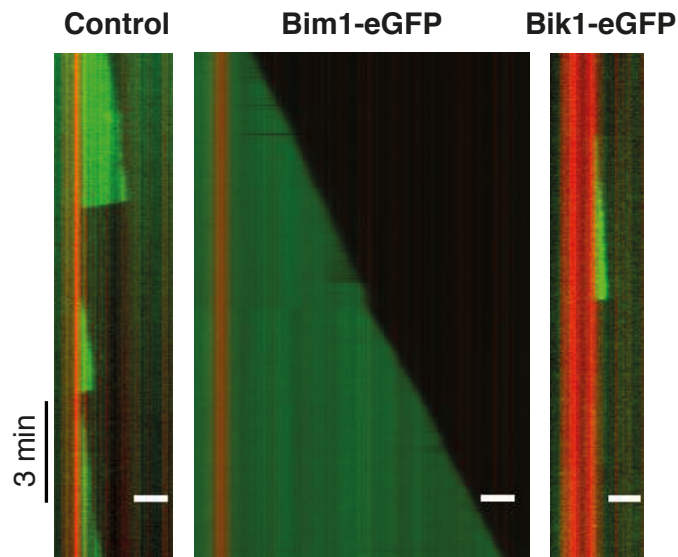
Figure 3.50. Bim1-eGFP and Bik1-eGFP have opposite effects on microtubule length.
Representative kymographs of microtubules grown with 12 µM porcine tubulin (left), tubulin plus 200 nM Bim1-eGFP (middle), or tubulin plus 22 nM Bik1-eGFP (right), in the presence of 1mM ATP. Scale bar = 2 µm.

As expected (Chapter 3.1), Kip2 increased the average microtubule length from 1.3 ± 0.16 µm to 7.0 ± 0.33 µm ($n = 48$ and 32 respectively, $p < .0001$ (Welch's unpaired t-test)). Bim1-eGFP also increased microtubule length to 8.8 ± 0.64 µm ($n = 29$, $p < .0001$ (Welch's unpaired t-test)). By contrast, Bik1-eGFP decreased the average microtubule length to 0.70 ± 0.14 µm ($n = 33$, $p < .01$ (Welch's unpaired t-test)).

Next, the effect on microtubule length of combinations of Kip2, Bim1-eGFP and Bik1-eGFP was probed (Figure 3.51, Figure 3.52). The combination of 200 nM Bim1-eGFP and 40 nM Kip2 further increased average microtubule length to 11.0 ± 0.37 µm ($n = 20$, $p < .0001$ (Welch's unpaired t-test)). By contrast, the combination of Bik1-eGFP and Kip2 did not affect microtubule length compared to Kip2 alone (7.0 ± 0.33 µm compared to 7.6 ± 0.47 µm ($n = 32$ and 21 respectively, $p = .35$ (Welch's unpaired t -test)). The combination of Bim1-eGFP and Bik1-eGFP did also not affect microtubule length compared to Bim1 alone (8.8 ± 0.64 µm compared to 7.9 ± 0.53 µm, $n = 29$ and 25 respectively, $p = .29$ (Welch's unpaired t-test)). Finally, the complete plus-end tracking protein complex Kip2-Bim1-eGFP-Bik1-eGFP affected microtubule length to the same extent as the combination of Kip2 with Bim1-eGFP

(11.0 ± 0.37 µm compared to 10.2 ± 0.44 µm, *n* = 20 in both conditions, *p* = .21 (Welch's unpaired t-test)).
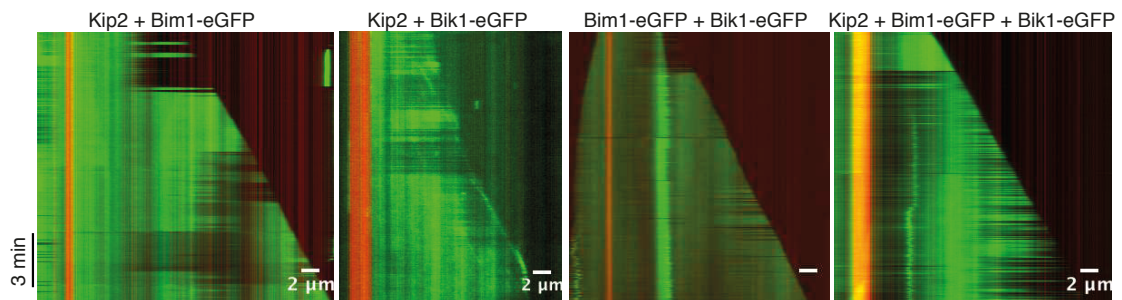
Figure 3.51. Combinatorial regulation of microtubule length.

Representative kymographs of microtubules grown with 12 µM porcine tubulin and combinations of 40 nM Kip2, 200 nM Bim1-eGFP and/or 22 nM Bik1-eGFP, in the presence of 1 mM ATP. Scale bar = 2 µm.
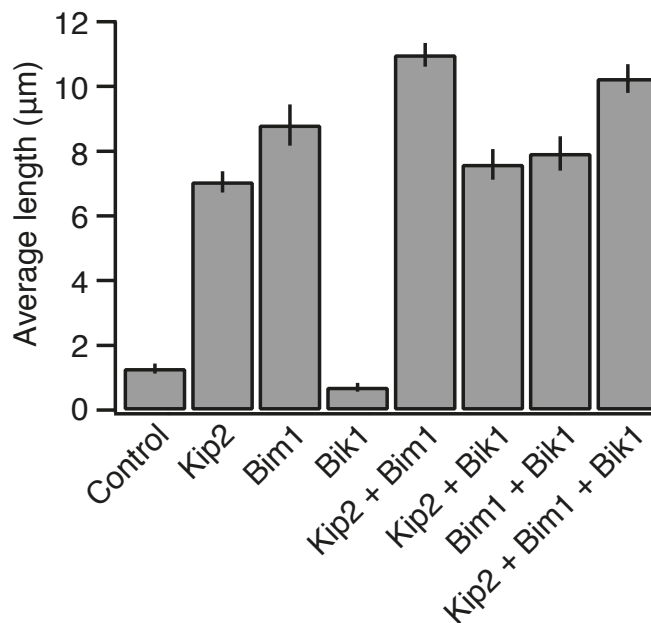
Figure 3.52. Combinatorial effects of Kip2, Bim1 and Bik1 on microtubule length *in vitro.*

Bar chart showing microtubule length (mean ± SE) at t = 10 minutes after the start of the experiment of microtubules grown with 12 µM porcine tubulin in 1 mM ATP for control and (combinations of) 40 nM Kip2, 200 nM Bim1-eGFP and 22 nM Bik1-eGFP. Kip2 and Bim1-eGFP increase the length of microtubules, both alone and in combination. Bik1-eGFP lowers microtubule length, but does not affect microtubule length when part of a bigger complex.

Thus, whereas both Kip2 and Bim1 alone are sufficient to increase microtubule length, Bik1 is neither necessary nor sufficient to increase microtubule length *in vitro,* in contrast to what was suggested by genetic studies in (Carvalho et al., 2004). In summary, the plus-end tracking protein complex Kip2-Bim1-Bik1 increases microtubule length *in vitro*, through partially additive effects of Kip2 and Bim1.

3.4.5.   Combinatorial regulation of microtubule growth rate by the complex Kip2-Bim1-Bik1

To quantify whether Bik1 and Bim1 influence microtubule dynamics, kymographs were created from the time-lapse images of the dynamic microtubule assay. These kymographs revealed that microtubules were dynamic both with and without Bik1-eGFP and Bim1-eGFP present in the assay. Next, to characterize the effect of Bik1-eGFP and Bim1-eGFP on microtubule dynamics, the microtubule growth rate was analyzed in the presence of (combinations of) these proteins. As a positive control, the effect of 40 nM Kip2 on microtubule growth rate was quantified. As expected (Chapter 3.1), 40 nM Kip2 increased the microtubule growth rate from 0.34 ± 0.01 µm/min to 0.76 ± 0.04 µm/min ($n = 116$ and 30 respectively, $p < .0001$ (Welch's unpaired t-test)). Bim1-eGFP also increased the microtubule growth rate, to 0.85 ± 0.04 µm/min ($n = 37$, $p < .0001$ (Welch's unpaired t-test)). By contrast, 22 nM Bik1-eGFP lowered the microtubule growth rate, to 0.30 ± 0.01 µm/min ($n = 78$, $p < .001$ (Welch's unpaired t-test)). Thus, in contrast to the indications from genetic studies, Bik1 does not portray microtubule polymerase activity. The measured stimulating effect of Bim1 on microtubule growth rate, as well as the growth rate decreasing effect of Bik1 are in agreement with (Blake-Hodek et al., 2010). However, Blake-Hodek and colleagues did not test the combinatorial effect of Bim1 and Bik1 with Kip2.

To reconstitute the combinatorial effects of the plus-end tracking protein complex Kip2-Bim1-Bik1, the dynamic microtubule assay was performed in the presence of 40 nM Kip2 plus 200 nM Bim1-eGFP, 40 nM Kip2 plus 22 nM Bik1-eGFP, 200 nM Bim1-eGFP plus 22 nM Bik1-eGFP and finally 40 nM Kip2, 200 nM Bim1-eGFP and 22 nM Bik1-eGFP (Figure 3.53).
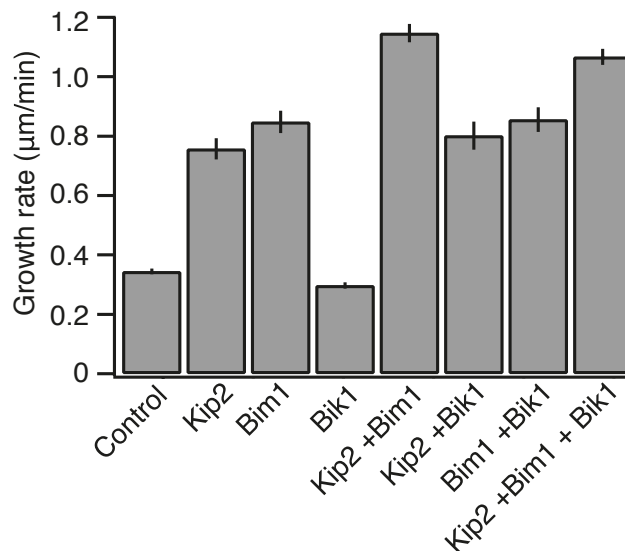
Figure 3.53. Combinatorial effects of Kip2, Bim1 and Bik1 on microtubule growth rate.
Microtubule growth rate (mean ± SE) of microtubules grown with 12 µM porcine tubulin in 1
mM ATP for control and (combination of) 40 nM Kip2, 200 nM Bim1-eGFP and 22 nM Bik1-
eGFP. Kip2 and Bim1-eGFP increase the growth rate of microtubules, both alone and in
combination. Bik1-eGFP lowers microtubule growth rate.

These experiments revealed that the combination of Kip2 and Bim1-eGFP increased
microtubule growth rate in a partially additive manner, from 0.76 ± 0.04 µm/min at 40
nM Kip2 to 1.15 ± 0.03 µm/min when both proteins were present in the assay (n = 30
and 26 respectively, $p < .0001$ (Welch's unpaired t-test)). By contrast, addition of
Bik1-eGFP to Kip2 did not affect microtubule growth rate compared to the growth
rate in the presence of only Kip2 (0.80 ± 0.47 µm/min and 0.76 ± 0.04 µm/min
respectively, n = 16 and 30 respectively, $p = .45$ (Welch's unpaired t-test)). The
addition of Bik1-eGFP to Bim1-eGFP did also not affect the growth rate compared to
the growth rate in the presence of only Bim1-eGFP (0.86 ± 0.04 µm/min and 0.85 ±
0.04 µm/min respectively, n = 33 and 37 respectively, $p = .89$ (Welch's unpaired t-
test)). Finally, the combination of Kip2, Bim1-eGFP and Bik1-eGFP increased the
microtubule growth rate to the same extent as the combination of Kip2 and Bim1-
eGFP (1.07 ± 0.03 µm/min and 1.15 ± 0.03 µm/min respectively, n = 25 and 26
respectively, $p = .06$ (Welch's unpaired t-test)).

In summary, Kip2 and Bim1 both increase microtubule growth rates. Their
partially additive effects suggest that they do so via different mechanisms. Bik1 alone
decreases microtubule growth rate, but in combination with either Kip2 or Bim1, its
effect is lost.

3.4.6.   Regulation of microtubule catastrophe frequency by the complex Kip2-Bim1-Bik1

To quantify how Bim1 and Bik1 affect microtubule catastrophe frequency, the total number of catastrophes observed per experimental condition was divided by the total duration of microtubule growth of all microtubules in that experimental condition. As a positive control, the effect of 40 nM Kip2 on microtubule catastrophe was quantified. As expected (Chapter 3.1), Kip2 decreased K_{cat} from 0.14 ± 0.02 per minute to < 0.001 per minute (mean $\pm$ SE, $n = 90$ and 0 respectively, $p < .0001$ (Welch's unpaired t-test)). Bim1-eGFP also decreased K_{cat}, albeit to a lesser extent, to 0.03 ± 0.01 per minute ($n = 10$, $p < .0001$ (Welch's unpaired t-test)). Bik1-eGFP did not affect K_{cat} (0.14 ± 0.02 per minute, $n = 60$, $p = .84$ (Welch's unpaired t-test)).
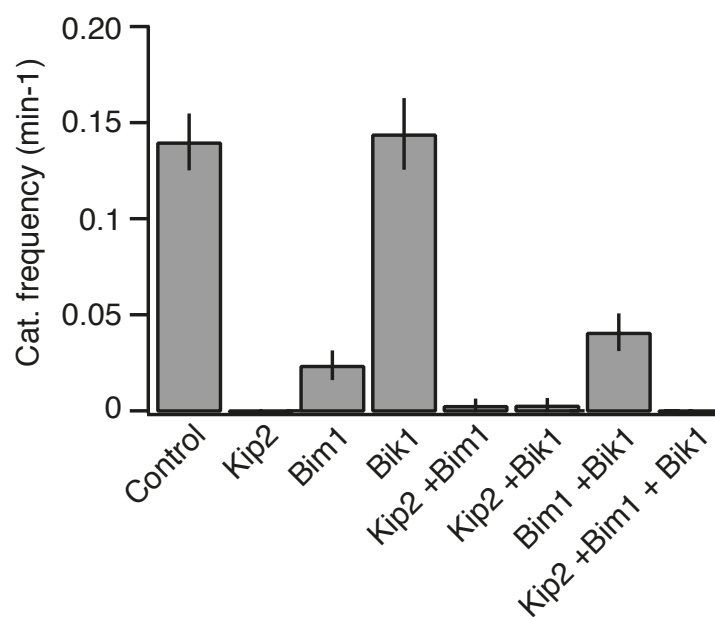
Figure 3.54. Combinatorial effects of Kip2, Bim1 and Bik1 on catastrophe frequency.
Catastrophe frequency (mean $\pm$ SE) of microtubules grown with 12 µM porcine tubulin in 1 mM ATP for control and (combination of) 40 nM Kip2, 200 nM Bim1 and 22 nM Bik1.

Kip2 in combination with either Bim1-eGFP or Bik1-eGFP decreased K_{cat} to the same extent as Kip2 alone (0.004 ± 0.004 per minute in both conditions, $n = 0$ in both conditions, $p = .05$ (Welch's unpaired t-test)). The addition of Bik1-eGFP to Bim1-eGFP did not affect K_{cat} compared to Bim1-eGFP alone (0.04 ± 0.01 per minute, $n = 18$, $p = .18$ (Welch's unpaired t-test)). Finally, Kip2, Bim1-eGFP and Bik1-eGFP in combination decreased K_{cat} to the same extent as Kip2 alone (< 0.001 per minute,

_____

$n = 0$, $p = .96$ (Welch's unpaired t-test)), but significantly more than Bim1-eGFP alone ($p < .05$ (Welch's unpaired t-test)). Thus, Kip2 alone and in complex with Bim1 or Bik1 completely suppresses microtubule catastrophe. Bim1 also prevents catastrophe, but to a lesser extent than Kip2 does. Bik1 does not affect K_{cat}, neither alone nor in complex. In summary, the plus-end tracking protein complex Kip2-Bim1-Bik1 prevents microtubule catastrophe.

3.4.7.   Bik1-eGFP localizes to microtubules in the presence of Kip2, but not autonomously

Bik1-eGFP on its own decreases the average length of microtubules by decreasing their growth rate, while it does not alter the catastrophe frequency. (Blake-Hodek et al., 2010) suggested that Bik1-eGFP scavenges tubulin from solution and thereby depletes the polymerizable tubulin pool, instead of acting directly on the microtubule. Blake-Hodek and colleagues only observed dim Bik1-eGFP labeling of microtubules grown from axonemes. To test whether Bik1-eGFP alone binds to microtubules *in vitro*, 22 nM Bik1-eGFP was added to dynamic microtubules grown with 12 µM unlabeled porcine tubulin. The rationale behind this experiment was that if Bik1-eGFP binds to microtubules, the dynamic extension should be visible using TIRF microscopy, as is the case when unlabeled microtubules are incubated with as little as 1 nM Kip2-eGFP (Figure 3.29C) or with Bim1-eGFP (Figure 3.56). However, no localized eGFP signal was detected in this assay (data not shown). Together with the fact that Bik1-eGFP was not visible on red GMPCPP-stabilized microtubule seeds in the dynamic microtubule assay (Figure 3.50, right panel), it is reasonable to assume that Bik1-eGFP on its own does not bind porcine microtubules.

To test whether Bik1-eGFP associates with Kip2 *in vitro*, as was shown in (Roberts et al., 2014) and *in vivo* (Carvalho et al., 2004; Caudron et al., 2008), the experiment described above was repeated with 22 nM Bik1-eGFP in the presence of 40 nM unlabeled Kip2. In this case, Bik1-eGFP did associate with dynamic microtubules (Figure 3.55). Thus, Kip2 binds Bik1-eGFP in dynamic microtubule assays and targets it to porcine microtubule plus-ends. The kymographs did not reveal obvious long traces of Kip2-transported Bik1-eGFP along stabilized microtubule seeds nor along the dynamic microtubule extensions. This suggests that the interaction between Kip2 and Bik1 on microtubules is transient. In summary, Bik1-eGFP alone does not bind to stabilized or growing microtubules. In the

presence of Kip2, Bik1-eGFP is transported to the microtubule plus-ends in the dynamic microtubule assay, which is consistent with (Roberts et al., 2014).
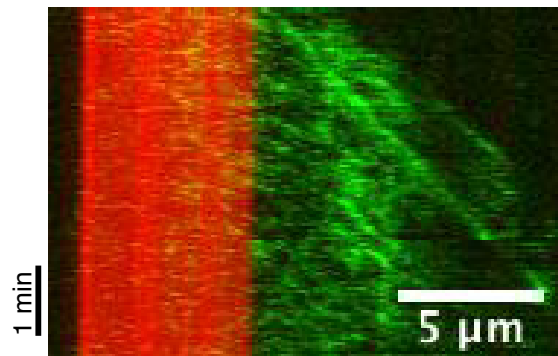
Figure 3.55. Kip2 transports Bik1-eGFP along GMPCPP-stabilized and dynamic microtubules.

Kymograph showing translocation of Kip2-associated Bik1-eGFP along unlabeled porcine microtubules in 1 mM ATP.

3.4.8.   Bim1-eGFP autonomously localizes to microtubule lattices

Bim1-eGFP on its own increases the average length of microtubules by increasing their growth rate, while decreasing the catastrophe frequency. To test whether Bim1-eGFP alone tracks growing microtubule plus-ends *in vitro*, 200 nM Bim1-eGFP was added to dynamic microtubules grown with 12 µM unlabeled porcine tubulin. Surprisingly, Bim1-eGFP did not tip-track the growing microtubule plus-end, but instead labeled the entire dynamic microtubule extension as well as the GMPCPP-stabilized microtubule seed (Figure 3.56). Possibly, Bim1-eGFP differentially recognizes porcine tubulin from yeast tubulin. Therefore, to draw definitive conclusions on the regulation of microtubule dynamics by the plus-end tracking protein complex Kip2-Bik1-Bim1, it is important that the interactions of Bik1 and Bim1 are probed on microtubules grown with yeast tubulin.

_____
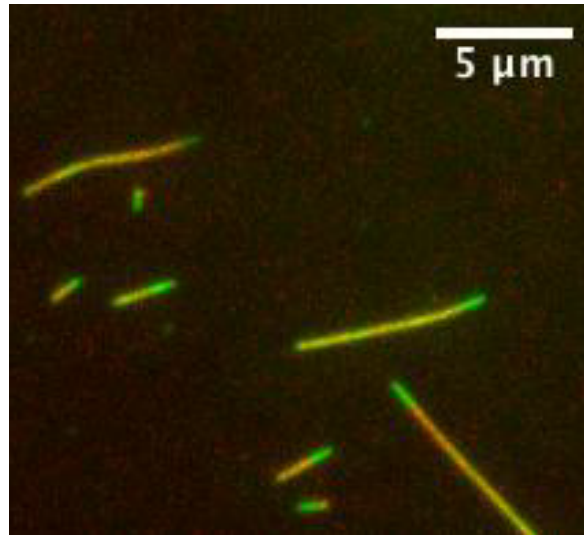
Figure 3.56. Bim1-eGFP autonomously binds to the GMPCPP-stabilized microtubule seed as well as to the dynamic microtubule lattice.

Microscopy image of dynamic, unlabeled porcine microtubules growing from rhodamine-labeled GMPCPP-stabilized microtubules in the presence of 200 nM Bim1-eGFP. Both the microtubule seeds and dynamic extensions are covered by Bim1-eGFP.

_____

4.   Discussion

4.1.   Summary of the main findings

In this work, an *in vitro* reconstitution approach was taken to decipher the mechanism by which budding yeast kinesin Kip2 regulates microtubule dynamics, in order to provide insight into how kinesins control microtubule length. Using dynamic microtubule assays, Kip2 was shown to increase the mean length of microtubules through polymerase and anti-catastrophe activities, both with porcine and yeast tubulin, in the absence of accessory proteins. Kip2 drives tubulin assembly by increasing the tubulin on-rate and decreasing the GTP-tubulin off-rate. These actions require ATP-hydrolysis. Strikingly, Kip2 increases the growth rate of microtubules and prevents catastrophe in a length-dependent manner.

Using single-molecule motility assays, Kip2 was shown to translocate in a highly processive, ATP-dependent manner and to dwell at microtubule plus-ends. This end-residence time decreased at higher Kip2 concentrations. Surprisingly, Kip2 was found to processively target tubulin oligomers to microtubule plus-ends. Although Kip2 bound to dynamic and stabilized microtubules at the same rate, the flux of Kip2 was lower on dynamic extensions than on stabilized microtubule seeds.

Using truncation mutants, it was shown that the N-terminus is dispensable for Kip2's polymerase activity, processive motility and tubulin binding *in vitro*. By contrast, the C-terminus of Kip2 is required for growth promotion and processive motility, but not for tubulin binding. This C-terminus harbors a conserved stretch of positively charges residues, which were hypothesized to function as a tubulin/ microtubule-binding site. Alanine substitution mutagenesis of four positively charged residues in this C-terminal region did not result in a loss of polymerase activity *in vitro*, or in a change in velocity, run-length or dwell-time. Over-expression of this mutant Kip2 in budding yeast cells resulted in an intermediate hyper-elongated microtubule phenotype.

Finally, using dynamic microtubule assays, the complex of Kip2 with its interaction partners Bik1 and Bim1 was shown to promote microtubule growth beyond the growth promotion by Kip2 alone. Individually, Bik1 and Bim1 had opposite effects on microtubule length, but the effect of Bik1 was lost in combination with either Bim1 or Kip2. Bik1 was shown to associate with microtubules as a cargo

of Kip2, whereas Bim1 autonomously bound stabilized as well as dynamic microtubules.

4.2.   Kip2 alone promotes microtubule growth *in vitro* at physiologically relevant protein concentrations

The *in vitro* reconstitution experiments on the interaction of Kip2 with dynamic microtubules show that Kip2 regulates microtubule dynamics as a polymerase and anti-catastrophe factor in the absence of accessory proteins. This effect of purified Kip2 on microtubule dynamics saturated at concentrations as low as 20 nM Kip2, both with porcine and yeast tubulin. By comparison, the cellular concentration of Kip2 in budding yeast is $\approx$ 25 nM (Ghaemmaghami et al., 2003). Thus, the effects of Kip2 on microtubule growth rate and catastrophe frequency *in vitro* were measured at physiologically relevant Kip2 concentrations. Addition of purified Bik1 did not alter the microtubule growth promoting function of Kip2. These findings disprove the hypothesis that Kip2 regulates microtubule dynamics as a translocase of the +TIP Bik1, as suggested by (Carvalho et al., 2004; Caudron et al., 2008). By contrast, this work demonstrates that a kinesin motor can act directly as a (length-dependent) microtubule polymerase and anti-catastrophe factor in the absence of accessory proteins.

4.3.   The Kip2 motor domain plays an essential role in microtubule growth promotion

The full effect of Kip2 on microtubule growth promotion requires ATP hydrolysis. Thus, although Kip2 has some similarities to XMAP215 (a processive polymerase), it differs in some fundamental aspects. XMAP215 acts as a catalyst that increases the tubulin on-rate, when the tubulin concentration is high, and increases the tubulin off-rate to the same extent, when the tubulin concentration is low (Brouhard et al., 2008). Therefore, XMAP215 has no effect on microtubule catastrophe frequency because changes in the on and off rates cancel out. By contrast, Kip2 increases the tubulin on-rate and decreases the tubulin off-rate, which results in a decrease in microtubule catastrophe frequency, as predicted by (Bowne-Anderson et al., 2013).

_____

Consistent with the non-catalytic behavior of Kip2, when the motor domain is fixed in the ATP state using the non-hydrolyzable ATP analog AMP-PNP, microtubule growth is no longer promoted. Thus, unlike XMAP215, Kip2 does not passively catalyze microtubule growth, but instead requires ATP hydrolysis. Kip2 therefore breaks the principle of 'detailed balance' for chemical kinetics (Wegscheider, 1901), where each process is equilibrated by its reverse process.

Possibly, Kip2 requires ATP-hydrolysis only for processive motility to localize to the microtubule plus-end. Once at the plus-end, Kip2 may promote microtubule growth without consuming energy, like XMAP215. One finding that argues in favor of this possibility is that in ADP, Kip2 protects stabilized microtubules from shrinking. Whether Kip2 increases microtubule growth rate in ADP could not be tested, due to experimental issues with ATP contaminations from multiple sources. In summary, the ATP-hydrolyzing motor domain of Kip2 plays an essential role in modulating microtubule dynamics. Whether Kip2 requires ATP-hydrolysis for its polymerase activity per se was not fully elucidated.

4.4. Similar biophysical properties of Kip2 and Kip3 result in opposite effects on microtubule dynamics

Kip2 is a highly processive motor, with an average run-length that exceeds the length of cytoplasmic microtubules in budding yeast, which is about 2 µm (Caudron et al., 2008). Therefore, every Kip2 that lands on the microtubule lattice will in principle reach the microtubule plus-end; the microtubule acts as an antenna for Kip2 to land on, as is the case for the kinesin-8 Kip3 (Figure 4.1 (Varga et al., 2006; 2009)). Furthermore, the measured velocity of Kip2 is five times higher than the fastest microtubule growth rate measured in the dynamic microtubule assays. In comparison, the *in vivo* velocity of Kip2 ranges from 3.2 to 15.2 µm/min (Carvalho et al., 2004), while yeast microtubules grow at a rate of 2.3 ± 0.4 µm/min (Caudron et al., 2008). Thus, Kip2 catches up with the growing microtubule plus-end, both *in vitro* and in the cell. The high processivity and long end-residence time of Kip2 lead to a substantial build-up of this protein at the plus-ends of microtubules, as was also observed for Kip3 (Leduc et al. 2012).

Kip3 disassembles microtubules in a length-dependent manner. This length-dependent disassembly results directly from the motor's high processivity, which assures that almost all motors that land on the microtubule reach the plus-end. Kip3

_____

depolymerizes this microtubule plus-end, by removing on average one or two tubulin dimers per Kip3 molecule. The number of motors that land on a microtubule scales with the length of the microtubule (antenna model (Varga et al., 2009): longer microtubules collect more Kip3 at their plus-ends and therefore depolymerize more quickly (Varga et al., 2009).

By stark contrast, Kip2 assembles microtubules in a length-dependent manner. In the absence of Kip2, microtubules grow at a length-independent rate. At low Kip2 concentrations, microtubule growth rate becomes dependent on microtubule length, as longer microtubules recruit more Kip2 to their plus-ends, which in turn leads to faster growth rates. This length-dependent acceleration of growth starts at shorter microtubule lengths for higher Kip2 concentrations, as seen from the steeper curves at intermediate Kip2 concentrations compared to low Kip2 concentrations. Finally, at high Kip2 concentrations, length dependent acceleration of growth already occurs at very short microtubule length. This length-dependent assemblyby Kip2 is also a result of high processivity: the number of Kip2 molecules that land on a microtubule is proportional to the length of the microtubule, as is the case for Kip3. Thus, Kip3 causes microtubule length-dependent disassembly, whereas the same antenna mechanism results in length-dependent microtubule growth promotion in the case of Kip2 (Figure 4.1).
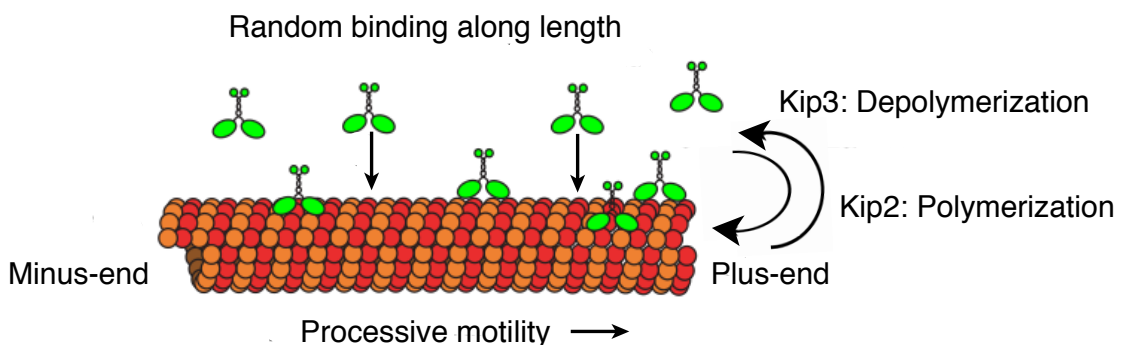
Figure 4.1. Antenna model for length-dependent microtubule depolymerization by Kip3 and length-dependent polymerization by Kip2. Adapted from (Varga et al., 2009).
In the antenna model described for kinesin-8 Kip3, motors randomly bind to the microtubule along its lattice. The number of binding events per unit of time scales with the length of the microtubule. As a result of high processivity, approximately all motors will reach the microtubule plus-end, where they cause depolymerization. Longer microtubules collect more motors and therefore depolymerize more quickly. This antenna model also applies to microtubule growth promotion by Kip2: instead of length-dependent depolymerization, Kip2 causes length-dependent microtubule polymerization.

_____

4.5.   Kip2 promotes microtubule growth through a positive feedback mechanism

Kip2 promotes microtubule growth in a length-dependent manner: as microtubules grow, Kip2 binds to them, which results in faster growth rates and prevention of catastrophe. As a consequence, microtubules become longer and through their antenna function will collect even more Kip2. This results in a positive feedback mechanism for promotion of microtubule growth. Likely, this positive feedback mechanism promotes the growth of cytoplasmic microtubules that grow into the yeast bud (Figure 4.2). Thus, Kip2 is believed to pave its own way on cytoplasmic microtubules by speeding up microtubule growth and inhibiting catastrophe.
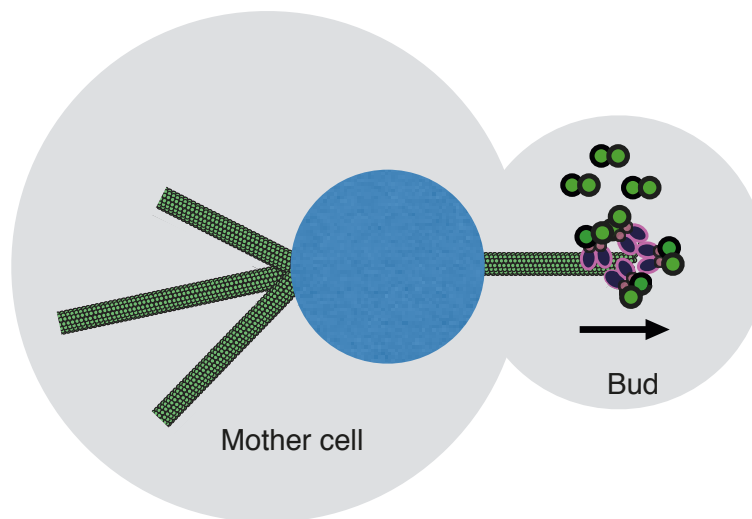
Figure 4.2. Kip2 paves its own way on cytoplasmic microtubules.
When cytoplasmic microtubules start growing from the SPB, they act as an antenna for Kip2 to land on. Next, Kip2 will walk to and catch up with the growing plus-end, where it increases the microtubule growth rate and prevents catastrophe. These behaviors result in a positive feedback mechanism: growing microtubules collect progressively more Kip2, Kip2 subsequently promotes the growth of its own track. Image is courtesy of Prof. Dr. J. Howard.

When enough Kip2 is present to continuously saturate the microtubule plus-end, this positive feedback mechanism should result in an unbounded state of microtubule growth, where the average velocity with which a population of microtubules grows is positive (Verde et al., 1992). Possibly, this unbounded growth is observed when Kip2 is over-expressed *in vivo* (Carvalho et al., 2004) and at higher Kip2 concentrations *in*

_____

vitro (this work). This suggests that in the wild-type budding yeast cell, the Kip2 concentration is lower than required for hyper-elongation, the activity of Kip2 is antagonized, or Kip2 is spatially and/or temporally down-regulated. In *kip3Δ* cells, cytoplasmic microtubules are longer than in wild-type (Cottingham and Hoyt, 1997)., suggesting that the antagonistic actions of Kip3 and Kip2 could balance microtubule length. In addition, Kip2 could be down-regulated by phosphorylation of Kip2's N-terminal phosphoserines (D. Liakopoulos, personal communication).

4.6.   Possible mechanisms for promotion of microtubule growth by Kip2: the tubulin shuttle model

Kip2 increases microtubule growth rates, but the mechanism by which it does so is currently unknown. A potential mechanism by which Kip2 increases microtubule growth rates is by shuttling tubulin to the microtubule plus-end and thereby locally increasing the tubulin concentration. In support of this mechanism, Kip2 is able to bind tubulin from solution, as is the case for Kip3 (Su et al., 2011). Moreover, Kip2 transports this soluble tubulin to the microtubule plus-end. This finding suggests that Kip2 has a tubulin-binding domain. However, efforts to identify such a domain (Chapter 3.3), were not successful.

If Kip2 increases microtubule growth rates by shuttling tubulin to the plus-end, then the flux of Kip2:tubulin complexes must be high enough to account for the measured increase in microtubule growth rate. At first sight, the flux of Kip2 to the plus-end appears too low to account for the increase in growth rate: at 20 nM Kip2 and 8 nM tubulin, 30 Kip2 molecules arrive at the plus-end per minute, whereas the microtubule growth rate is ~640 dimers per minute of which ~360 are attributed to Kip2. Thus, each Kip2 molecule would need to carry at least 12 tubulin dimers to account for the measured increase in microtubule growth rate. While the transport of tubulin oligomers seems unlikely in light of the lack of obvious tubulin-binding domain in the Kip2 sequence, the measured average number of tubulin dimers transported per particle was 9-12. Thus, the flux of these tubulin oligomers approximates the flux necessary to account for the measured increase in microtubule growth rate.

Depending on the number of Kip2 molecules at the microtubule plus-end (1 to 13), the total rate by which Kip2 departs from the plus-end is 10 to 130 molecules per minute. In the shuttle model, this would require that every Kip2 carries 36 to 3 tubulins (because Kip2 adds 360 dimers per minute). However, because the

microtubule growth rate is limited by the lower value of either the arrival rate or the departure rate, each Kip2 would have to carry 12-36 tubulin dimers. The measured average number of 9-12 tubulin dimers per transport particle is at the low end of the required number to account for the increase in microtubule growth rate.

One important prediction of the shuttle model is that an increase in the Kip2 concentration leads to an increase in the amount of tubulin being delivered at the plus-end, which in turn should result in a higher microtubule growth rate. At 40 nM Kip2 and 8 nM tubulin, 90 Kip2 molecules arrive at the plus-end per minute, compared to 30 molecules per minute at 20 nM Kip2. By contrast, the microtubule growth rate saturates between 20-40 nM Kip2.

In addition, another important prediction of the shuttle model is that the amount of tubulin being delivered at the plus-end scales with the length of the microtubule. Longer microtubules should collect more Kip2:tubulin, which in turn should result in higher microtubule growth rates. The data show that Kip2 indeed is a length-dependent polymerase. However, the length-dependence saturates at a certain microtubule length and the higher the Kip2 concentration, the shorter the microtubules are when growth rates saturate. Together, these findings strongly argue against the shuttle model.

The shuttle model could only explain the observed saturation of the microtubule growth rate in the case of the existence of Kip2 traffic jams at the microtubule plus-end. If the arrival rate of Kip2 to the microtubule plus-end would exceed the departure rate of Kip2 from the plus-end, a Kip2 traffic jam would form on the microtubule lattice that would prevent the delivery of tubulin cargo to the site of microtubule growth. At 20 nM, 30 Kip2 molecules arrive at the plus-end per minute. Each of these Kip2 molecules spends on average 6 s at the microtubule plus-end: the departure rate therefore is 10 molecules per minute. However, because there are 13 protofilaments to dissociate from, the total departure rate will be 130 Kip2 molecules per minute. Thus, the departure rate exceeds the Kip2 arrival rate about 4-fold. This means that traffic jams are not expected to occur under the experimental conditions where microtubule growth rate was saturated. At 40 nM Kip2, 90 Kip2 molecules arrive at the microtubule plus-end per minute, whereas the departure rate is 130 per minute. Therefore, no traffic jams should form below 40 nM Kip2. This argument holds independent of how many tubulin dimers are carried per Kip2 molecule.

_____

In conclusion, the data is inconsistent with a tubulin shuttle model, because:

a) the measured arrival and departure rates are at the lower boundary to account for the increase in microtubule growth rate.

b) the shuttle model can not reconcile the increased flux of Kip2 to the plus-end with the saturation of microtubule growth at 20-40 nM Kip2, as the measured Kip2 arrival and departure rates indicate that traffic jams should not form on dynamic microtubules under these experimental conditions.

c) the length-dependent increase in growth rate also saturates at high Kip2 concentrations.

d) no evidence for a functional tubulin-binding domain was found in the Kip2 sequence.

4.7.   Possible mechanisms for promotion of microtubule growth by Kip2: the polymerase model

Rather than promoting microtubule growth by shuttling tubulin to the microtubule plus-end, Kip2 is thought to promote microtubule growth by acting as a processive polymerase while at the plus-end. The limited number of Kip2 binding sites at the growing plus-end appears to be the rate-limiting factor for microtubule growth. Increasing the Kip2 concentration from 20 to 40 nM Kip2 neither affects the end-residence time of Kip2 at the growing microtubule plus-end, nor the microtubule growth rate. This indicates that it is not the rate of arrival, but the saturation of Kip2 at the growing plus-end that is rate-limiting for microtubule growth. Thus, Kip2 uses its processive motility to reach and track the growing plus-end, where it functions primarily as a processive polymerase that adds multiple tubulin dimers to the microtubule plus-end.

Kip2 dwells at the microtubule plus-end for 6 seconds. During these 6 seconds, the microtubule grows by 64 dimers, of which 36 are added by Kip2. If the microtubule plus-end is saturated with Kip2, then ~13 Kip2 molecules are present. Thus, each Kip2 is adding about 3 tubulin dimers during its time at the plus-end. During this time, the microtubule grows about 40 nm. Therefore, each Kip2 molecule must surf about 5 tubulin dimers to stay at the growing microtubule plus-end. In summary, each Kip2 is adding 3-36 tubulin dimers, depending on how many active molecules are present at the plus-end.

4.8.   Possible mechanisms by which Kip2 affects tubulin binding kinetics

A key question is how Kip2 affects tubulin binding kinetics. Three possible, yet speculative mechanisms are described here. In the absence of Kip2, tubulin dimers encounter the microtubule plus-end by diffusion. These interactions are short lived, and the tubulin dimer often diffuses away (Figure 4.3A).
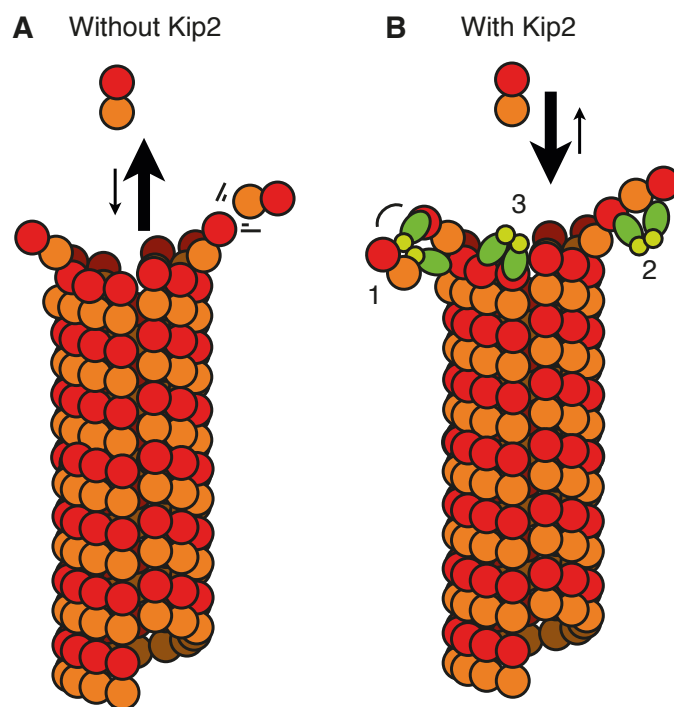
Figure 4.3. Possible mechanisms by which Kip2 could affect tubulin binding kinetics.
Schematic of a growing microtubule in the absence (A) or presence (B) of Kip2.

1). Kip2 binds and processively adds tubulin to the growing microtubule.

2). Kip2 stabilizes an intermediate microtubule:tubulin state and thereby facilitates incorporation.

3). Kip2 stabilizes the microtubule via lateral protofilament interactions.

Kip2 present at the microtubule plus-end (Figure 4.3B) could increase the tubulin on-rate by binding tubulin dimers from solution and processively adding them to the growing microtubule. Alternatively, Kip2 could increase the tubulin on-rate and decrease the GTP-tubulin off-rate by stabilizing an intermediate state in which the incoming tubulin dimer is only weakly attached to the protofilament, thereby reducing

_____

the likelihood of the tubulin dimer to diffuse away. Finally, Kip2 could decrease the tubulin off-rate by increasing lateral protofilament interactions. These (possibly combined) mechanisms would result in the reported increase in microtubule growth rate and decrease in catastrophe frequency. Other mechanisms, such as facilitated tubulin dimer straightening by Kip2 upon incorporation into the lattice, are also imaginable. To elucidate exactly how Kip2 affects tubulin binding kinetics, its crystal structure (in combination with tubulin) should be determined.

4.9. Kip2 decreases catastrophe frequency by increasing the on-rate and decreasing the off-rate of tubulin

Kip2 increases microtubule growth rate and decreases microtubule catastrophe frequency by increasing the rate of tubulin association with the growing microtubule plus-end, and through a decrease in the GTP-tubulin dissociation rate. A recent theoretical model postulates that a GTP cap protects the microtubule plus-end, as long as dissociation of the terminal GTP-tubulin from a protofilament end does not expose a hydrolyzed GDP-tubulin in the next position. This model predicts that the catastrophe frequency increases with both the rate of GTP hydrolysis (h) and the GTP-tubulin dissociation rate (k_{off}) and decreases with the microtubule growth rate $k_{on} \cdot [Tb]$ (Bowne-Anderson et al., 2013) following Equation 4.

$$k_{cat} \approx 4 \frac{h k_{off}}{k_{on}[Tb]}$$
(4)

Interestingly, the decrease in catastrophe frequency induced by Kip2 was much larger than the 3-fold increase in growth rate; this suggests that the increased tubulin on-rate by Kip2 only partly explains the strongly decreased catastrophe frequency. Following Equation 4, the 3-fold decrease in microtubule shrinkage rate, together with the measured 3-fold increase in microtubule growth rate, should result in a 9-fold decrease in catastrophe frequency. Indeed, at 20 nM Kip2, an 8-fold decrease in catastrophe frequency was measured. Whether Kip2 further reduces the catastrophe frequency by inhibiting the rate of GTP hydrolysis was not tested.

_____

4.10. The binding rate of Kip2 at low concentrations is high enough to saturate the growing plus-end

Kip2 prevents microtubule catastrophe in a length-dependent manner. This length-dependence became apparent at 5 nM Kip2 of microtubule grown with porcine tubulin. This finding suggests that the longer microtubules that escape from catastrophe have between 1 and 13 Kip2 molecules at the microtubule plus-end at any time (to prevent catastrophe). This raises the question whether the binding rate of Kip2 is high enough to saturate the dynamic microtubule plus-end.

At 5 nM, Kip2 binds to stabilized microtubules at a rate of 0.03 $\mu m^{-1} \cdot s^{-1}$ (extrapolated from the binding rates at 21 nM and 41 nM Kip2). Assuming a seed length of 2 μm and 14 protofilaments per microtubule seed, it takes on average (14/0.06) = 4 minutes for 14 Kip2 molecules to bind to the microtubule. During this time, the microtubule would have grown 2.4 μm (4 min * 0.6 μm/min). On dynamic microtubules, Kip2 walks at a pace of 2.8 μm/min. Therefore, bound Kip2 molecules reach the growing plus-end within 1 minute. Thus, at a seed length of 2 μm and 5 nM Kip2, it takes less than 5 minutes to saturate the growing plus-end with Kip2. In the absence of Kip2, microtubules catastrophe on average once every six minutes. Thus, the first Kip2 molecules that land on the microtubule would have enough time to reach the plus-end and prevent catastrophe. At 2 nM Kip2, it takes 22 minutes for 14 Kip2 molecules to reach the microtubule plus-end: the Kip2 binding rate is too low to saturate the growing plus-end before the microtubule experiences catastrophe. At Kip2 concentrations above 5 nM, increasingly shorter microtubules will escape catastrophe.

4.11. The microtubule plus-end tracking protein complex Kip2-Bim1-Bik1 promotes microtubule growth

Kip2 promotes microtubule growth, both alone and in combination with accessory budding yeast MAPs Bik1 and Bim1. Others showed that Bik1 and Bim1 act as processivity factors for Kip2 *in vitro* (Roberts et al., 2014). Roberts and colleagues reported an average run- length of Kip2-Atto647 along taxol-stabilized microtubules of only 1.2 ± 0.1 μm, which is much shorter than the run length of Kip2-eGFP in this work (4.1 ± 0.2 μm along GMPCPP-stabilized microtubules). This discrepancy in run-

_____

length could be due to the differences in protein source (yeast compared to insect cells), the difference in nucleotide state of the stabilized microtubule (taxol-stabilized compared to GMPCPP-stabilized), the ionic strength and composition of the experimental buffers (160 mM compared to 140 mM) and/or the fluorescent labels of the purified proteins (Atto-647 compared to eGFP). Recently, it was shown that some fluorescent tags, amongst which eGFP, artificially increase the run-length of kinesin-1 (Norris et al, 2015). The finding that both labeled and unlabeled Kip2 promote microtubule growth to a similar extent strongly suggests that unlabeled Kip2 is highly processive and reaches the growing microtubule plus-end. Thus, any putative over-estimation of the run-length of Kip2 due to the eGFP tag should not affect the overall conclusions of this work. Interestingly, Roberts and colleagues found that in the presence of both Bik1 and Bim1, the run-length of Kip2 increased to 4.8 ± 0.3 µm, similar to the run-length observed in this work with Kip2 alone. Perhaps Bik1 and Bim1 increase the affinity of Kip2 to microtubules in their assays to the affinity that Kip2 has in the assays described in this work.

Bik1 alone decreases average microtubule length, however, in combination with either Kip2 or Bim1 its inhibitory effect on microtubule length is lost. This is in agreement with (Blake-Hodek et al., 2010), who reported that Bim1 and Bik1 in combination affect microtubule dynamics in the same way as Bim1 alone. Interestingly, the fact that the combination of Bim1 with Kip2 increases microtubule length beyond the effect of these proteins alone strongly suggests that Kip2 and Bim1 affect length through different mechanisms. However, Bim1 binding did not discriminate between microtubule seeds and extensions in this work. The fact that Bim1-eGFP does not behave as a microtubule plus-end tip-tracker *in vitro* was also observed in other labs (D. Liakopoulos, personal communication). Possibly, this aberrant unspecific microtubule localization is due to the use of porcine instead of yeast tubulin. Therefore, to draw firm conclusions about the differential growth promoting effects of Kip2 and Bim1, these experiments have to be repeated using conspecific yeast tubulin.

4.12. Kip2 is a weaker polymerase with yeast tubulin than with porcine tubulin

The finding that Kip2 has a weaker polymerase effect on its conspecific yeast tubulin than on porcine tubulin is unexpected: others have reported enhanced enzyme

activity as a result of using conspecific tubulins (Alper et al., 2013; Podolski et al., 2014). Possibly, the reduced propensity of Kip2 to polymerize yeast tubulin is due to the differential treatment of the two tubulin pools: the porcine tubulin was cycled prior to being used in the dynamic microtubule assays, whereas the yeast tubulin was not cycled, due to its low starting concentration and volume. The cycling step removes inactive tubulin and aggregates and therefore may have caused higher purity and affinity of the porcine tubulin pool. Future experiments using cycled yeast tubulin should show whether Kip2 truly is a weaker polymerase of yeast compared to porcine tubulin.

4.13.   Conclusion and outlook

The aim of this project was to decipher the mechanism by which budding yeast kinesin Kip2 regulates microtubule dynamics, in order to provide insight into how kinesins control microtubule length. The outcome of this work shows that a kinesin motor can act directly as a length-dependent microtubule polymerase and anti-catastrophe factor in the absence of accessory proteins.

The mechanism by which Kip2 affects tubulin binding kinetics remains unknown. One way to start approaching this question would be to solve the crystal structure of Kip2 associated with tubulin using X-ray crystallography and to study Kip2 at microtubule plus-ends using cryoelectron microscopy.

The regulation of microtubule dynamics by Kip2 results in microtubule hyper-elongation. In the budding yeast cell, however, microtubule dynamics are simultaneously under regulation of Kip2's antagonist, Kip3. In light of the resemblance between Kip2 and Kip3 in both biophysical properties and their regulation of microtubule dynamics, it will be exciting to learn how microtubule length is affected when the microtubule is exposed to both motors simultaneously. Kip3 and Kip2 will compete for the same kinesin binding site at the microtubule plus-end, which is limited in number. Therefore, one prediction for this experiment is that the motor that has the highest affinity for the microtubule plus-end will out-compete the other motor in terms of length-dependent polymerase or depolymerase activities.

5.   Materials and Methods

5.1.   Protein expression and purification protocols

5.1.1.   Cloning of Kip2

The coding region of *KIP2* was PCR amplified, using genomic DNA of *Saccharomyces cerevisiae* strain W303 as a template, with the following primers:

Forward: AATAATAACAT<u>GCGGCCGC</u>AATGATTCAAAAAATGAGCCCAAGC

Reverse: AATAATAACAT<u>GGCGCGCC</u>TTTATCGTTATCCACGACAGGGTG

The resulting PCR product was run on a 0.8% agarose gel and purified from this gel using a Qiaquick gel extraction kit (Qiagen). The purified PCR product was digested overnight at 37^{0}C with restriction enzymes NotI-HF and AscI (New England Biolabs) to expose its ligation sites. After digestion, the PCR product was purified using a PCR purification kit (Qiagen).

Next, the PCR product was ligated into destination vector pOCC5 (Table 10) and transformed into *E.coli* DH5α cells by heat shock. Bacteria were grown on LB plates supplemented with ampicilin. Plasmids were extracted using a miniprep kit (Qiagen) and sequenced by the MPI-CBG in-house sequencing facilities to confirm sequence and reading frame. Finally, the correct DNA fragment was ligated into destination vectors (Table 10), resulting in the protein constructs 6xHis-Kip2, 6xHis-Kip2–eGFP and Kip2-HA3.

5.1.2.   Cloning of Kip2 truncation mutants

C-terminally or N-terminally truncated coding regions of *KIP2* were PCR amplified from 6xHis-Kip2 plasmid DNA using the following primers:

Kip2pΔC
Forward: AATAATAACAT<u>GCGGCCGC</u>AATGATTCAAAAAATGAGCCCAAGC
Reverse: AATAATAACAT<u>GGCGCGCC</u>CCCGTTACTGATGATGGATTTTTTGGA

_____

Kip2pΔN

Forward:AATAATAACAT<u>GCGGCCGC</u>AATGAGAAAAAACGATACATATACTGGGTCA

Reverse: AATAATAACAT<u>GGCGCGCC</u>TTTATCGTTATCCACGACAGGGTG

Next, PCR products were digested with NotI and AscI and then ligated into destination vector pOCC16, following the procedure described above for Kip2, to obtain 6xHis-Kip2ΔN-eGFP and 6xHis-Kip2ΔC-eGFP (Table 10).

5.1.3.   Cloning of Kip2_ala mutant using alanine substitution mutagenesis

To mutate 4 amino acids in the KIP2 gene (K670A, K672A, R684A and K686A), a synthesized KIP2 fragment with corresponding nucleotide substitutions was ordered from Genscript. This fragment starts at the OliI restriction site (bp 1971) and runs up to the stop codon, with addition of a 3' AScI restriction site. To obtain the Kip2_ala-HA3 mutant expression construct, the wild-type OliI-AScI fragment was replaced by the mutated fragment and ligated into the yeast expression plasmid OCC78 (Table 10). The mutated DNA fragment was sequenced by the MPI-CBG in-house sequencing facilities to confirm sequence and reading frame. Finally, the DNA fragment was digested from the yeast plasmid and ligated into destination vector OCC16 for expression in insect cells (Table 10).

5.1.4.   Protein expression of Kip2 constructs in insect cells

Kip2 protein constructs were expressed in SF+ cells via baculovirus infection. Baculovirus was obtained using the Bac-to-Bac system (Invitrogen). Expression of the protein of interest was checked by SDS-PAGE gel and confirmed by Western blot using anti-6xHis antibody. A time-course was conducted to find the peak in protein expression. Cells were harvested at the time of peak expression, washed with PBS and frozen at -80°C for later purification.

_____

5.1.5.   Protein purification of Kip2 constructs

Proteins were purified via affinity chromatography using 1 ml His-affinity columns (GE Healthcare). The purification protocol was based on The Qiaexpressionist handbook protocol #16 for purification of 6xHis-tagged proteins (Qiagen) and optimized for purification of Kip2, as follows:

1. Cell pellets of 2.5 ml were melted on ice in the cold room, 25 ml lysis buffer was added and the suspension was vigorously dounced 20 times on ice using a glass dounce homogenizer.

2. Cells were left on for 10 additional minutes for complete lysis.

3. 10 µl Benzonase (Novagen) was added to degrade DNA and RNA and a sample was taken for analysis on SDS-PAGE gel.

4. The cell suspension was spun at 40.000 rpm. for 1 hour at 4°C in a Beckman Coulter Optima ultracentrifuge using a Ti45 rotor. Afterwards, a sample was taken for analysis on SDS-PAGE gel.

5. Next, the supernatant was loaded on a 1 ml 6xHis-affinity column (GE Heathcare) at a flowrate of ~1 ml/minute. A sample of the flow-through was taken for analysis on SDS-PAGE gel.

6. The column was washed with 10 column volumes of lysis buffer and a sample of the flow-through was taken for analysis on SDS-PAGE gel.

7. The column was washed with 10 column volumes of wash buffer containing 100 mM imidazole and protein inhibitors. A sample of the flow-through was taken for analysis on SDS-PAGE gel.

8. The column was washed with 10 column volumes of wash buffer containing 100 mM imidazole without protein inhibitors.

9. The protein of interest was eluted from the column in 1 ml fractions using elution buffer containing 300 mM imidazole.

10. Protein concentrations of the eluted fractions were monitored using Bradford reagent (Biorad): 4 µl of eluted protein into 200 µl of 5x diluted Bradford solution.

11. Peak elution fractions were pooled and further purified. A sample of the pooled fractions was taken for analysis on SDS-PAGE gel.

12. Affinity column purification success was checked by SDS-PAGE and Western blot using anti-6xHis antibody. The used buffers used are listed in Table 13.

_____

5.1.6.   Enzymatic cleaving of the 6xHis-tag

The 6xHis-tag was enzymatically cleaved from the protein of interest as follows:

1. Directly after elution, PreScission protease (GE Heathcare) was added to the 300 mM imidazole elution fraction in a 1:50 dilution.
2. This elution fraction containing PreScission protease was incubated overnight on a rotary wheel at 4°C.
3. The next day, the stability of protein of interest was confirmed by SDS-PAGE and enzymatic cleavage of the 6xHis-tag from the protein of interest was confirmed by Western blot using anti-6xHis-antibody.

5.1.7.   Gel filtration of purified proteins

After His-affinity column purification and enzymatic cleavage of the 6xHis-tag, proteins of interest were purified to homogeneity by gel filtration over a Sephadex 200 column using storage buffer (Table 13). Final protein purity was checked by mass spectroscopy at the MPI-CBG in-house Mass Spec facility. Purified proteins were snap-frozen using liquid nitrogen and stored at -80 °C.

5.1.8.   Determination of protein concentration

Purified protein concentrations were determined by spectrophotometry. Bradford reagent (Biorad) was diluted 1:4 with H2O in 1 ml plastic cuvettes. Next, 33 µl and 66 µl reagent were replaced by purified protein in storage buffer or by storage buffer alone (blank). Light absorbance was measured at 595 nm. These measurements were done in duplicate. As a control, protein concentrations of Kip2 and Kip2-eGFP were also determined by SDS-PAGE using BSA standards of known concentration and the purified protein of interest. These two techniques yielded the same results.

_____

5.1.9.   Cloning of Bik1 and Bim1

The coding region of *BIK1* was PCR amplified, using genomic DNA of *Saccharomyces cerevisiae* strain W303 as a template, with the following primers:

Forward: AATAATAACAT<u>GCGGCCGC</u>AATGGATAGATATCAAAGAAAGATAGGATG

Reverse: AATAATAACAT<u>GGCGCGCC</u>GAAGAACTGCTGGTTGTCAGGATTG

The coding region of *BIM1* was PCR amplified from *Saccharomyces cerevisiae* genomic DNA using the following primers:

Forward: AATAATAACAT<u>GCGGCCGC</u>AATGAGTGCGGGTATCGGAGAATC

Reverse: AATAATAACAT<u>GGCGCGCC</u>AAAAGTTTCCTCGTCGATGATCAAGTTG

Next, the PCR products were digested with Not1 and Asc1 and then ligated into destination vectors, following the procedure described above for Kip2, to obtain 6xHis-Bik1-eGFP for expression in SF+ cells and 6xHis-Bim1-eGFP for expression in *E. coli* (Table 10). Plasmids were extracted using a miniprep kit (Qiagen) and sequenced by the MPI-CBG in-house sequencing facilities to confirm protein sequence and reading frame.

5.1.10.   Protein purification of Bik1-eGFP from SF+ cells

6xHis-Bik1-eGFP was expressed in insect cells as described in § 5.1.4. and affinity purified following the protocol described in (Blake-Hodek et al., 2010). Next, the 6xHis-tag was cleaved off as described in § 5.1.6. and proteins were purified to homogeneity using gel filtration as described in § 5.1.7.

5.1.11.   Expression of 6xHis-Bim1-eGFP in *E.coli*

6xHis-Bim1-eGFP was transformed by heat shock into BL21 pRARE cells. Cells were plated on LB plates supplemented with kanamycin. 6xHis-Bim1-eGFP was expressed in bacterial cells as follows:

1.   A start culture of 20 ml cells strain was grown overnight at 37°C.

_____

2.   The next day, 2 ml of start culture was diluted 500x in 1L LB supplemented with kanamycin and chloramphenicol and grown until OD = 0.5.

3.   Cells were then placed at 18°C for 1 hour after which expression was induced by 1 mM IPTG.

4.   Cells were grown overnight at 18°C and then harvested, washed with PBS, snap-frozen and stored at -80°C.

5.1.12.   Protein purification of Bim1-eGFP

6xHis-Bim1-eGFP was kindly affinity purified by Dr. Aliona Bogdanova, following the protocol described in (Blake-Hodek et al., 2010). Next, the 6xHis-tag was cleaved off as described in § 5.1.6. and proteins were purified to homogeneity using gel filtration as described in § 5.1.7.

5.2.   Tubulin protocols

5.2.1.   Purification of porcine brain tubulin

Porcine brain tubulin was purified as described in (Gell et al., 2011) in a joint effort with members of the Howard lab. Final PC tubulin was concentrated prior to cycling using 15 ml spin-filters with a 30 kDa cut-off (Amicon).

5.2.2.   Cycling of tubulin

All porcine tubulin was cycled prior to usage to remove inactive (unpolymerizing) tubulin, free nucleotides in solution and aggregates, as described in (Gell et al., 2010). The cycled tubulin concentration was measured by absorbance at 595 nm using Bradford reagent (Biorad) in a spectrophotometer.

_____

5.2.3.   Labeling of tubulin

Porcine tubulin was labeled with Alexa Fluor 488 or TAMRA (Invitrogen), as described in (Hyman et al., 1991).

5.2.4.   Purification of yeast tubulin

Purification of yeast tubulin was described in (Widlund et al., 2012). The yeast tubulin used in this thesis work was provided by Dr. Marija Podolski. Due to its low abundance, yeast tubulin was not cycled nor labeled prior to usage in microscopy experiments.

5.2.5.   Ready-to-use and biotinylated tubulin preparations

The 30% tetrarhodamine-labeled ready-to-use tubulin used in this thesis work was kindly provided by Heike Petzold. Biotynilated tubulin was kindly provided by Corina Braeuer.

5.2.6.   Polymerization of GMPCPP-stabilized microtubules

Reagents used to polymerize GMPCPP-stabilized microtubules are listed in Table 11. Reagents were mixed, incubated on ice for 5 minutes and transferred to 37°C to allow polymerization of microtubules. For dynamic microtubule assays, GMPCPP-stabilized microtubules were incubated at 37°C for 20 minutes, while for stabilized microtubule assays, GMPCPP-stabilized microtubules were incubated for 2-3 hours. Subsequently, microtubules were diluted in 350 µl BRB80 at room temperature and centrifuged for 6 minutes using a Beckman airfuge to remove free tubulin. After centrifugation, the supernatant was aspired and the pellet was resuspended in 200 µl BRB80.

5.2.7. Polymerization of taxol-stabilized microtubules

Reagents used to polymerize taxol-stabilized microtubules are listed in Table 12. Reagents were mixed, incubated on ice for 5 minutes and transferred to 37°C to allow microtubule polymerization for 30 minutes. Meanwhile, 10 µl of 1mM taxol in DMSO was diluted 1:100 in BRB80. After incubation, 10 µl of polymerized microtubules were diluted in 990 µl taxol-BRB80. Taxol stabilized microtubules were centrifuged for 6 minutes using a Beckman airfuge to remove free tubulin. After centrifugation, the supernatant was aspired and the pellet was resuspended in 200 µl taxol-BRB80.

5.3. Microscopy assay protocols

5.3.1. Glass silanization

Glass cover slips sized 22x22 ± 0.005 mm and 18x18 ± 0.005 mm (Menzel-Glaeser) were silanized as described in (Gell et al., 2010).

5.3.2. Flow cell preparation

Flow cell chambers were made as described in (Gell et al., 2010), using silanized coverslips but parafilm instead of double-sided scotch.

Flow cell channels were prepared at the bench as follows:

1. 20 µl BRB80 was flown into the flow cells.

2. Anti-rhodamine antibodies (Sigma-Aldrich) diluted 1:50 in BRB80 were flown into the channel and incubated for 10 minutes.

3. The channel was washed with 40 µl BRB80 to remove unbound antibodies.

4. 20 µl F127 (Sigma-Aldrich) was flushed in and incubated for 30 minutes to passify the coverglass surface.

_____

5.   Channels were washed with 80 µl BRB80 to remove unbound F127.

6.   20 µl of stabilized rhodamine-labeled microtubule seeds, diluted 1:10 in
       BRB80, were perfused into the channel using filter paper and incubated for
       10 minutes.

7.   The channel was washed 2 times with 20 µl BRB20 to remove unbound
       microtubule seeds and to substitute BRB80 for BRB20.

Next, the chamber holder was mounted onto the microscope to allow the flow cell
channels to heat to 28°C.

5.3.3.   Dynamic microtubule assay - porcine tubulin

Dynamic microtubule assays were performed to measure effects of Kip2 on dynamic
microtubules grown with labeled porcine tubulin. For dynamic microtubule assays,
flow cell channel preparation continued as follows:

8.   20 µl polymerization buffer including 12 µM 8% Alexa-488 labeled tubulin and
       Kip2 or Kip2-eGFP in solution was perfused into the channel.

TIRF microscopy time-lapse imaging was started exactly 10 minutes after perfusion
of the polymerization buffer.

5.3.4.   Dynamic microtubule assay - yeast tubulin

Dynamic microtubule assays were performed to measure effects of Kip2 on dynamic
microtubules grown with unlabeled yeast tubulin. For dynamic microtubule assays,
flow cell channel preparation continued as follows:

8.   20 µl polymerization buffer including unlabeled yeast tubulin and Kip2 in
       solution was perfused into the channel.

DIC microscopy time-lapse imaging was started after perfusion of the polymerization
buffer.

_____

5.3.5.   Single-molecule motility assay

Single-molecule motility assays were performed to measure biophysical properties of Kip2p-eGFP on nondynamic microtubules. For single-molecule motility assays, flow cell channel preparation continued as follows:

8.   20 µl motility buffer including Kip2-eGFP in solution was perfused into the channel.

TIRF microscopy time-lapse imaging was started directly after perfusion of motility buffer into the channel.

5.3.6.   Tubulin transport assay

Tubulin transport assay on tetrarhodamine-labeled GMPCPP-stabilized tubulin seeds was performed as follows:

1.   Surface-bound microtubules were pre-washed with 20 µl imaging buffer, supplemented with 40 nM Kip2 and 1 mM AMP-PNP.

2.   Next, 20 µl imaging buffer supplemented with 1 µM 60% Alexa-488 labeled tubulin and 1 mM AMP-PNP was flushed in.

3.   Finally, unbound tubulin was washed out with 20 µl imaging buffer supplemented with 1 mM AMP-PNP or 1 mM ATP.

TIRF microscopy time-lapse imaging was started directly after perfusion of motility buffer into the channel.

5.3.7.   TIRF Microscopy

Rhodamine-labeled proteins were excited by EPI-fluoresence using a HBO100 mercury lamp. EGFP-labeled proteins were excited using a 488 nm laser line (Ion Laser Technology). Imaging was performed with an Andor iXon camera on a Zeiss Axiovert 200M microscope with a Zeiss ×100/1.46 plan apochromat oil objective and standard filter sets. An objective heater (Zeiss) was used to warm the sample to 28 °C. All experiments were performed at least three times on three different days.

5.3.8.   DIC Microscopy

The set-up used in the DIC microscopy experiments was described in (Bormuth et al., 2007).

5.3.9.   Image and data analysis

Image analysis was performed by creating kymographs of microtubule growth events and single-molecule motility events in ImageJ. Data analysis was performed using Matlab, Graphpad, Excel, Igor Pro and Motiontracking software packages.

5.3.10.   Statistics and graphics

Statistical analyses were performed using Matlab, Graphpad, Excel, Igor Pro, Motiontracking and Adobe Illustrator software packages.

5.4.   Budding yeast protocols

5.4.1.   Budding yeast transformation

Kip2-HA3 and Kip2_ala-HA3 plasmids (§ 5.1.3.) were expressed in *Saccharomyces cerevisiae* strain TH663 W303, MATα his3::GFP-TUB1-HIS3, which expresses GFP-labeled α-tubulin. This strain was kindly provided by Prof. Dr. Anthony Hyman. To make cells competent for heat shock transformation, 50 ml of cells were grown in

_____

YPD medium until OD = 0.5-0.7 and pelleted at 4000 rpm. for 5 minutes at room temperature. Next, cells were washed once with 25 ml of 1M Sorbitol/1M LiAc solution, pelleted again and after removal of the supernatant by decanting, cells were resuspended in the remaining liquid.

The transformation reaction mix consisted of 25 µl of linearized plasmid (cut with Cla1), 15 µl of salmon sperm DNA (Sigma-Aldrich), 100 µl of competent cells and 280 µl of 50% PEG 40000 in water. This mix was incubated at for 1 hour at room temperature. Next, 40 µl of DMSO was added, followed by 15 minutes of heat shock at 42 degrees. After the heat shock, 1 ml of YPD was added to the reaction mix. Cells were then pelleted at 4000 rpm. for 5 minutes, the pellet was resuspended is 100 µl YPD buffer, plated on -leu plates to grow for 2 days at 30 °C. To select against false positives, 8 single colonies per plate were streaked on SD -Leu plates to again grow for 2 days at 30 °C.

5.4.2.   Induction of Kip2 expression in budding yeast

Single colonies were inoculated overnight at 30 °C in 2 ml YP medium containing 2% raffinose. The next morning, cultures were diluted in 13 ml of YP medium containing 2% raffinose and incubated for 5 hours. Next, protein expression was induced by addition of 1.5 ml 2% galactose. Cells were grown for 1 hour at 30 °C and subsequently handled for protein extraction or for microscopy experiments.

5.4.3.   Protein extraction from budding yeast

To check the expression level of Kip2 protein constructs in budding yeast cells, proteins were extracted using the following trichloroacetic acid (TCA) protein extraction protocol:

1. Cells were spun down for 5 min at 4000 rpm on a table top centrifuge. The supernatant was removed and tubes were kept on ice.
2. 800 µl of cold 10 % TCA was added. Cells were resuspend, moved to clean 1.5 ml centrifuge tube and kept on ice.

_____

3. Cells were once more spun down at 4000 rpm for 5 min and the supernatant was removed.

4. Cell pellets were frozen in liquid nitrogen.

5. 200 µl of 10 % TCA and 300 µl of glass beads were added to the frozen cell pellet. The cell pellet was vortexed for 20 minutes.

6. 800 µl of 10 % TCA was added, mixed and the supernatant was transferred liquid to a clean centrifuge tube.

7. Supernatant was spun down for 10 minutes at 3000 rpm in a table top centrifuge. Supernatant was removed as precisely as possible.

8. Depending on pellet volume, 50-200 µl of 1 x Laemmli buffer was added, followed by 25-100 µl (half the total volume) of 1 M Tris base to neutralize.

9. The pellet was resuspend by pipetting, boiled for 5 minutes at 95°C and spun down for 10 minutes at 13.000 rpm.

10. Supernatant was moved to a clean centrifuge tube.

11. Protein concentration was measured using Bradford: 800 µl of H2O + 0.5-1 µl of protein sample + 200 µl of Biorad protein assay reagent in a spectrophotometer at 595 nm.

12. Protein samples were analysed using SDS-PAGE.

5.4.4.   Microscopy on budding yeast cells

Kip2 over-expression was induced as described in § 5.4.2. Exactly 45 minutes after galactose addition, cells were pelleted at 4000 rpm for 5 minutes, the supernatant was decanted and cells were resuspended in the remaining medium. Next, cells were perfused into a flow cell. Flow cells were sealed using valap and imaged on a Zeiss 2-photon upright laser scanning microscope with a 63x oil objective using a 488 nm laser line.

References

Akhmanova, A., and Steinmetz, M.O. (2010). Microtubule +TIPs at a glance. J. Cell. Sci. *123,* 3415–3419.

Alper, J.D., Tovar, M., and Howard, J. (2013). Displacement-weighted velocity analysis of gliding assays reveals that Chlamydomonas axonemal dynein preferentially moves conspecific microtubules. Biophys. J. *104,* 1989–1998.

Amos, L.A. (2004). Microtubule structure and its stabilisation. Org. Biomol. Chem. *2,* 2153–2160.

Arnal, I., Heichette, C., Diamantopoulos, G.S., and Chrétien, D. (2004). CLIP-170/ tubulin-curved oligomers coassemble at microtubule ends and promote rescues. Current Biology *14,* 2086–2095.

Bieling, P., Laan, L., Schek, H., Munteanu, E.L., Sandblad, L., Dogterom, M., Brunner, D., and Surrey, T. (2007). Reconstitution of a microtubule plus-end tracking system in vitro. Nature *450,* 1100–1105.

Blake-Hodek, K.A., Cassimeris, L., and Huffaker, T.C. (2010). Regulation of microtubule dynamics by Bim1 and Bik1, the budding yeast members of the EB1 and CLIP-170 families of plus-end tracking proteins. Molecular Biology of the Cell *21,* 2013–2023.

Bormuth V., Howard J. and Schäffer E. (2007). LED illumination for video-enhanced DIC imaging of single microtubules. Journal of Microscopy *226,* 1-5.

Bowne-Anderson, H., Zanic, M., Kauer, M., and Howard, J. (2013). Microtubule dynamic instability: A new model with coupled GTP hydrolysis and multistep catastrophe. Bioessays *35,* 452–461.

Brady, S.T. (1985). A novel brain ATPase with properties expected for the fast axonal transport motor. Nature *317,* 73–75.

Braun, M., Lansky, Z., Bajer, S., Fink, G., Kasprzak, A.A., and Diez, S. (2013). The human kinesin-14 HSET tracks the tips of growing microtubules in vitro. Cytoskeleton *70,* 515–521.

Brouhard, G.J., Stear, J.H., Noetzel, T.L., Al-Bassam, J., Kinoshita, K., Harrison, S.C., Howard, J., and Hyman, A.A. (2008). XMAP215 Is a Processive Microtubule Polymerase. Cell *132,* 79–88.

Browning, H., Hayles, J., Mata, J., Aveline, L., Nurse, P., and McIntosh, J.R. (2000). Tea2p is a kinesin-like protein required to generate polarized growth in fission yeast. The Journal of Cell Biology *151,* 15–28.

Brunner, D., and Nurse, P. (2000). CLIP170-like tip1p spatially organizes microtubular dynamics in fission yeast. Cell *102,* 695–704.

Byers, B., and Goetsch, L. (1975). Behavior of spindles and spindle plaques in the cell cycle and conjugation of Saccharomyces cerevisiae. J. Bacteriol. *124,* 511–523.

Caplow, M., and Shanks, J. (1996). Evidence that a single monolayer tubulin-GTP cap is both necessary and sufficient to stabilize microtubules. Molecular Biology of the Cell *7,* 663.

Carminati, J.L., and Stearns, T. (1997). Microtubules orient the mitotic spindle in yeast through dynein-dependent interactions with the cell cortex. The Journal of Cell Biology *138,* 629–641.

Carvalho, P., Gupta, M.L., Jr, Hoyt, M.A., and Pellman, D. (2004). Cell Cycle Control of Kinesin-Mediated Transport of Bik1 (CLIP-170) Regulates Microtubule Stability and Dynein Activation. Dev. Cell *6,* 815–829.

Caudron, F., Andrieux, A., Job, D., and Boscheron, C. (2008). A new role for kinesin-directed transport of Bik1p (CLIP-170) in Saccharomyces cerevisiae. J. Cell. Sci. *121,* 1506–1513.

Cottingham, F.R., and Hoyt, M.A. (1997). Mitotic spindle positioning in Saccharomyces cerevisiae is accomplished by antagonistically acting microtubule motor proteins. The Journal of Cell Biology *138,* 1041–1053.

Coy, D.L., Wagenbach, M., and Howard, J. (1999). Kinesin takes one 8-nm step for each ATP that it hydrolyzes. Journal of Biological Chemistry *274,* 3667–3671.

Dimitrov, A., Quesnoit, M., Moutel, S., Cantaloube, I., Pous, C. and Perez, F. (2008). Detection of GTP-tubulin conformation in vivo reveals a role for GTP remnants in microtubule rescues. Science *322*, 1353-6.

Cui, W., Sproul, L.R., Gustafson, S.M., Matthies, H.J., Gilbert, S.P., and Hawley, R.S. (2005). Drosophila Nod protein binds preferentially to the plus ends of microtubules and promotes microtubule polymerization in vitro. Molecular Biology of the Cell *16,* 5400–5409.

Dagenbach, E.M., and Endow, S.A. (2004). A new kinesin tree. J. Cell. Sci. *117,* 3–7. Desai, A., and Mitchison, T.J. (1997). Microtubule polymerization dynamics. Annu. Rev. Cell Dev. Biol. *13,* 83–117.

Dixit, R., Barnett, B., Lazarus, J.E., Tokito, M., Goldman, Y.E., and Holzbaur, E.L.F. (2009). Microtubule plus-end tracking by CLIP-170 requires EB1. Proc. Natl. Acad. Sci. U.S.A. *106,* 492–497.

Drechsel, D.N., and Kirschner, M.W. (1994). The minimum GTP cap required to stabilize microtubules. Current Biology *4,* 1053–1061.

Drummond, D.R. (2011). Regulation of microtubule dynamics by kinesins. Seminars in Cell and Developmental Biology *22,* 927–934.

Eshel, D., Urrestarazu, L.A., Vissers, S., Jauniaux, J.C., van Vliet-Reedijk, J.C., Planta, R.J., and Gibbons, I.R. (1993). Cytoplasmic dynein is required for normal nuclear segregation in yeast. Proc. Natl. Acad. Sci. U.S.a. *90,* 11172–11176.

Fink, G., Hajdo, L., Skowronek, K.J., Reuther, C., Kasprzak, A.A., and Diez, S. (2009). The mitotic kinesin-14 Ncd drives directional microtubule–microtubule sliding. Nat. Cell Biol. *11,* 717–723.

Fridman, V., Gerson-Gurwitz, A., Shapira, O., Movshovich, N., Lakamper, S., Schmidt, C.F., and Gheber, L. (2013). Kinesin-5 Kip1 is a bi-directional motor that stabilizes microtubules and tracks their plus-ends in vivo. J. Cell. Sci. *126,* 4147–4159.

Friel, C.T., and Howard, J. (2011). The kinesin-13 MCAK has an unconventional ATPase cycle adapted for microtubule depolymerization. The EMBO Journal *30,* 3928–3939.

Friel, C.T. and Howard, J. (2012). Coupling of kinesin ATP turnover to translocation and microtubule regulation: one engine, many machines. J Muscle Res Cell Motil. 33, 377-83.

Fukuda, Y., Luchniak, A., Murphy, E.R., and Gupta, M.L., Jr (2014). Spatial Control of Microtubule Length and Lifetime by Opposing Stabilizing and Destabilizing Functions of Kinesin-8. Current Biology *24,* 1826–1835.

Ghaemmaghami, S., Huh, W.-K., Bower, K., Howson, R.W., Belle, A., Dephoure, N., O'Shea, E.K., and Weissman, J.S. (2003). Global analysis of protein expression in yeast. Nature *425,* 737–741.

Gard, D.L., and Kirschner, M.W. (1987). A microtubule-associated protein from Xenopus eggs that specifically promotes assembly at the plus-end. The Journal of Cell Biology *105,* 2203–2215.

Gardner, M.K., Haase, J., Mythreye, K., Molk, J.N., Anderson, M., Joglekar, A.P., O'Toole, E.T., Winey, M., Salmon, E.D., Odde, D.J., et al. (2008). The microtubule-based motor Kar3 and plus end-binding protein Bim1 provide structural support for the anaphase spindle. The Journal of Cell Biology *180,* 91–100.

Gardner, M.K., Zanic, M., Gell, C., Bormuth, V., and Howard, J. (2011). Depolymerizing Kinesins Kip3 and MCAK Shape Cellular Microtubule Architecture by Differential Control of Catastrophe. Cell *147,* 1092–1103.

Gardner, M.K., Zanic, M., and Howard, J. (2013). Microtubule catastrophe and rescue. Current Opinion in Cell Biology *25,* 14–22.

Gell, C., Bormuth, V., Brouhard, G.J., Cohen, D.N., Diez, S., Friel, C.T., Helenius, J., Nitzsche, B., Petzold, H., Ribbe, J., et al. (2010). Chapter 13 - Microtubule Dynamics Reconstituted In Vitro and Imaged by Single-Molecule Fluorescence Microscopy (Elsevier).

Gell, C., Friel, C.T., Borgonovo, B., Drechsel, D.N., Hyman, A.A., and Howard, J. (2011). Purification of tubulin from porcine brain. Methods Mol. Biol. *777,* 15–28.

Gibbons, I.R., and Rowe, A.J. (1965). Dynein: A Protein with Adenosine Triphosphatase Activity from Cilia. Science *149,* 424–426.

Goshima, G., Wollman, R., Goodwin, S.S., Zhang, N., Scholey, J.M., Vale, R.D., and Stuurman, N. (2007). Genes Required for Mitotic Spindle Assembly in Drosophila S2 Cells. Science *316,* 417–421.

Gupta, M.L., Carvalho, P., Roof, D.M., and Pellman, D. (2006). Plus end-specific depolymerase activity of Kip3, a kinesin-8 protein, explains its role in positioning the yeast mitotic spindle. Nat. Cell Biol. *8,* 913–923.

Hackney, D.D. (1994). Evidence for alternating head catalysis by kinesin during microtubule-stimulated ATP hydrolysis. Proc Natl Acad Sci. *91,* 6865-9.

Hancock, W.O. and Howard J. (1999). Kinesin's processivity results from mechanical and chemical coordination between the ATP hydrolysis cycles of the two motor domains. Proc Natl Acad Sci. *96,* 13147-52.

Helenius, J., Brouhard, G., Kalaidzidis, Y., Diez, S., and Howard, J. (2006). The depolymerizing kinesin MCAK uses lattice diffusion to rapidly target microtubule ends. Nat. Cell Biol. *441,* 115–119.

Hepperla, A.J., Willey, P.T., Coombes, C.E., Schuster, B.M., Gerami-Nejad, M., McClellan, M., Mukherjee, S., Fox, J., Winey, M., Odde, D.J., et al. (2014). Minus-End-Directed Kinesin-14 Motors Align Antiparallel Microtubules to Control Metaphase Spindle Length. Dev. Cell *31,* 61–72.

Hildebrandt, E.R., and Hoyt, M.A. (2000). Mitotic motors in Saccharomyces cerevisiae. Biochimica Et Biophysica Acta (BBA)-Molecular Cell Research *1496,* 99–116.

Hirokawa, N., Noda, Y., Tanaka, Y., and Niwa, S. (2009). Cytoskeletal motors: Kinesin superfamily motor proteins and intracellular transport. 1–15.

Hirokawa, N., and Tanaka, Y. (2015). Kinesin superfamily proteins (KIFs): Various functions and their relevance for important phenomena in life and diseases. Exp. Cell Res. *15,* S0014-4827.

Honnappa, S., Gouveia, S.M., Weisbrich, A., Damberger, F.F., Bhavesh, N.S., Jawhari, H., Grigoriev, I., van Rijssel, F.J.A., Buey, R.M., Lawera, A., et al. (2009). An EB1-Binding Motif Acts as a Microtubule Tip Localization Signal. Cell *138,* 366–376.

Howard, J. (2001). Mechanics of motor proteins and the cytoskeleton. Sunderland MA, Sinauer Associates, Inc.

Howard, J., and Hyman, A.A. (2003). Dynamics and mechanics of the microtubule plus end. Nature *422,* 753–758.

Howard, J., and Hyman, A.A. (2007). Microtubule polymerases and depolymerases. Curr. Opin. Cell Biol. *19,* 31–35.

Hoyt, M.A., He, L., Loo, K.K., and Saunders, W.S. (1992). Two Saccharomyces cerevisiae kinesin-related gene products required for mitotic spindle assembly. The Journal of Cell Biology *118,* 109–120.

Hunter, A.W., Caplow, M., Coy, D.L., Hancock, W.O., Diez, S., Wordeman, L., and Howard, J. (2003). The kinesin-related protein MCAK is a microtubule depolymerase that forms an ATP-hydrolyzing complex at microtubule ends. Molecular Cell *11,* 445–457.

Huyett, A., Kahana, J., Silver, P., Zeng, X., and Saunders, W.S. (1998). The Kar3p and Kip2p motors function antagonistically at the spindle poles to influence cytoplasmic microtubule numbers. J. Cell. Sci. *111,* 295–301.

Hyman, A., Drechsel, D., Kellog, D., Salser, S., Sawin, K., Steffen, P., Wordeman, L. and Mitchison, T. (1991). Preparation of modified tubulins. Methods in Enzymology *196,* 478-485.

Hyman, A.A., Salser, S., Drechsel, D.N., Unwin, N., and Mitchison, T.J. (1992). Role of GTP hydrolysis in microtubule dynamics: information from a slowly hydrolyzable analogue, GMPCPP. Molecular Biology of the Cell *3,* 1155.

Janke, C., and Chloë Bulinski, J. (2011). Post-translational regulation of the microtubule cytoskeleton: mechanisms and functions. Nat. Rev. Mol. Cell Biol. *12,* 773–786.

Jolly, A.L., and Gelfand, V.I. (2014). Cytoplasmic microtubule sliding. Communicative & Integrative Biology *3,* 589–591.

Kahana, J.A., Schnapp, B.J., and Silver, P.A. (1995). Kinetics of Spindle Pole Body Separation in Budding Yeast. Proc. Natl. Acad. Sci. *92,* 9707–9711.

Kinoshita, K., Arnal, I., Desai, A., Drechsel, D.N., and Hyman, A.A. (2001). Reconstitution of physiological microtubule dynamics using purified components. Science *294,* 1340–1343.

Kinoshita, K., Noetzel, T.L., Arnal, I., Drechsel, D.N., and Hyman, A.A. (2006). Global and local control of microtubule destabilization promoted by a catastrophe kinesin MCAK/XKCM1. J. Muscle Res. Cell. Motil. *27,* 107–114.

Kline-Smith, S.L., and Walczak, C.E. (2002). The microtubule-destabilizing kinesin XKCM1 regulates microtubule dynamic instability in cells. Molecular Biology of the Cell *13,* 2718–2731.

Kozielski, F., Sack, S., Marx, A., Thormählen, M., Schönbrunn, E., Biou, V., Thompson, A., Mandelkow, E.-M., and Mandelkow, E. (1997). The crystal structure of dimeric kinesin and implications for microtubule-dependent motility. Cell *91,* 985–994.

Kühne, W. (1859). Untersuchungen über Bewegungen und Veränderungen der contractilen Substanzen. *Archiv für Anatomie. Physiologie und wissenschaftliche Medicin, 1859,* 748-835.

Kurihara, L.J., Beh, C.T. Latterich, M., Schekman, R. and Rose, M.D. (1994). Nuclear congression and membrane fusion: two distinct events in the yeast karyogamy pathway. The Journal of Cell Biology *126,* 911-23.

Lansbergen, G., and Akhmanova, A. (2006). Microtubule plus end: a hub of cellular activities. Traffic *7,* 499–507.

Lawrence, C.J., Dawe, R.K., and Christie, K.R. (2004). A standardized kinesin nomenclature. The Journal of Cell Biology, 167, 19-22.

Lee, J.C., and Timasheff, S.N. (1977). In vitro reconstitution of calf brain microtubules: effects of solution variables. Biochemistry *16,* 1754–1764.

Li, Y.-Y., Yeh, E., Hays, T., and Bloom, K. (1993). Disruption of mitotic spindle orientation in a yeast dynein mutant. Proc. Natl. Acad. Sci. U.S.A. *90,* 10096–10100.

Lillie, S.H. and Brown, S.S. (1994). Immunofluorescence localization of the unconventional myosin, Myo2p, and the putative kinesin-related protein, Smy1p, to the same regions of polarized growth in Saccharomyces cerevisiae. The Journal of Cell Biology *125,* 825-42.

Liu, A.P., and Fletcher, D.A. (2009). Biology under construction: in vitro reconstitution of cellular function. Nat. Rev. Mol. Cell Biol. *10,* 644–650.

Maekawa, H., Usui, T., Knop, M., and Schiebel, E. (2003). Yeast Cdk1 translocates to the plus end of cytoplasmic microtubules to regulate bud cortex interactions. Embo J. *22,* 438–449.

Manning, B.D., Barrett, J.G., Wallace, J.A., Granok, H., and Snyder, M. (1999). Differential Regulation of the Kar3p Kinesin-related Protein by Two Associated Proteins, Cik1p and Vik1p. The Journal of Cell Biology *144,* 1219–1233.

Marx, A., Müller, J., and Mandelkow, E. (2005). The structure of microtubule motor proteins. Adv. Protein Chem. *71,* 299–344.

Maurer, S.P., Cade, N.I., Bohner, G., Gustafsson, N., Boutant, E., and Surrey, T. (2014). EB1 Accelerates Two Conformational Transitions Important for Microtubule Maturation and Dynamics. Current Biology *24,* 372–384.

McVicker, D.P., Chrin, L.R., and Berger, C.L. (2011). The nucleotide-binding state of microtubules modulates kinesin processivity and the ability of tau to inhibit kinesin-mediated transport. Journal of Biological Chemistry *286,* 42873–42880.

Meluh, P.B., and Rose, M.D. (1990). Kar3, a kinesin-related gene required for yeast nuclear-fusion. Cell *60,* 1029–1041.

Mickey, B., and Howard, J. (1995). Rigidity of microtubules is increased by stabilizing agents. The Journal of Cell Biology *130,* 909–917.

Mieck, C., Molodtsov, M.I., Drzewicka, K., van der Vaart, B., Litos, G., Schmauss, G., Vaziri, A., and Westermann, S. (2015). Non-catalytic motor domains enable processive movement and functional diversification of the kinesin-14 Kar3. eLife *4.*

Miller, R.K., Heller, K.K., Frisèn, L., Wallack, D.L., Loayza, D., Gammie, A.E., and Rose, M.D. (1998). The kinesin-related proteins, Kip2p and Kip3p, function differently in nuclear migration in yeast. Molecular Biology of the Cell *9,* 2051–2068.

Mimori-Kiyosue, Y., Shiina, N., and Tsukita, S. (2000). The dynamic behavior of the APC-binding protein EB1 on the distal ends of microtubules. Current Biology *10,* 865–868.

Mitchison, T., and Kirschner, M. (1984a). Dynamic instability of microtubule growth. Nature *312,* 237–242.

Mitchison, T., and Kirschner, M. (1984b). Microtubule assembly nucleated by isolated centrosomes. Nature *312,* 232–237.

Moore, J.K., Stuchell-Brereton, M.D., and Cooper, J.A. (2009). Function of dynein in budding yeast: Mitotic spindle positioning in a polarized cell. Cell Motil. Cytoskeleton *66,* 546–555.

Morrison, E.E., Wardleworth, B.N., Askham, J.M., Markham, A.F., and Meredith, D.M. (1998). EB1, a protein which interacts with the APC tumour suppressor, is associated with the microtubule cytoskeleton throughout the cell cycle. Oncogene *17,* 3471–3477.

Nogales, E. (1999). A structural view of microtubule dynamics. Cellular and Molecular Life Sciences CMLS *56,* 133–142.

Nogales, E., Wolf, S.G., and Downing, K.H. (1998). Structure of the αβ tubulin dimer by electron crystallography. Nature *391,* 199–203.

Norris, S. R., Nunez, M.F. and Verhey, K.J. (2015). Influence of fluorescent tag on the motility properties of kinesin-1 in single-molecule assays. Biophysical Journal *108,* 1133–1143.

Palmer, R.E., Sullivan, D.S., Huffaker, T., and Koshland, D. (1992). Role of astral microtubules and actin in spindle orientation and migration in the budding yeast, Saccharomyces cerevisiae. The Journal of Cell Biology *119,* 583–593.

Pecreaux, J., Röper, J.-C., Kruse, K., Jülicher, F., Hyman, A.A., Grill, S.W., and Howard, J. (2006). Spindle oscillations during asymmetric cell division require a threshold number of active cortical force generators. Current Biology *16,* 2111– 2122.

Perez, F., Diamantopoulos, G.S., Stalder, R., and Kreis, T.E. (1999). CLIP-170 highlights growing microtubule ends in vivo. Cell *96,* 517–527.

Podolski, M., Mahamdeh, M., and Howard, J. (2014). Stu2, the budding yeast XMAP215/Dis1 homolog, promotes assembly of yeast microtubules by increasing growth rate and decreasing catastrophe frequency. Journal of Biological Chemistry *289,* 28087-93.

Pollard, T.D., and Korn, E.D. (1973). Acanthamoeba myosin. I. Isolation from Acanthamoeba castellanii of an enzyme similar to muscle myosin. Journal of Biological Chemistry *248,* 4682–4690.

Reber, S.B., Baumgart, J., Widlund, P.O., Pozniakovsky, A., Howard, J., Hyman, A.A., and Jülicher, F. (2013). XMAP215 activity sets spindle length by controlling the total mass of spindle microtubules. Nat. Cell Biol. *15,* 1116–1122.

Rizk, R.S., DiScipio, K.A., Proudfoot, K.G., and Gupta, M.L. (2014). The kinesin-8 Kip3 scales anaphase spindle length by suppression of midzone microtubule polymerization. The Journal of Cell Biology *204,* 965–975.

Roberts, A.J., Goodman, B.S., and Reck-Peterson, S.L. (2014). Reconstitution of dynein transport to the microtubule plus end by kinesin. eLife *3.*

Rogers, S.L., Rogers, G.C., Sharp, D.J., and Vale, R.D. (2002). Drosophila EB1 is important for proper assembly, dynamics, and positioning of the mitotic spindle. The Journal of Cell Biology *158,* 873–884.

Roof, D.M., Meluh, P.B., and Rose, M.D. (1992). Kinesin-related Proteins required for Assembly of the Mitotic Spindle. The Journal of Cell Biology *118,* 95–108.

Sardar, H.S., Luczak, V.G., Lopez, M.M., Lister, B.C., and Gilbert, S.P. (2010). Mitotic Kinesin CENP-E Promotes Microtubule Plus-End Elongation. Current Biology *20,* 1648–1653.

Schatz, P.J., Pillus, L., Grisafi, P., Solomon, F., and Botstein, D. (1986). Two functional alpha-tubulin genes of the yeast Saccharomyces cerevisiae encode divergent proteins. Molecular and Cellular Biology *6,* 3711–3721.

Schnitzer, M.J., and Block, S.M. (1997). Kinesin hydrolyses one ATP per 8-nm step. Nature *388,* 386–390.

Snyder, M., Gehrung, S., and Page, B.D. (1991). Studies Concerning the Temporal and Genetic-Control of Cell Polarity in Saccharomyces-Cerevisiae. The Journal of Cell Biology *114,* 515–532.

Spellman, P.T., Sherlock, G., Zhang, M.Q., Iyer, V.R., Anders, K., Eisen, M.B., Brown, P.O., Botstein, D., and Futcher, B. (1998). Comprehensive identification of cell cycle-regulated genes of the yeast Saccharomyces cerevisiae by microarray hybridization. Molecular Biology of the Cell *9,* 3273–3297.

Su, X., Arellano-Santoyo, H., Portran, D., Gaillard, J., Vantard, M., Thery, M., and Pellman, D. (2013). Microtubule-sliding activity of a kinesin-8 promotes spindle assembly and spindle-length control. Nat. Cell Biol. *15,* 1–8.

Su, X., Qiu, W., Gupta, M.L., Jr, Pereira-Leal, J.B., Reck-Peterson, S.L., and Pellman, D. (2011). Mechanisms Underlying the Dual-Mode Regulation of Microtubule Dynamics by Kip3/Kinesin-8. Molecular Cell *43,* 751–763.

Su, X., Ohi, R., and Pellman, D. (2012). Move in for the kill: motile microtubule regulators. Trends in Cell Biology 1–9.

Sullivan, D.S., and Huffaker, T.C. (1992). Astral microtubules are not required for anaphase-B in Saccharomyces cerevisiae. The Journal of Cell Biology *119,* 379–388.

Svoboda, K., and Block, S.M. (1994). Force and velocity measured for single kinesin molecules. Cell *77,* 773–784.

Svoboda, K., Schmidt, C.F., Schnapp, B.J., and Block, S.M. (1993). Direct observation of kinesin stepping by optical trapping interferometry. Nature *365,* 721–727.

Tirnauer, J.S., O'Toole, E., Berrueta, L., Bierer, B.E., and Pellman, D. (1999). Yeast Bim1p promotes the G1-specific dynamics of microtubules. The Journal of Cell Biology *145,* 993–1007.

Tran, P.T., Walker, R.A., and Salmon, E.D. (1997). A metastable intermediate state of microtubule dynamic instability that differs significantly between plus and minus ends. The Journal of Cell Biology *138,* 105–117.

Tropini, C., Roth, E.A., Zanic, M., Gardner, M.K. and Howard, J. (2012). Islands containing slowly hydrolyzable GTP analogs promote microtubule rescues. Plos One *7*, e30103.

Vaart, B.V.D., Akhmanova, A., and Straube, A. (2009). Regulation of microtubule dynamic instability. Biochem. Soc. Trans *37,* 1007.

Vale, R.D., and Fletterick, R.J. (1997). The design plan of kinesin motors. Annu. Rev. Cell Dev. Biol. *13,* 745–777.

Vale, R.D., and Milligan, R.A. (2000). The way things move: looking under the hood of molecular motor proteins. Science *288,* 88–95.

Vale, R.D., Reese, T.S., and Sheetz, M.P. (1985). Identification of a Novel Force-Generating Protein, Kinesin, Involved in Microtubule-Based Motility. Cell *42,* 39–50.

Varga, V., Helenius, J., Tanaka, K., Hyman, A.A., Tanaka, T.U., and Howard, J. (2006). Yeast kinesin-8 depolymerizes microtubules in a length-dependent manner. Nat. Cell Biol. *8,* 957–962.

Varga, V., Leduc, C., Bormuth, V., Diez, S., and Howard, J. (2009). Kinesin-8 motors act cooperatively to mediate length-dependent microtubule depolymerization. Cell *138,* 1174–1183.

Verde, F., Dogterom, M., Stelzer, E., Karsenti, E., and Leibler, S. (1992). Control of microtubule dynamics and length by cyclin A- and cyclin B-dependent kinases in Xenopus egg extracts. The Journal of Cell Biology *118,* 1097–1108.

Verde, F., Mata, J., and Nurse, P. (1995). Fission yeast-cell morphogenesis - identification of new genes and analysis of their role during the cell-cycle. The Journal of Cell Biology *131,* 1529–1538.

Vicente, J.J., and Wordeman, L. (2015). Mitosis, microtubule dynamics and the evolution of kinesins. Exp. Cell Res. 1–9.

Walczak, C.E., Mitchison, T.J., and Desai, A. (1996). XKCM1: a Xenopus kinesin-related protein that regulates microtubule dynamics during mitotic spindle assembly. Cell *84,* 37–47.

Walker, J.E., Saraste, M., Runswick, M.J., and Gay, N.J. (1982). Distantly related sequences in the alpha- and beta-subunits of ATP synthase, myosin, kinases and other ATP-requiring enzymes and a common nucleotide binding fold. Embo J. *1,* 945–951.

Walker, R.A., Inoue, S., and Salmon, E.D. (1989). Asymmetric behavior of severed microtubule ends after ultraviolet microbeam irradiation of individual microtubules in vitro. The Journal of Cell Biology *108,* 931–937.

Walker, R.A., O'Brien, E.T., Pryer, N.K., Soboeiro, M.F., Voter, W.A., Erickson, H.P., and Salmon, E.D. (1988). Dynamic instability of individual microtubules analyzed by video light microscopy: rate constants and transition frequencies. The Journal of Cell Biology *107,* 1437–1448.

Wegscheider, R. (1901). Über simultane Gleichgewichte und die Beziehungen zwischen Thermodynamik und Reactionskinetik homogener Systeme. Monatshefte für Chemie *32,* 849–906.

Weisenberg, R. C., Borisy, G. G., and Taylor, E. W. (1968). Biochemistry 7, 4466-4479.

Weisenberg, R. C., and Timasheff, S. N. (1970). Biochemistry 9, 4110-4116.

Wickstead, B., Gull, K., and Richards, T.A. (2010). Patterns of kinesin evolution reveal a complex ancestral eukaryote with a multifunctional cytoskeleton. BMC Evol Biol *10,* 110.

Widlund, P.O., Podolski, M., Reber, S., Alper, J., Storch, M., Hyman, A.A., Howard, J., and Drechsel, D.N. (2012). One-step purification of assembly-competent tubulin from diverse eukaryotic sources. Molecular Biology of the Cell *23,* 4393–4401.

Yang, J.T., Laymon, R.A., and Goldstein, L.S. (1989). A three-domain structure of kinesin heavy chain revealed by DNA sequence and microtubule binding analyses. Cell *56,* 879–889.

Yeh, E., Skibbens, R.V., Cheng, J.W., Salmon, E.D., and Bloom, K. (1995). Spindle dynamics and cell-cycle regulation of dynein in the budding yeast, Saccharomyces cerevisiae. The Journal of Cell Biology *130,* 687–700.

Yildiz, A., Tomishige, M., Vale, R.D., and Selvin, P.R. (2004). Kinesin walks hand-over-hand. Science *303,* 676–678.

Zanic, M., Widlund, P.O., Hyman, A.A., and Howard, J. (2013). Synergy between XMAP215 and EB1 increases microtubule growth rates to physiological levels. Nat. Cell Biol. *15,* 688–693

Appendices

**Appendix I. Kip2 protein stability and 6xHis-tag cleavage success probed by SDS-PAGE and Western blot.**
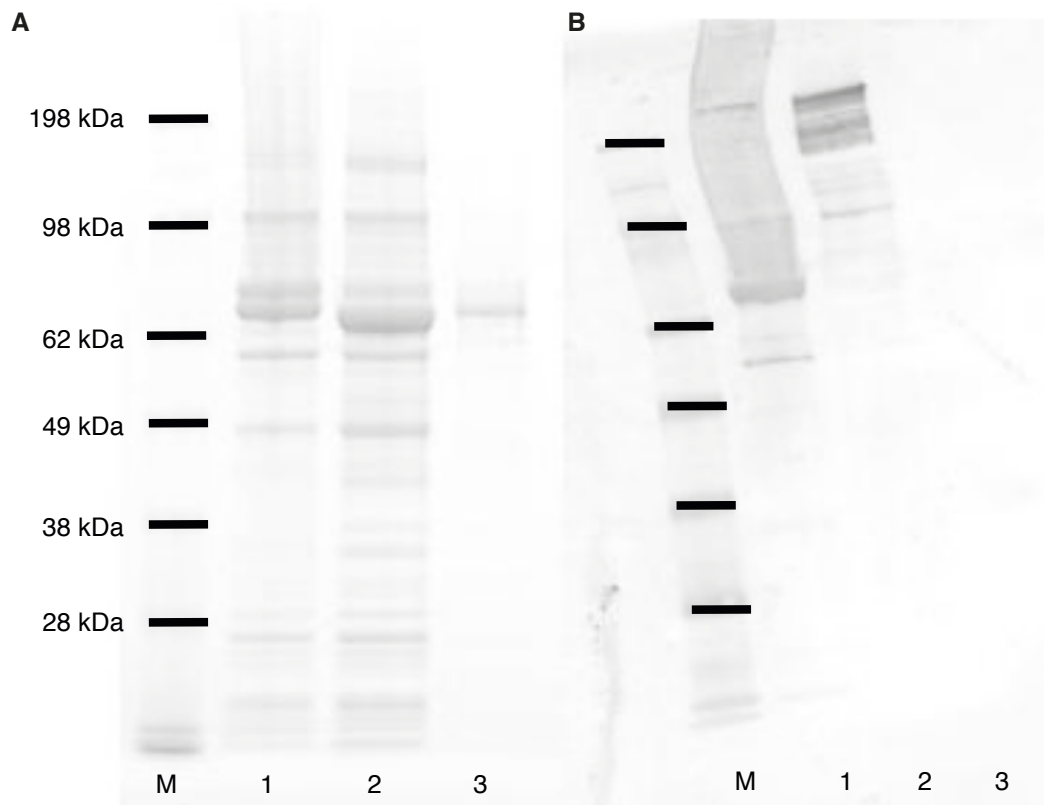
A). SDS-PAGE gel of Kip2 fractions following subsequent purification steps. Per lane, 8 µl protein was loaded. Lane M: SeeBlue® Plus2 prestained protein standard (Lifetechnologies). Lane 1: The 300 mM imidazole elution fraction of the His-affinity column purification. The fraction is enriched for 6xHis-Kip2. Lane 2: Kip2 fraction after PreScission protease treatment over-night on a rotary at 8 °C. Lane 3: Pooled Kip2 fractions after gel filtration. Only the Kip2 protein band remains visible on the SDS-page gel, Kip2 is stable after removal of the 6xHis-tag.

B). Western blot of Kip2 fractions following subsequent purification steps, using THE-his antibody (Genscript) as primary anti-body in a 1:10.000 dilution. Per lane, 8 µl protein was loaded. Lane M: SeeBlue® Plus2 prestained protein standard. Lane 1: The 300 mM imidazole elution fraction of the His-affinity column purification. The fraction is enriched for 6xHis-Kip2 and oligomers of 6xHis-Kip2 (smear). Lane 2: Kip2 fraction after PreScission protease treatment over-night on a rotary at 8 °C. The Kip2-band is no longer visible, which indicates that PreScission protease successfully cleaved off the 6xHis-tag. Lane 3: Pooled Kip2 fractions after gel filtration. The Kip2 protein band is invisible on the Western blot.

Appendix 2. SDS-PAGE gel to determine Kip2 concentration.
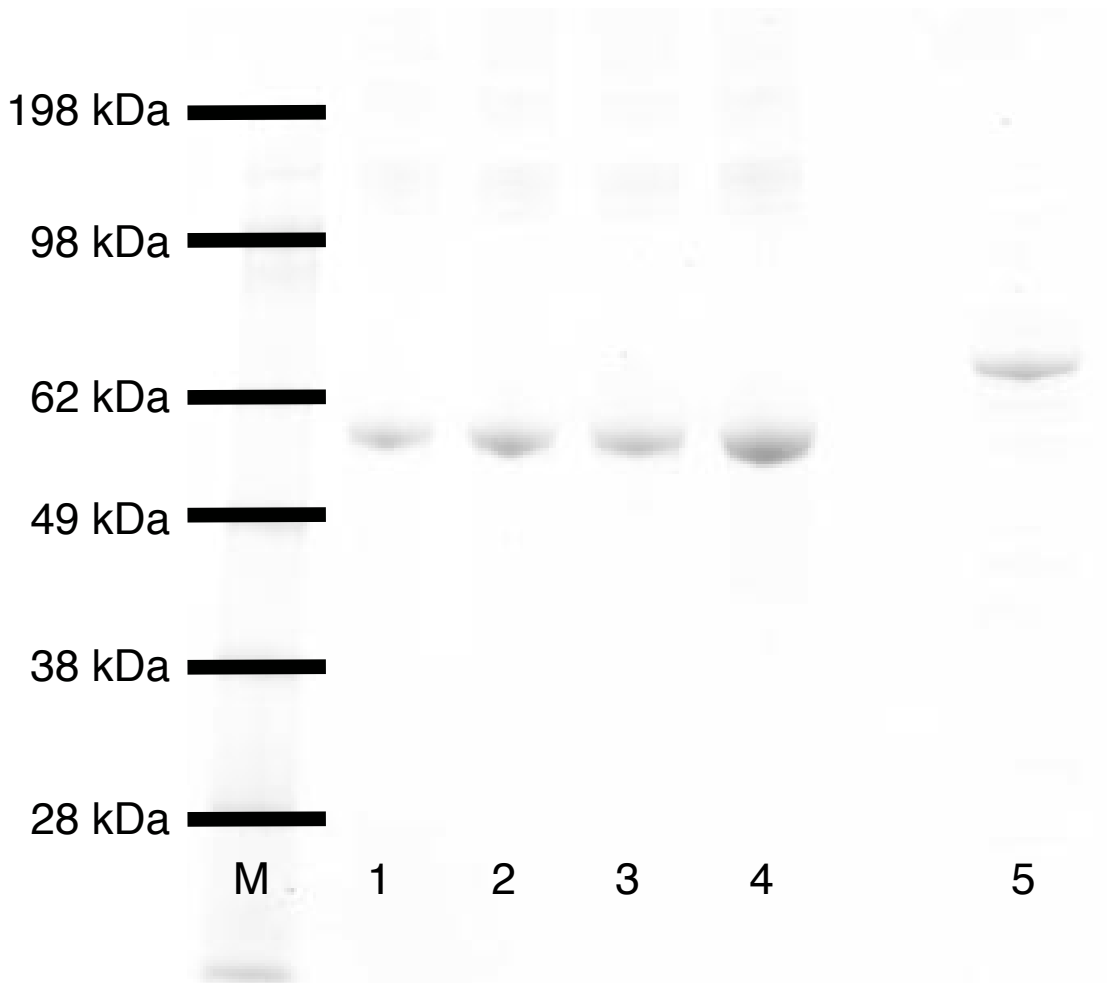

SDS-PAGE gel of BSA (66.5 kDa) dilutions and purified Kip2 (78 kDa) to determine Kip2 concentration. Per lane, 10 µl protein was loaded. Lane M: SeeBlue® Plus2 prestained protein standard (Lifetechnologies). Lane 1: 0.2 mg/ml BSA. Lane 2: 0.3 mg/ml BSA. Lane 3: 0.4 mg/ml BSA. Lane 4: 0.5 mg/ml BSA. Lane 5: Pooled Kip2 gel filtration fractions.

Appendix 3. SDS-PAGE gel to determine Kip2-eGFP concentration.
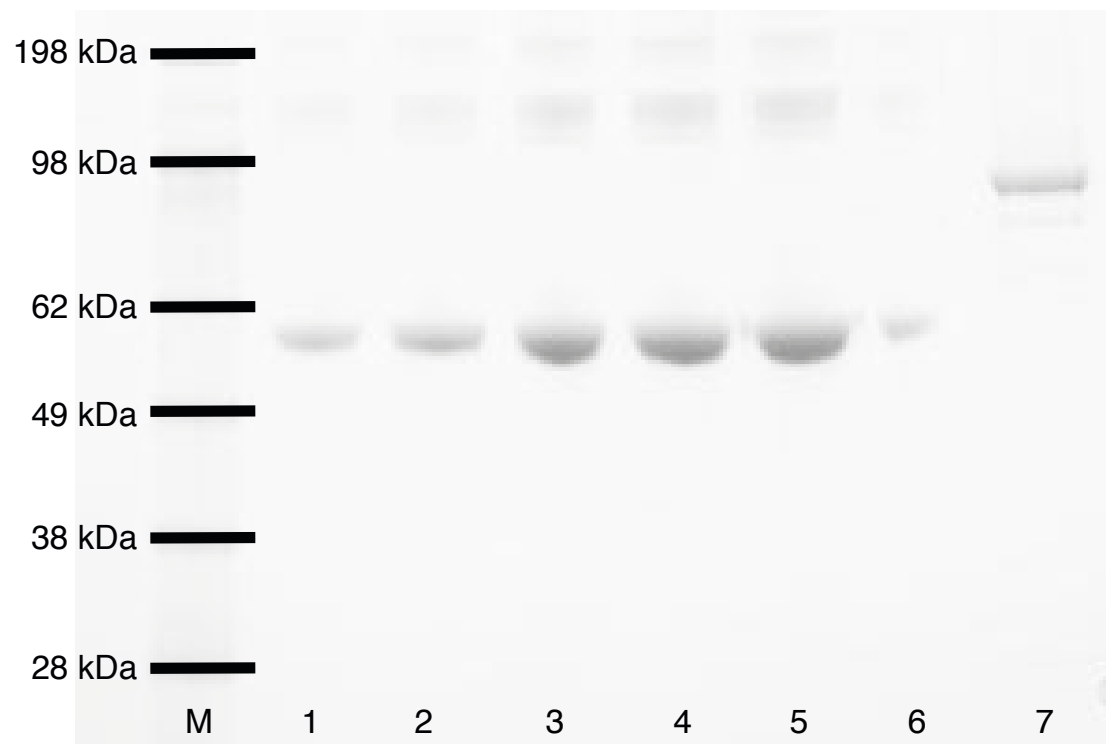
A). SDS-PAGE gel of BSA dilutions (66.5 kDa) and purified Kip2-eGFP (105 kDa) to determine Kip2 concentration-eGFP. Per lane, 15 µl protein was loaded. Lane M: SeeBlue® Plus2 pre-stained protein standard (Lifetechnologies). Lane 1: 0.1 mg/ml BSA. Lane 2: 0.2 mg/ml BSA. Lane 3: 0.3 mg/ml BSA. Lane 4: 0.4 mg/ml BSA. Lane 5: 0.5 mg/ml BSA (leaked into lane 6). Lane 7: Pooled Kip2-eGFP gel filtration fractions.

Appendix 4. 6xHis-Kip2_ala-eGFP protein stability and enzymatic cleavage success probed by SDS-PAGE Western blot.
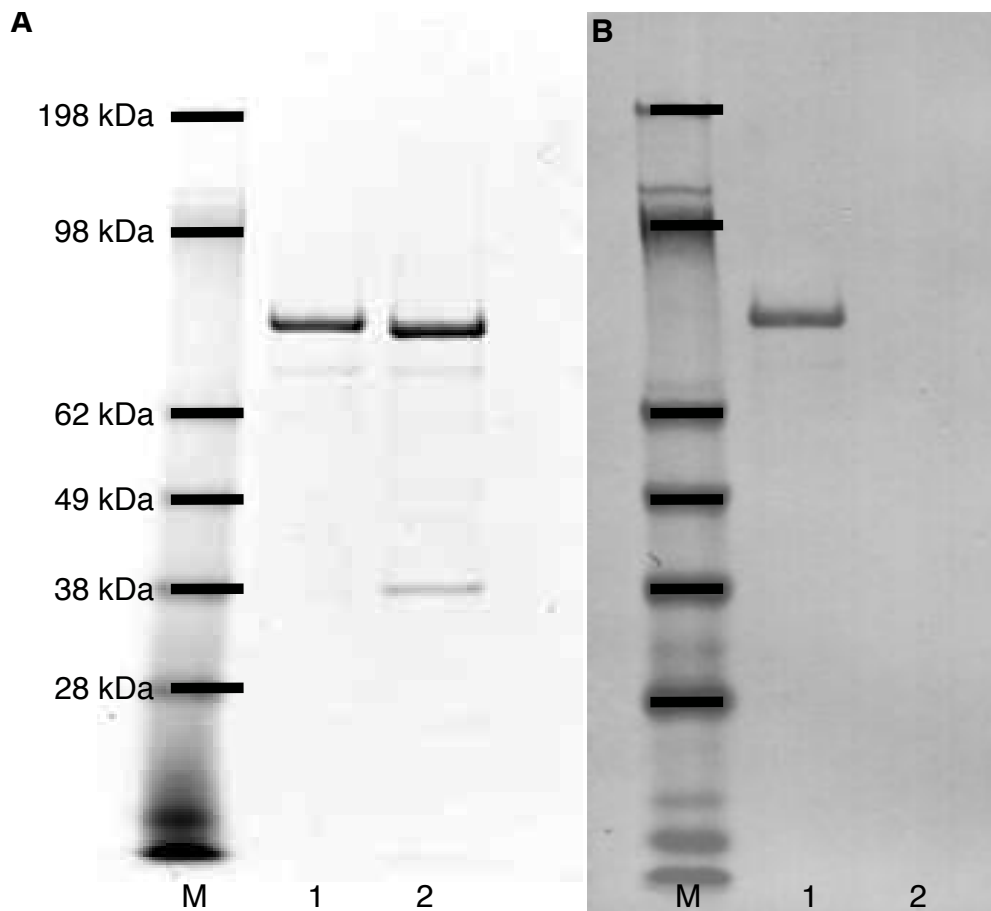
A). SDS-PAGE gel of Kip2_ala-eGFP fractions following subsequent purification steps. Per lane, 7 µl protein was loaded. Lane M: SeeBlue® Plus2 prestained protein standard (Lifetechnologies). Lane 1: The 300 mM imidazole elution fraction of the His-affinity column purification. The fraction is enriched for 6xHis-Kip2_ala-eGFP. Lane 2: Kip2 fraction after PreScission protease treatment over-night on a rotary at 8 °C. Only the Kip2 protein band remains visible on the SDS-page gel, Kip2 is stable after removal of the 6xHis-tag. The second band of lower molecular mass is the PreScission protease.

B). Western blot of Kip2_ala-eGFP fractions following subsequent purification steps, using THE-his antibody (Genscript) as primary anti-body in a 1:3.000 dilution. Per lane, 7 µl protein was loaded. Lane M: SeeBlue® Plus2 prestained protein standard. Lane 1: The 300 mM imidazole elution fraction of the His-affinity column purification. The fraction is enriched for 6xHis-Kip2_ala-eGFP. Lane 2: Kip2 fraction after PreScission protease treatment over-night on a rotary at 8 °C. The Kip2_ala-eGFP band is no longer visible, which indicates that PreScission protease successfully cleaved off the 6xHis-tag.

Appendix 5. Protein expression in budding yeast probed by Western blot.
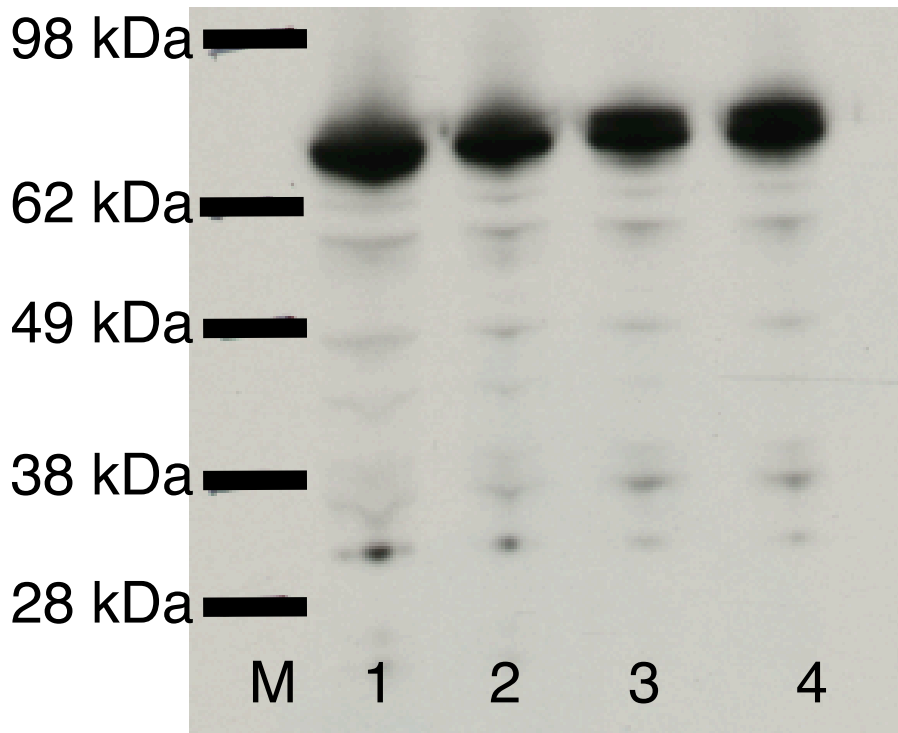
Western blot of full-length Kip2-HA3 or Kip2_ala-Ha3 over-expression in budding yeast strains, using rabbit HA-antibody (Santa Cruz Biotechnology) as primary anti-body in a 1:200 dilution and anti-rabbit-IgG (Sigma) in a 1:5000 dilution as secondary antibody. Per lane, 6 µg protein was loaded. Lane 1 & 2: Over-expression of Kip2-HA (duplicates). Lane 3 & 4: Over-expression of Kip2_ala-HA (duplicates). Protein levels of full-length Kip2 and Kip2-ala are approximately the same.

Tables

Table 1. Microtubule lengths at t = 10 minutes (12 μM porcine tubulin).

Kip2 (nM)	Mean (μm)	SD (μm)	n	SE (μm)
0	0.99	0.87	54	0.12
1	1.0	1.4	75	0.16
2	2.1	1.5	88	0.16
5	5.3	1.9	82	0.21
10	6.4	1.7	75	0.19
20	7.7	2.3	68	0.28
40	8.8	3.3	26	0.64

Table 2. Parameters.

Parameter		Mean	Error	
Catastrophe frequency	K_{cat}	$\dfrac{n}{T_+}$	$\dfrac{\sqrt{n}}{T_+}$	n is the the number of catastrophes observed T_+ is the total time of observed microtubule growth
Rescue frequency	K_{res}	$\dfrac{n}{L_-}$	$\dfrac{\sqrt{n}}{L_-}$	n is the the number of rescues observed L_- is the total length of observed microtubule shrinkage
Kip2 flux on dynamic microtubules	J_d	$\dfrac{n}{T_+}$	$\dfrac{\sqrt{n}}{T_+}$	n is the number of Kip2 molecules arriving at the microtubule plus-end T_+ is the total time of observed microtubule growth
Kip2 flux on stabilized microtubules	J_s	$\dfrac{n}{T}$	$\dfrac{\sqrt{n}}{T}$	n is the number of Kip2 molecules arriving at the microtubule plus-end T is the total duration of the experiment
Kip2 binding rate to dynamic microtubules	K_d^{Kip2}	$\dfrac{2n}{T^2 \cdot V_+}$	SD	n is the number of binding events observed T is the total duration of the experiment V_+ is the microtubule growth rate
Kip2 binding rate to stabilized microtubules	K_s^{Kip2}	$\dfrac{n}{L \cdot T}$	SD	n is the number of binding events observed L is the length of the microtubule seed T is the total duration of the experiment

Table 3. Microtubule growth rates (12 µM porcine tubulin).

Kip2 (nM)	Mean (µm/min)	SD (µm/min)	n	SE (µm/min)
0	0.32	0.31	172	0.02
1	0.37	0.13	152	0.01
2	0.35	0.15	159	0.01
5	0.62	0.28	77	0.03
10	0.78	0.20	38	0.03
20	0.99	0.24	36	0.04
40	0.94	0.22	18	0.05

Table 4. Microtubule catastrophe frequencies (12 µM porcine tubulin).

Kip2 (nM)	Mean (min^{-1})	n	SE (min^{-1})
0	0.17	126	0.02
1	0.13	104	0.01
2	0.13	115	0.01
5	0.07	33	0.01
10	0.04	16	0.01
20	0.02	10	0.01
40	0.004	1	0.004

Table 5. Microtubule rescue lengths (12 µM porcine tubulin).

Kip2 (nM)	Mean (µm)	n	SE (µm)
0	0.03	7	0.01
1	0.01	2	0.01
2	0.02	5	0.01
5	0.08	9	0.03
10	0.06	6	0.03
20	0.19	6	0.08
40	N.A.	N.A.	N.A.

Table 6. Microtubule shrinkage rates (12 μM porcine tubulin).

Kip2 (nM)	Mean (μm/min)	SD (μm/min)	n	SE (μm/min)
0	27.6	11.0	130	0.96
1	27.7	7.9	85	0.85
2	29.7	9.3	110	0.89
5	28.4	11.8	45	1.76
10	28.9	17.2	18	4.1
20	N.A.	N.A.	N.A.	N.A.
40	N.A.	N.A.	N.A.	N.A.

Table 7. Theoretical lengths at t = 10 minutes (12 μM porcine tubulin).

Kip2 (nM)	Growth rate (μm/min)	Lifetime (min)	calculation	Theor. length (μm)
0	0.32	6	(10 - 6) * 0.32	1.3
1	0.37	7.5	(10 - 7.5) * 0.37	0.9
2	0.35	7.5	(10 - 7.5) * 0.35	0.9
5	0.62	14	10 * 0.62	6.2
10	0.78	25	10 * 0.78	7.8
20	0.99	50	10 * 0.99	9.9
40	0.94	250	10 * 0.94	9.4

Table 8. Microtubule growth rates (4 μM yeast tubulin).

Kip2 (nM)	Mean (μm/min)	SD (μm/min)	n	SE (μm/min)
0	0.26	0.07	300	0.004
5	0.30	0.08	263	0.005
10	0.35	0.09	146	0.008
20	0.57	0.07	57	0.010
40	0.59	0.08	48	0.012

Table 9. Microtubule catastrophe frequencies (4 µM yeast tubulin).

Kip2 (nM)	Mean (min^{-1})	n	SE (min^{-1})
0	0.23	191	0.02
5	0.14	141	0.01
10	0.10	116	0.01
20	0.02	13	0.01
40	0.009	5	0.004

Table 10. DNA fragment and destination vectors.

Vector (in CBG-list)	DNA construct	Expression system
pOCC5	6xHis-Kip2	SF+ cells
pOCC16	6xHis-Kip2-eGFP	SF+ cells
pOCC16	6xHis-Kip2ΔN-eGFP	SF+ cells
pOCC16	6xHis-Kip2ΔC-eGFP	SF+ cells
pOCC16	6xHis-Bik1-eGFP	SF+ cells
pOCC13	6xHis-Bim1-eGFP	*E. coli*
pOCC16	6xHis-Kip2_ala-eGFP	SF+ cells
pOCC78	Kip2_ala-HA3	*S. cerevisiae*
pOCC78	Kip2-HA3	*S. cerevisiae*

Table 11. Reagents used to polymerize GMPCPP-stabilized microtubules.

Volume	Reagents	[Stock]	[Final]
10 µl	RTU tubulin	1mg/ml [10 µM]	2 µM
5 µl	GMPCPP	10 mM	1 mM
0.5 µl	MgCl2	100 mM	1 mM
34.5 µl	BRB80	1x	

50 µl final volume

Table 12. Reagents used to polymerize taxol-stabilized microtubules.

Volume	Reagents	[Stock]	[Final]
10 µl	RTU tubulin	1mg/ml [10 µM]	x µM
0.6 µl	DMSO	100%	5%
0.5 µl	MgCl2	100 mM	1 mM
0.5 µl	GTP	25 mM	1 mM
0.9 µl	BRB80	1x	
12.5 µl final volume			

Table 13. Purification buffers.

Buffer	*Reagents*
Lysis buffer	50 mM NaH_2PO_4, 300 mM NaCl, 0.1% tween-20, 10 mM imidazole, protease inhibitors, 2 mM Mg-ATP, pH = 8.0
Wash buffer	50 mM NaH_2PO_4, 300 mM NaCl, 100 mM imidazole, 2 mM Mg-ATP, pH = 8.0
Elution buffer	50 mM NaH2PO4, 300 mM NaCl, 300 mM imidazole, 2 mM Mg-ATP, pH = 8.0
Storage buffer	1x BRB80 supplemented with 10% glycerol, 1 mM Mg-ATP, 1 mM dithiothreitol
Imaging buffer TIRF and DIC assays	1x BRB20 supplemented with 100 mM KCl, 20 mM glucose, 20 µg ml^{-1} glucose oxidase, 8 µg ml^{-1} catalase, 0.1 mg ml^{-1} casein, 1mM dithiothreitol, 0.001% tween-20, 1 mM GTP and 1 mM Mg-ATP or AMP-PNP

Acknowledgement

I profoundly thank my supervisor Prof. Dr. Jonathon Howard for the opportunity to work in his lab on such a great PhD project, for his supervision, for showing me how to do the numbers, for offering many opportunities to travel; to learn and to teach others, and for supporting my decision to not join the lab at Yale. I could not have wished for a more satisfying PhD experience.

I sincerely thank Prof. Dr. Tony Hyman, Prof. Dr. Stefan Diez and Dr. Simon Alberti for their excellent scientific guidance as my Thesis Advisory Committee members. In addition, I thank Stefan for being a great mentor.

I thank Dr. Jan Brugues for the stimulating and fun discussions.

I thank all members of the Howard lab in Dresden and at Yale, for providing a challenging work environment. I learned a lot.

It has been a great pleasure to share a bench with Dr. Aliona Bogdanova for three years. Aliona taught me all I know about molecular biology, she was always happy to brainstorm on my project and she never failed to boost my confidence. Thank you, Aliona!

I am grateful to Heike Petzold for the 1001 things she did in the lab that made my PhD easier. My project would have taken twice as long if not for her work. My hair would have been twice as grey if not for our relaxing daily chats.

I sincerely thank Dr. Joshua Alper, Dr. Vikram Mukundan and Dr. Sujoy Ganguly, who selfishly invested a huge amount of time and energy to teach the basics of biophysics during the 'Howard lab book club' and the 'Physics for Biologists' lecture series.

I am thankful to Antje Franz for her happy energy.

Erklärung entsprechend §5.5 der Promotionsordnung

Hiermit versichere ich, dass ich die vorliegende Arbeit ohne unzulässige Hilfe Dritter und ohne Benutzung anderer als der angegebenen Hilfsmittel angefertigt habe; die aus fremden Quellen direkt oder indirekt übernommenen Gedanken sind als solche kenntlich gemacht. Die Arbeit wurde bisher weder im Inland noch im Ausland in gleicher oder ähnlicher Form einer anderen Prüfungsbehörde vorgelegt.

Die Dissertation wurde im Zeitraum vom 01. Oktober 2011 bis 30. März 2015 verfasst und von Prof. Dr. Jonathon Howard, MPI-CBG Dresden/Yale University und Prof. Dr. Stefan Diez, TU Dresden betreut.

Meine Person betreffend erkläre ich hiermit, dass keine früheren erfolglosen Promotionsverfahren stattgefunden haben.

Ich erkenne die Promotionsordnung der Fakultät für Mathematik und Naturwissenschaften, Technische Universität Dresden an.

28.8.2020

Date,   Signature